"Instrumentation Engineering, Electronics and Telecommunications – 2019"

Proceedings of the V International Forum

November 20–22, 2019
Izhevsk, Russia

"INSTRUMENTATION ENGINEERING, ELECTRONICS AND TELECOMMUNICATIONS - 2019"

Proceedings of the V International Forum

(Izhevsk, Russia, November 20-22, 2019)

UDC 681.2(06)

This volume contains papers on wide range of problems in fields of instrumental engineering, electronics, telecommunications and related areas discussed during the V International Forum "Instrumentation Engineering, Electronics and Telecommunications - 2019", IEET-2019, November 20-22, 2019, Izhevsk, Russia. All presented papers were selected after double-blind peer-rewiew. The Forum takes place annually in the Kalashnikov Izhevsk State Technical University.

UDC 681.2(06)

«ПРИБОРОСТРОЕНИЕ, ЭЛЕКТРОНИКА И ТЕЛЕКОММУНИКАЦИИ – 2019»

Сборник статей V Международного форума

(Россия, Ижевск, 20–22 ноября 2019 г.)

УДК 681.2(06)
П75

Президиум организационного комитета

В. П. Грахов – председатель, д-р экон. наук, ректор ИжГТУ имени М. Т. Калашникова
А. Л. Кузнецов – зам. председателя, д-р экон. наук, ИжГТУ имени М. Т. Калашникова
А. В. Абилов – зам. председателя, канд. техн. наук, ИжГТУ имени М. Т. Калашникова

Программный комитет

Редакционная коллегия

А. В. Абилов – гл. редактор, председатель, канд. техн. наук, ИжГТУ имени М. Т. Калашникова, Россия
А. Лобов – соредактор, зам. председателя, Dr. Tech., Университет Тампере, г. Тампере, Финляндия
С. А. Мурашов – канд. техн. наук, ИжГТУ имени М. Т. Калашникова, Россия

Рецензенты

К. Е. Аббакумов – д-р техн. наук, Санкт-Петербургский государственный электротехнический университет «ЛЭТИ» им. В. И. Ульянова (Ленина), Россия
М. А. Аль Аккад – канд. техн. наук, ИжГТУ имени М. Т. Калашникова, Россия
Д. С. Васильев – канд. техн. наук, ИжГТУ имени М. Т. Калашникова, Россия
Л. В. Волкова – канд. техн. наук, ИжГТУ имени М. Т. Калашникова, Россия
Я. Котон – PhD, Технический университет г. Брно, Чехия
Д. Кубанек – PhD, Технический университет г. Брно, Чехия
А. Кубанкова – PhD, Технический университет г. Брно, Чехия
О. В. Муравьева – д-р техн. наук, ИжГТУ имени М. Т. Калашникова, Россия
П. Райхерт – гл. операционный директор, CONDOR Maritime LTD., Германия
А. В. Хомченко – д-р физ.-мат. наук, Белорусско-Российский университет, г. Могилев, Беларусь

Приборостроение, электроника и телекоммуникации – 2019 [Электронный ресурс] :
П75   сб. ст. V Междунар. форума (Россия, Ижевск, 20–22 ноября 2019 г.). – Ижевск : Изд-во ИжГТУ имени М. Т. Калашникова, 2019. – 123 с. – 10,6 Мб.

ISSN 2658-3658

Сборник содержит статьи на английском языке по широкому кругу вопросов в области приборостроения, электроники, связи и смежных им, которые обсуждались на V Международном форуме "Instrumentation Engineering, Electronics and Telecommunications – 2019" («Приборостроение, электроника и телекоммуникации – 2019»), IEET-2019, 20–22 ноября 2019 года, Россия, г. Ижевск. Все представленные статьи были отобраны по результатам двойного слепого рецензирования. Форум проводится ежегодно в Ижевском государственном техническом университете имени М. Т. Калашникова.

На дату публикации ИжГТУ имени М.Т. Калашикова принадлежат эксклюзивные права на первую публикацию каждой статьи, представленной в сборнике, а также неэксклюзивные права на их репродукцию в любом виде. Права на дизайн и верстку сборника принадлежат Издательству ИжГТУ имени М. Т. Калашникова. Остальные права на каждую статью сборника остаются за авторами.

УДК 681.2(06)

TABLE OF CONTENTS

Experimental Investigation of the Characteristics of the Information Sensing Module Based on the Optical Tunneling Effect of the Angular Velocity Transducer by Using a Piezoelectric Module

V. I. Busurin, A. V. Kazaryan, Yin Naing Win, K. A. Korobkov

Moscow Aviation Institute (National Research University)
Volokolamskoe Road, 4, Moscow, A-80, GPS-3, 125993, Russia
E-mail: vbusurin@mai.ru, integratedchip.88@gmail.com

Abstract. This article presents an experimental investigation of the characteristics of the module based on the optical tunneling effect, which provides information on the nano displacements resonator of the angular velocity transducer. The analysis of the sensitivity of the module based on the optical tunneling effect with increasing amplitude of forced displacements excited by a piezoelectric module is produced. The principle of operation of the module based on the optical tunneling effect, which is based on the dependence of the reflection coefficient of the radiation source structure "medium-gap-medium" on the size of the gap, is determined. The transfer function of the piezoelectric transducer based on the optical tunneling effect with the total optical losses is determined. The theoretical investigation of the transfer function based on the tunneling effect using the module "optical prism – medium – surface simulator of the edge of the ring resonator" is carried out. The results of the experimental investigation are confirmed that when the amplitudes of the input voltages increase, asymmetric amplitudes of the positive and negative half-waves of the output voltages of the module based on the optical tunneling effect are formed. The scheme of the experimental investigation of the transfer function of the module based on the optical tunneling effect, providing the implementation of optical information retrieval in the measurement of angular velocity, is described. The results of the experimental investigation of the optical information sensing unit at different signals of the wave generator show a good agreement with the theoretical model of the module based on the optical tunneling effect and a small change in sensitivity with increasing the angular velocity and amplitude of the displacement of the resonator edge simulator, which should be compensated for the formation of the output signal.

Keywords: transducer, angular velocity, optical tunnel effect, piezoelectric transducer, experimental investigation

INTRODUCTION

The principle of operation of the module based on the optical tunneling effect (MOTE) is based on the dependence of the reflection coefficient of the radiation source for the structure

V. I. Busurin, A. V. Kazaryan, Yin Naing Win, K. A. Korobkov
"Experimental investigation of the characteristics of the information sensing module based on the
optical tunneling effect of the angular velocity transducer by using a piezoelectric module"

"medium-gap-medium" of the gap. In MOTE, optical radiation passes through the optical prism interacting with the ring resonator (RR) and reaches the photodetector [1-4]. The angle of incidence of the radiation source on the interface between the prism and the gap is chosen such that at a large gap, compared with the wavelength of optical radiation, there is a total internal reflection (TIR). If the size of the gap is comparable with the wavelength of light, then part of the radiation passes (tunnels) through the gap into the second medium and the reflection coefficient of the structure "medium-gap-medium" decreases. Thus, the power of optical radiation reflected from the structure "medium-gap-medium" carries information about the magnitude of the change in the gap and the measured angular velocity[5-10].

When developing an angular velocity transducer, it is necessary to have an adequate description of the real transfer function of the module based on the optical tunnel effect (MOTE), depending on the size of the nano-displacements of the resonator when the measured angular velocity is applied. The validity of the obtained characteristics of the transducer should be based on the results of a comparison of theoretical calculations and experimental studies.

INVESTIGATION OF THE CHARACTERISTICS OF THE MODULE BASED ON THE OPTICAL TUNNELING EFFECT USING THE PIEZOELECTRIC TRANSDUCER

To check the transfer function of the MOTE of the angular velocity transducer, an experimental investigation was conducted using a piezoelectric transducer based on OTE[11]. For the experimental investigation of the transfer function of MOTE, the scheme is developed that consists of prism of quartz glass 1, collimating device 2, fiber optic cable 3, wave generator 4, laser module (KIWI-4100) 5, simulator of the edge of the ring resonator 6, piezoelectric transducer 7, photodiode 8, current to voltage Converter 9, digital oscilloscope 10, computer 11 (Fig. 1).
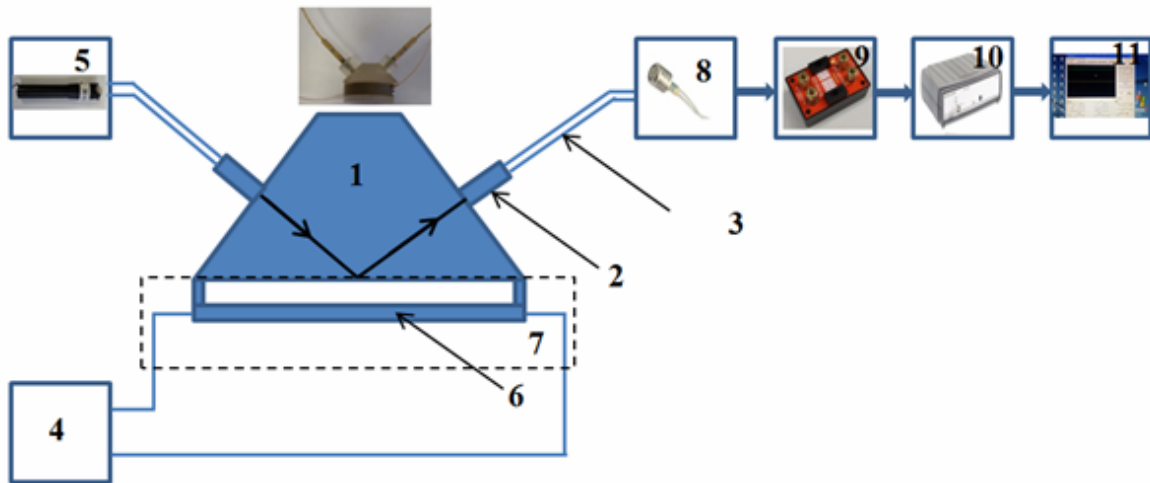
Figure 1. Schematic diagram of experimental setup for the investigation of characteristics for MOTE using piezoelectric transducer

In the mode of generating radiation a laser module (KIWI-4100) was used as a radiation source with a wavelength $\lambda = 0.65$ μm while maintaining a constant power of optical radiation. Periodic changes in the gap were made using excitation of a piezoelectric transducer with different amplitude of the alternating voltage. When applying the exciting voltage to the

piezoelectric transducer, occurs changing of the working gap d between the surface of the simulator of a part of the edge of the ring resonator and the base of the prism. From the radiation source, the optical signal passes the structure "prism-medium-simulator of a part of the edge of a ring resonator" through an optical fiber. Under the action of the voltage of the wave generator, the magnitude of the nano-displacement of the piezoelectric transducer changes: $y = k_{PT} \cdot U_{WG}$, where k_{PT} – coefficient of piezoelectric transducer, U_{WG} – voltage of wave generator [12-17].

The size of the working gap d between the surface of the piezoelectric transducer and the base of the prism is determined by the initial gap d_0 and nano-displacement of the piezoelectric transducer $y(U_{WG})$:

$$d\left(U_{WG}\right) = d_0 - y\left(U_{WG}\right). \tag{1}$$

When reducing the working gap d due to the approach of the simulator of the edge of the piezoelectric transducer, there is a decrease in the power of the optical signal fed to the photodetector. In this case, the transfer function of such a converter based on OTE, taking into account the total optical loss, is determined by the following formula[18-20].:

$$U_{I-U}\left(U_{WG}\right) = K_{I-U} \cdot S_{PD} \cdot P_{RS} \cdot K_{OL} \cdot R\left[d\left(U_{WG}\right)\right], \tag{2}$$

where K_{OL} – coefficient of total optical loss, K_{I-U} – coefficient of current to voltage converter, S_{PD} – sensitivity of the photodiode, P_{RS} – power of the radiation source, $R\left[d\left(U_{WG}\right)\right]$ – the reflectivity of the structure "prism-medium-simulator of a part of the edge of a ring resonator".

A theoretical investigation of the transfer function of the module "prism-medium-simulator of a part of the edge of a ring resonator" was performed with the following parameters: incidence angle of radiation $\theta = 47°$, wavelength $\lambda = 0.65$ μm, power of radiation source $P_{RS} = 20$ μW, refractive indices of prism and simulator of the interacting part of the resonator $n1 = n3 = 1.544$, respectively (Fig. 2).
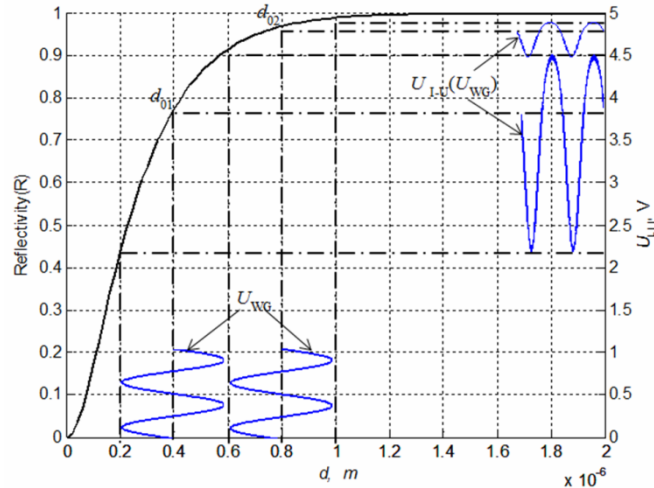
Figure 2. Transfer function of MOTE with variation of the initial gap

It is shown that when the initial gap deviates from the value corresponding to the middle of the quasilinear section, reflectivity of the MOTE changes and the sensitivity of the module "prism-medium-simulator of a part of the edge of a ring resonator" decreases, leading to a decrease in output voltage amplitudes $U_{I-U\,m}(U_{WG\,m})$. An increase in the amplitudes of the

V. I. Busurin, A. V. Kazaryan, Yin Naing Win, K. A. Korobkov
"Experimental investigation of the characteristics of the information sensing module based on the
optical tunneling effect of the angular velocity transducer by using a piezoelectric module"

oscillations of the gap d_m ($U_{WG\,m}$), proportional to the angular velocity and created by the imitating voltage U_{WG} supplied to the piezoelectric transducer, leads to the formation of an asymmetrical output voltage with different amplitudes of positive and negative half waves.

The experimental investigation of the transfer function of the piezoelectric transducer was carried out at various voltage of the wave generator at a frequency of $f = 1$ kHz (Fig. 3).

(a)   (b)

(c)   (d)

(e)   (f)
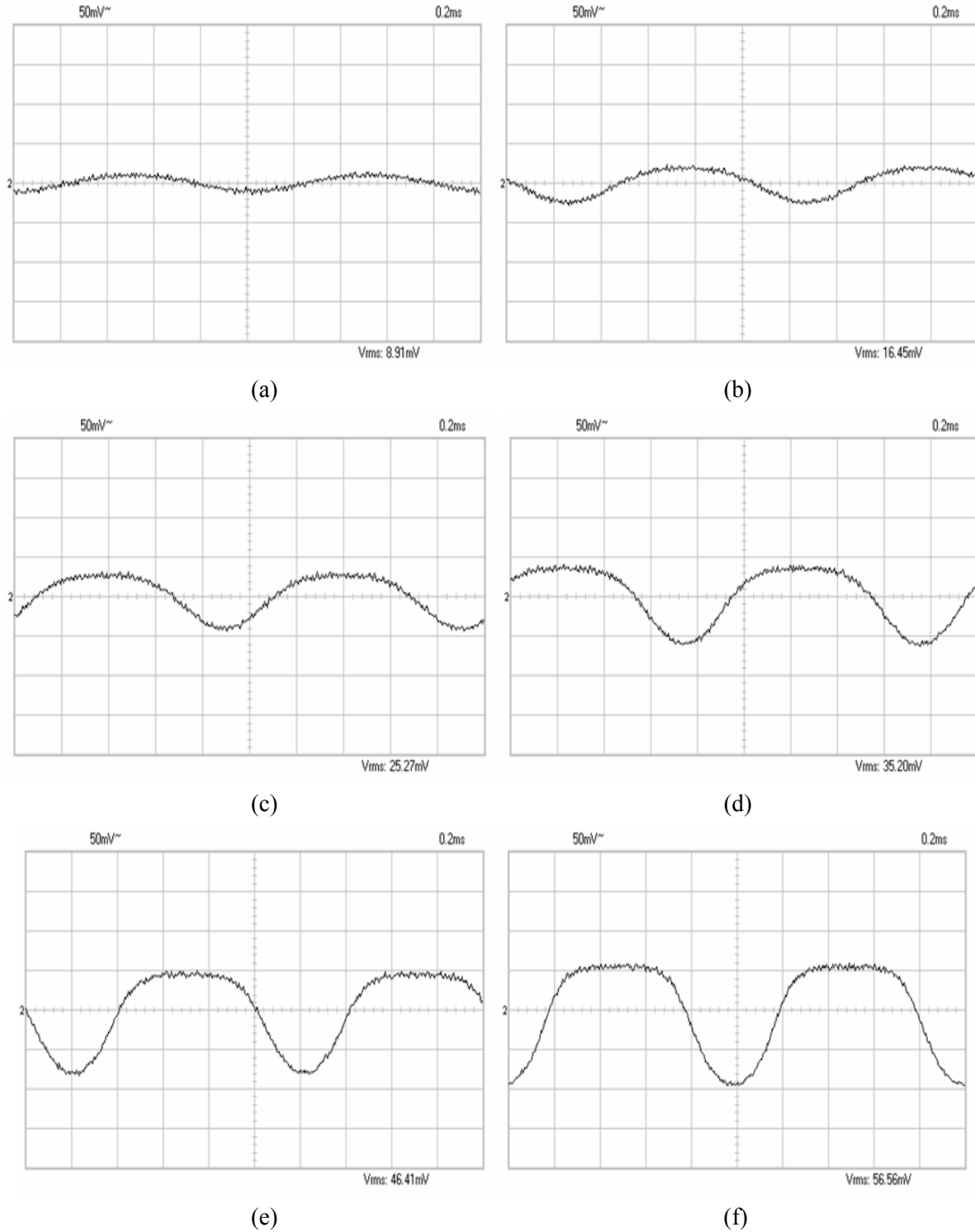
Figure 3. The relationship of the output voltage of MOTE at a frequency $f = 1$ kHz on various input voltages: $U_{WG\,m} = 20$ V (a); $U_{WG\,m} = 40$ V (b); $U_{WG\,m} = 60$ V (c); $U_{WG\,m} = 80$ V (d); $U_{WG\,m} = 100$ V (e); $U_{WG\,m} = 120$ V (f)

It was confirmed that as the amplitudes of the input voltages increase, asymmetric amplitudes of the positive and negative half-wavelengths of the MOTE output voltages are formed (see Fig. 3), having a difference of up to 38 % according to the results of the experiment (Fig. 4, *a*). This leads to a decrease in the linearity of the transfer function when simulating the measurement of angular velocity, which requires the introduction of compensating effects. The sensitivity of MOTE to periodic changes in the gap remains approximately the same due to the compensation of the decrease in sensitivity for a positive half-wave with its increase for a negative half-wave.

A comparison was made of experimental and theoretical data on the transfer function of the piezoelectric transducer for various signals of wave generator and initial gaps (Fig. 4, *b*).

(*a*)   (*b*)
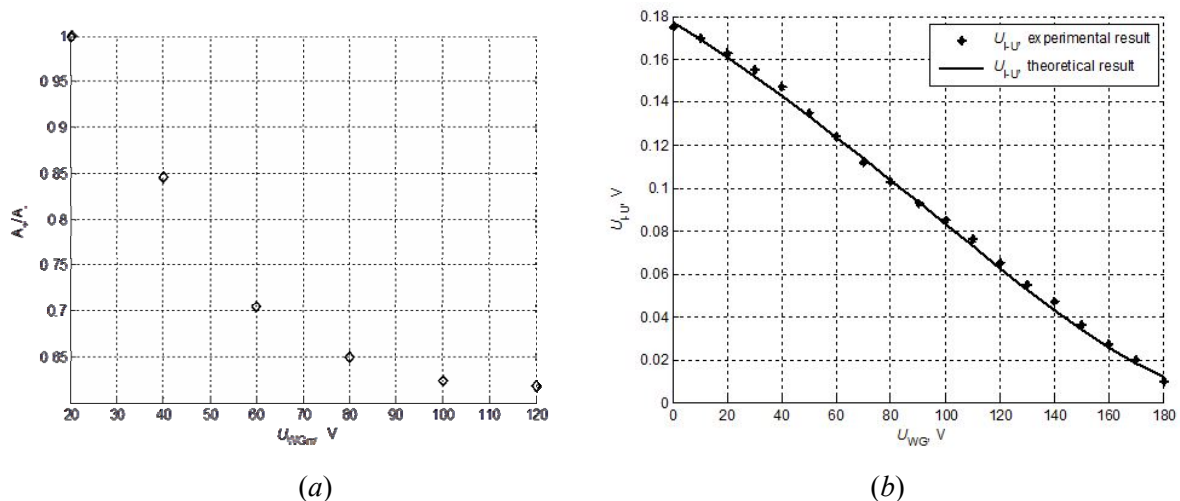
Figure 4. The ratio of the amplitude of the positive and negative half-waves $U_{WG\,m}$ (*a*); comparison of theoretical calculations and experimental investigation of the information retrieval module based on the optical tunneling effect (*b*)

A comparison of theoretical calculations and experimental studies shows that the use of theoretical dependences in the calculation of transducers based on the optical tunnel effect gives good agreement with the experimental data.

CONCLUSION

A theoretical investigation of the transfer function based on the optical tunneling effect using the module "prism - medium - surface of the simulator of the edge of the ring resonator" is described. A scheme for the experimental investigation of the MOTE transformation function is described, which provides the realization of optical information retrieval module in measuring the angular velocity. The results of an experimental investigation of an optical information pickup site with various wave generator signals show good agreement with the theoretical model of MOTE and a small change in sensitivity with increasing angular velocity and amplitude of displacements of the resonator edge simulator, which should be compensated for when forming the output signal.

V. I. Busurin, A. V. Kazaryan, Yin Naing Win, K. A. Korobkov
"Experimental investigation of the characteristics of the information sensing module based on the
optical tunneling effect of the angular velocity transducer by using a piezoelectric module"

References

1. Udd, E., & Spillman, W. B. Jr. (Eds.) (2011). *Fiber optic sensors: An introduction for engineers and scientists* (2nd ed.). New Jersey : John Wiley & Sons, Incp.

2. Xia, D., Yu, C., & Kong, L. (2014). The development of micromachined gyroscope structure and circuitry technology. *Sensors, 14,* 1394–1473. doi: 10.3390/s140101394.

3. Gallacher, B. J., Burdess, J. S., & Harris, A. J.(2001) Principles of a three-axis vibrating gyroscope. *IEEE Transactions on Aerospace and Electronic Systems, 37*, 1333–1343. doi: 10.1109/7.976969.

4. Busurin, V. I., Korobkov, V. V., & Win, Yin Naing. (2017). Issledovaniye vliyaniya parametrov kol'tsevogo rezonatora na kharakteristiki tryokhosevogo optoelektronnogo preobrazovatelya uglovoy skorosti [Investigation of the ring resonator parameters influence on the characteristics of the three-axis optoelectronic angular velocity transducer]. *Doklady TUSUR [Proceedings of TUSUR], 20*(4), 43-49. doi: 10.21293/1818-0442-2017-20-4-43-49. (in Russian).

5. Dennis, D. (Ed.). (1998). *Fiber optic test and measurement.* Prentice-Hall PRT.

6. Fraden, J. (2010). *Handbook of modern sensors: Physics, designs and applications* (4th ed.). New York : Springer-Verlag. doi: 10.1007/978-1-4419-6466-3.

7. Nash, W. A., & Potter, M. C. (2011). Schaum's outline of strength of materials (5th ed.). New York : The McGraw-Hill Companies, Inc.

8. Kostsov, E. G. (2009). Status and prospects of micro- and nanoelectromechanics. *Optoelectronics, Instrumentation and Data Processing, 45,* 189–226. doi: 10.3103/S8756699009030017.

9. Busurin, V. I., Win, Yin Naing, & Zheglov, M. A. (2019). Effect of linear acceleration on the characteristics of an optoelectronic ring transducer of angular velocity and its compensation. *Optoelectronics, Instrumentation and Data Processing, 55*, 309–316. doi: 10.3103/S8756699019030142.

10. Evstifeev, M. I., Kovalev, A. S., & Eliseev, D. P. (2014). Electromechanical model of RR type MEMS gyro with consideration for the platform vibrations. *Gyroscopy and Navigation, 5*, 174–180. doi: 10.1134/S2075108714030043.

11. He C., Zhao Q., Huang Q., Liu D., Yang Z., Zhang D., & Yan G. (2015).A MEMS vibratory gyroscope with real-time mode-matching and robust control for the sense mode. IEEE Sens. J. 15:2069–2077. doi: 10.1109/JSEN.2014.2371456.

12. Cheng Li, Bo Yang, Xin Guo, & Lei Wu.(2019). A Digital Calibration Technique of MEMS Gyroscope for Closed-Loop Mode-Matching Control. Micromachines (Basel). 2019 Jul 25;10(8). pii: E496. doi: 10.3390/mi10080496.

13. Busurin, V. I., Korobkov, V. V., Lwin, Naing Htoo, & Tuan, Phan Anh. (2016). Static and dynamic characteristics of angular velocity and acceleration transducers based on optical tunneling effect. *Journal of Physics: Conference Series, 737*, 012045. doi: 10.1088/1742-6596/737/1/012045.

14. Ovchinnikova, N., Panferov, A., Ponomarev, V., & Severov, L. (2014). Control of vibrations in a micromechanical gyroscope using inertia properties of standing elastic waves. In: *Preprints of the 19th World Congress "The International Federation of Automatic Control"* (pp. 2679–2684). Cape Town, South Africa: IFAC.

15. Busurin, V. I., Gorshkov, B. G., Gorshkov, G. B., Grinshtein, M. L., & Taranov, M. A. (2017). A factor limiting the accuracy of optical loss measurements in single-mode fibres: 'frozen-in' inhomogeneities of the Rayleigh backscatter coefficient. *Quantum Electronics, 47,* 83–86. doi: 10.1070/QEL16201

16. Evstifeev M.I., & Eliseev D.P. (2016). Mathematical model of RR-type micromechanical gyro capacitive comb-type sensors with account for vibrations. *Scientific and Technical Journal of Information Technologies, Mechanics and Optics*, Vol. 16, No. 3, pp. 541–549.

17. Evstifeev M.I., Eliseev D.P., & Chelpanov I.B. (2015). Enhancing the mechanical resistance of micromechanical gyros. *Gyroscopy and Navigation*, Vol. 6, No. 2, pp. 115–122. doi: 10.1134/S2075108715020042

18. Geen J. (2004). Progress in integrated gyroscopes. *IEEE Aerospace and Electronic Systems Magazine,* Vol. 19, No. 11, pp. 12–17. doi: 10.1109/MAES.2004.1365660

19. Busurin, V. I., & Tuan, P. A. (2016). Micro-opto-electro-mechanical angular velocity transducer based on the optical tunneling effect. *Optoelectronics, Instrumentation and Data Processing, 52,* 210–215. doi: 10.3103/S8756699016020151.

20. Busurin, V. I., Korobkov, V. V., & Yin Naing Win.(2016). Investigation of Characteristics of the Optoelectronic Ring Wave Angular Velocity Transducer. *Merhatronika, Avtomatizatsiya, Upravlenie, Vol.17, no 5, pp.* 340–346. doi: 10.17587/mau/16.340-346.

A Unified Ontology Namespace
for Enterprise Integration – a Digital Twin Case Study

Joe David [1], Antti Martikkala [1], Andrei Lobov [1, 2], Minna Lanz [1]

[1] Automation Technology and Mechanical Engineering Unit, Tampere University, Tampere, Finland
E-mail: {joe.david, andrei.lobov, minna.lanz}@tuni.fi
[2] Mechanical and Industrial Engineering, Norwegian University of Science and Technology,
Trondheim, Norway
E-mail: andrei.lobov@ntnu.no

Abstract. In order to be able to scale business enterprises and digitally transform them, we need to be able to readily integrate business data. Traditional systems have business data travelling through different layers of the automation stack vertically. This study presents an architecture that employs a unified ontology namespace for integration of business data. Such an architecture is thought to enhance transparency and visibility easing integrations. A use-case exploiting such an architecture with web-services is presented to convey the ease at which different applications, such as a digital twin, can be "plugged in" to realize further business potential of enterprises.

INTRODUCTION

Product Lifecycle Management (PLM), Enterprise Resource Planning (ERP) and Manufacturing Execution Systems (MES) have been the cornerstones of many (manufacturing) industries for decades but they have traditionally functioned as distinct and disparate systems coupled by means of proprietary protocols that prevent data from freely flowing across them. In order to obtain the best product in each level of the stack, often enterprises make use of different vendors at each level that have been implemented in completely different platforms and their convergence would generally take place only by means of software API integration done by software experts.

Fig. 1 shows the automation pyramid based on the standard that depicts the various level of automation in a factory. It constitutes of the following levels:

– **Level 0** is the field level contains the field devices, i.e. sensors that senses an event or measures one or more input variables and actuators that manipulate variables.

– **Level 1** is the control level that consists of programmable logic controllers (PLCs) or distributed control systems (DCS). They take in the information from the field layer to act upon them, make decisions based on programmed logic and pass back the outputs to the field layer.

 – **Level 2** is the supervisory level that primarily uses supervisory control and data acquisition (SCADA) systems and other human machine interfaces (HMIs). Operators make use of these systems to monitor and control process data which may be stored in databases.

 – **Level 3** is the planning level that constitutes mainly of the manufacturing execution systems (MES) that monitors the manufacturing processes in the plant that transforms products from its raw form to finished goods.

 – **Level 4** is the business planning and logistics level that comprises mainly of the enterprise resource planning (ERP) systems that is a suite of computer applications to monitor business processes such as purchasing, sales, finance and payroll among others.
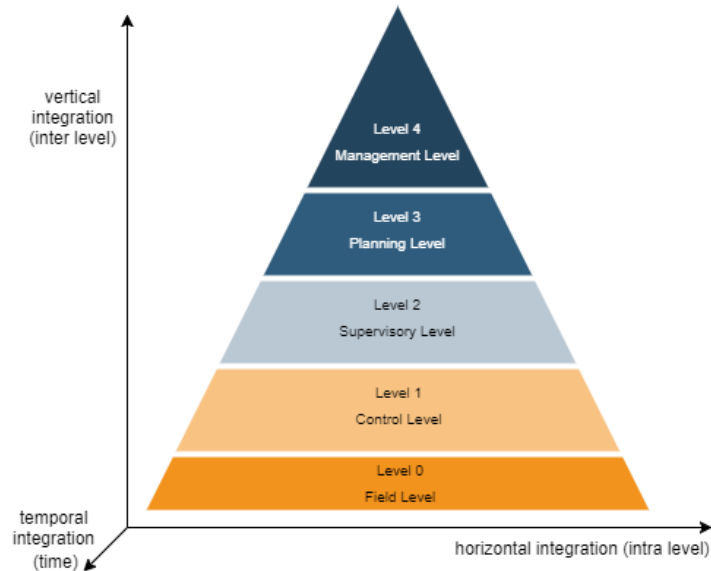
Figure 1. The Automation Pyramid

Integration in automation can take place along three directions, namely horizontal, vertical and temporal (longitudinal) (Sauter, 2005). Horizontal integration refers to the integration that takes place within each level (intra-level), vertical integration takes place along different levels (inter-level) and temporal integration takes place along the lifecycle of the plant.

To attain the holy grail of tri-system integration (PLM, ERP, MES), this paper envisions an architecture that publishes information from each of the layers of the pyramid to common unified knowledge base. Although the architecture allows for horizontal and vertical integration, the focus of the study is on temporal integration. Temporal integration refers to the changes that the automation system undergoes during its life-cycle. The different phases of the life-cycle include design, engineering, commissioning, operation and maintenance. Specifically, we look into reconfiguration of the automation system during operation as a use case. The unified architecture is expected to facilitate data sharing between constituent systems to offer visibility that would help eliminate redundant processes and waste, reduce product delivery times and ensure optimal overall running of the plant.

The remainder of the paper is structured as follows. The next section presents a background on the technologies underpinning the approach undertaken in the study and related work. The approach presents the conceptual architecture. A use-case where a digital twin for PLM is developed for a system that is developed based on the approach is discussed in the case study section. Discussions take place in the subsequent section and are followed by a conclusion where future work is presented.

BACKGROUND AND RELATED WORK

Work undertaken in this study revolves around two main technologies, web services that expose functionalities of applications as services and ontologies by means of which the domain knowledge or the current state of the system is represented. In this paper, the term web services is used loosely and does not necessarily mean connected to web, although this may be the case. It is used synonymous to Application Programming Interface (API) and is used to connote a medium of communication. Clarifying further, applications can make use of the service-oriented architecture using HypeTtext Transfer Protocol (HTTP) in local area networks without be connected to the World Wide Web.

Technologies

Webservices

A Web service is "software system designed to support interoperable machine-to-machine interaction over a network"("Web Services Glossary § Web service, W3C," 2004).Such a generic definition allows for REST architectures to be seen as one and consequently we look into two dominant paradigms in service oriented architectures, REST and the simple object access protocol (SOAP).

SOAP interactions occur with data in the XML format. SOAP web service descriptions are expressed using WSDL, an XML-based standard used to publish service descriptions using ports (service address), port types (operations that can be performed) and bindings (protocol used) (Gudgin et al., 2007). Universal Description, Discovery, and Integration (UDDI) is a standard for describing, publishing and discovering these services.

REST is the abbreviation for representational state transfer. A REST(ful) service is one that is built on a REST architecture that stipulates six architectural constraints (Fielding & Taylor, 2002): Uniform Interface, Stateless, Cacheable, Client-Server, Layered and Code-on-Demand. REST makes use of create, read update and delete (CRUD) operations using HTTP verbs typically on HTTP protocol. Web Application Description Language (WADL) (Haldey, 2009) is typically used to describe RESTful services .

Thus, while SOAP is a protocol that is formally defined using official web standards developed by the World Wide Web Consortium (W3C), a REST service is an architectural style that needs to be followed in order to qualify as a REST service. SOAP uses XML while REST can use a variety of formats including JSON, HTML, XML, etc. As such, SOAP requires more resources and bandwidth, while REST is rather lightweight and requires fewer resources. While SOAP services are mainly function driven, i.e. used for the transfer of structured information, REST services are mainly data driven and used for accessing a resource for data. As far as security of exchanged information is concerned, REST inherits the security features from the underlying transport protocol (HTTP(S)), while SOAP benefits from its own message level security via the WS-Security standard. Thus, REST offers only a faster point-to-point security while the data is being exchanged over the wire while SOAP offers a reliable end-to-end security.

When choosing between the two for a business application the following may be considered:

• **Complexity:** REST is to be used for simpler and faster access to a resource. SOAP's application is different in the sense that it is used mostly when maintaining open stateful connections with a complex client is necessary. REST transactions are stateless and independent of each other.

- **Data formats:** REST services can make use of data in various formats including JSON, CSV, XML, etc. while SOAP is limited to XML. XML is verbose and is less easy to parse than JSON or CSV and can accumulate on computation costs.
- **Standardization and Security:** If standardization is key, SOAP offers support for Web Services specifications. As for security, both support Secure Sockets Layer for point to point protection but SOAP offers WS-Security for end-to-end enterprise level protection.\\
- **Legacy applications:** Legacy systems are another argument in favour of SOAP. REST have gained popularity in recent times and many applications may still have only an implemented SOAP API.

Thus, it can be said that both REST and SOAP make use of different semantics and format to provide similar functionality and operate with separate security concerns.

Ontologies

Ontologies originated in research areas of metaphysics where philosophers used to describe the existence and nature of reality. A simple definition of ontology is that of Agarwal (2005) who states that "an ontology is, therefore, the manifestation of a shared understanding of a domain that is agreed between a number of agents and such agreement facilitates accurate and effective communications of meaning, which in turn leads to other benefits such as interoperability, reuse and sharing".

The rise of the semantic web has seen the emergence of ontology markup languages based on XML, of which Web Ontology Language (OWL), a W3C recommendation ("OWL - Semantic Web Standards"), is the most prominent. Ontologies have since been pursued by many, in various fields and domains to simplify and represent complex, unstructured and heterogeneous information as will be seen in the following section.

Related Work

Existing literature referring to ontology as a representation of manufacturing domain knowledge is plentiful. Specifically for enterprise integration that includes work of Zoubeidi, Kazar, Mesbahi, & Benharzallah, (2014) which presents an architecture towards integration of Enterprise Resource Planning systems (ERP) with a focus on semantic integration based on the context of use. The PABADIS'PROMISE (Diep, Alexakos, & Wagner, 2007) project deals with heterogeneity in a manufacturing environment and presents an interoperability framework based on ontology. Kalogeras, Gialelis, Alexakos, Georgoudakis, & Koubias (2006) present an architecture for vertical integration of the enterprise by using workflows to represent enterprise processes.

Different approaches to formalizing ontologies can be found as well. Nach & Lejeune, (2008) present an ontology that supports the ERPs for SMEs. A generic ontology for resources in an enterprise formulated from competency questions have has been presented by (Fadel, Fox, & Gruninger, 2002). MASON, a manufacturing upper ontology has been presented by Lemaignan, Siadat, Dantan, & Semenenko (2006).

APPROACH

The automation pyramid presented in the previous section saw a tightly coupled stack of applications that only interacted with applications in the adjacent layers. If for some reason we have to diverge from the traditional flow of information, say for example that we need some information from the ERP system to alert the operators at the SCADA layer, this would

have to flow through the MES system. This would require integrations at both the ERP-MES level and the MES-SCADA level. It is clear to see how the existing architecture is suboptimal. If we consider another scenario, where one would like to deploy an application that would use data from different layers of the stack, this would mean making discrete connections from distinct applications on disparate platforms, which is both time consuming and requires expert intervention.

Topology

Fig. 2 shows the conceptual architecture of the approach taken in this study. It consists of the systems that constitute the automation pyramid in Fig. 1. However, it takes the form of a star topology as opposed to the vertical stack. The central component is the domain ontology that each of the systems update to maintain a comprehensive updated knowledge model of the plant.
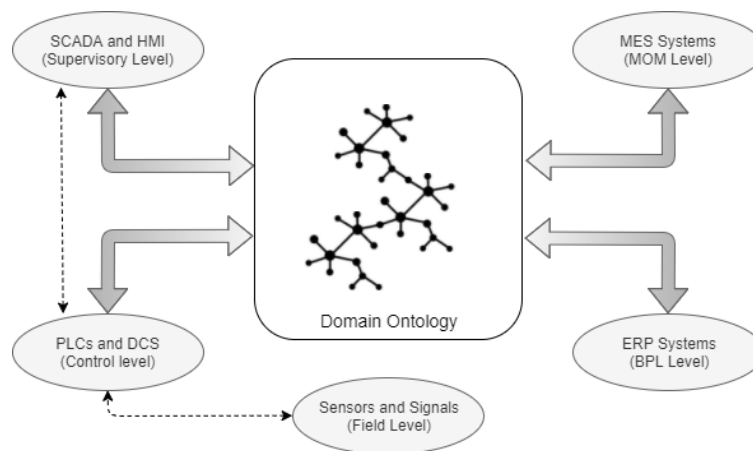
Figure 2. Conceptual Architecture

Discrete connections may still exist between these systems. For example, time critical applications may necessitate discrete connections from the field sensors and the control layer for real-time decision making based on programmed logic. This could be via any industrial (fieldbus) protocols, Profibus for example.

In some cases, especially in the case of legacy systems, the domain ontology acts as a knowledge base in addition to the existing vertical stack and does not replace it. This can be thought of as a generalization of the first point.

Information Interchange

Interaction of heterogeneous systems on disparate platforms requires standardized interfaces that foster information exchange between them and the unified knowledge base. Web services for long have provided just this interoperability is an obvious choice in the undertaken approach. There are mainly two kind of web services; web services that employs the simple object access protocol (SOAP) and RESTful web services, the relevant details of which was discussed in the previous section. We make use of both depending on the application requirements.

SOAP is to be used for applications where security is of prime importance or in cases where the endpoint under consideration is already implemented in SOAP. These include applications at the enterprise level such as payment gateways in financial services, customer re-

lationship management (CRM) systems, etc. REST is to be used for applications where efficiency involving a lightweight architecture is needed or where the endpoint of the application is a RESTful one. This would be in the case of field devices, or devices in the control (PLCs) and supervisory layer (SCADA Systems).

Knowledge Representation

Domain knowledge is represented using ontologies introduced in the earlier section. Fig. 3 shows the relationships between classes (entities) in the ontology. They are associated by means of need-feed relationships that exist between them. Here the relationship need takes the meaning of requires while feed relationships can be viewed as supply with or produces.

The Resource entity: A resource is any object that plays a role with respect to an activity (Fadel et al., 2002). As such, resources could be equipments such as work centers that process products, humans that perform activities that require human intervention such as loading of pallets, maintenance, electricity required to operate equipments, etc.

The product entity: A product is the produce of the production system or line obtained via the transformation of raw goods.

The process entity: The transformation of raw goods to products takes place by the

Figure 3. Relationship between entities constituting the ontology

means of processes. The ontology developed is available online[1]. It must be noted that object and data property axioms are included for illustrtation purposes only. Those axioms are automatically created during runtime depending on the response from the production systems during runtime.

USE CASE – DIGITAL TWIN FOR PLM

This section presents an example of a use-case that utilizes the architecture described in the section III. The use-case is that of a digital twin of a production system that interacts with the domain knowledge to facilitate product lifecycle management functions.

Architecture

The conceptual architecture of the use-case is depicted in Fig. 4. It consists of a production system interfaced with a RESTful interface and its description which is stored in a WADL document that is made available for necessary integrations. A knowledge broker exists which acts as an intermediary between the source of the information in the production system and its ontological representation as the domain knowledge and consists of a web service discovery component and an ontology broker. It performs two basic functions: (1) Translation and transformation of necessary knowledge to be stored in the unified ontology namespace and (2) Discovery of web services to be able to perform the previous function. The knowledge base is developed in OWL remains synchronized with the current state of the production system with the help of the knowledge broker. The digital twin utilizes a SPARQL wrapper to query the knowledge base.

---

[1] https://github.com/joedavid91/unifiednamespace
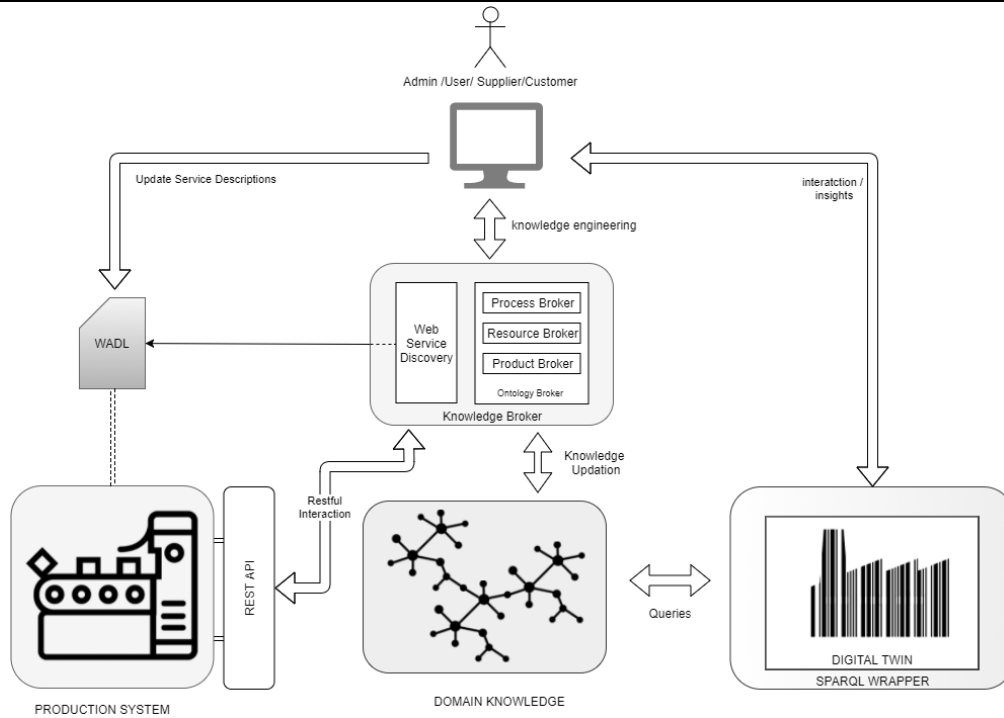
Figure 4. Realized Digital Twin Architecture

Implementation

The production line is that of a Flexible Manufacturing System (FMS), the specifics of which are introduced in an earlier work (David, Lobov, & Lanz, 2018). The system consists of components typical of an FM system such as machining centers, loading and material stations, washing machines, crane and its associated storage. The knowledge broker is a software component developed in python using libraries *urlib2* for the restful requests, *rdflib* to express the information in RDF, *wadllib* for the discovery of services. The knowledge base is developed using Protégé, an open source ontology editor and expressed in the Resource Description Framework. The domain knowledge can either exist as a file or can be served via HTTP via a Jena Fuseki Server implementing a SPARQL endpoint. The digital twin is developed using the software Visual Components, a leading developer of 3D simulation software for manufacturing. One of key concepts underlying the development of the digital twin is the separation of concerns by developing modular components. Each of the components exist independently and have a description of itself that is made available by its manufacturer in the XML format. The description contains all specifications of the component and describes it in its entirety. For example, a machining centre has information such as the PLC parameters, Pallet Changer parameters, Address parameters, Tool parameters, NC program parameters among a lot of others. The digital twin uses these specs from the domain knowledge to initialize the components in its 3D world. The digital twin behaviors are also implemented in python in Visual Components and makes use of the *SPARQLWrapper* python library to be able to query the domain knowledge. Thus, although the knowledge is centralized the intelligence is distributed.

Case Study

As a particular scenario, we examine a case that allows for automatic re-configuration of production systems during commissioning and operation and demonstrate how the architec-

ture envisioned in the earlier section allows for it. It must be noted that, the intention is not to deal with spontaneous dynamic networks at the protocol level but show that the digital twin can make use of such an architecture to incorporate dynamic networks.

The devices registered in the production line are made available in a device discovery API exposed through the REST interface. This service is discovered by the WS discovery component of the knowledge broker and the domain knowledge is updated accordingly. Fig. 5*a* shows the REST request and response from a third-party REST client. Similarly, the location coordinates of the devices are made available in a device data API exposed through the REST interface which is updated in the domain knowledge via the knowledge broker. The domain knowledge that exists in the resource description (RDF) format is updated by the knowledge broker simultaneously (Fig. 5*b*). The knowledge base in itself can be considered as a "raw" digital twin with potent information. The digital twin queries the domain knowledge base via SPARQL, an RDF query language. A sample query that initializes the components of the digital twin and locates them in the layout is shown in Fig. 5*c*. The digital twin (Fig. 6) makes use of this and a host of other information in the same manner to function and provide value to the entire business enterprise.

(a)

(b)

(c)

Figure 5. (*a*) Example RESTful information exchanged between Knowledge Broker and Production System (*b*) Machining Centre Description stored in RDF format in the Domain Ontology (c) SPARQL query to obtain coordinates of the devices in the production system

Figure 6. Digital Twin

DISCUSSION AND CONCLUSION

As the digitalization of the manufacturing enterprises gains momentum, the integration of its systems is considered to play a crucial role. By closing the loop between the ERP, MES and PLM the domain knowledge facilitates just this and the central repertoire of domain knowledge offers visibility and access that would help streamline manufacturing operations and help reduce redundant communication.

The use case presented a digital twin that exploits the architecture presented in the approach section. The use of an ontology expressed in OWL to represent domain knowledge can be justified by the fact that it offers high level of expressivity while allowing to model complex constructs typical of manufacturing systems. Inference of new knowledge (not in use-case) based on existing knowledge can also take place via inference engines using rule languages such as SWRL. Serializing it as RDF/XML helps existing and inferred knowledge to be queried by query languages such as SPARQL. The use of webservices further helps encapsulate business functionality while taking care of security concerns.

Moreover, such an architecture can have several other advantages. It provides scalability. As the physical asset scales, only the description of the services needs to be added or modified. If the scaling involves just increase in the quantity of existing components, the architecture allows for automatic discovery and updation in the domain knowledge. The knowledge broker further allows for easy access of all information stored in the knowledge base to any administrator or other users such as customers or suppliers.

With the data going vertically from the business planning and logistics system, to the field level we miss a big opportunity. Rather having a unified namespace for data across a common data model simplifies scalability and eliminates one-off integrations. Being able to "plug-in" applications and allowing applications to consumer necessary data greatly enhances the factories ability to adapt to change and maintenance, a key necessity for the factory of tomorrow.

REFERENCES

1. Agarwal, P. (2005). Ontological considerations in GIScience. *International Journal of Geographical Information Science, 19*(5), 501–536. doi: 10.1080/13658810500032321.

2. David, J., Lobov, A., & Lanz, M. (2018). Leveraging digital twins for assisted learning of flexible manufacturing systems. In: *2018 IEEE 16th International Conference on Industrial Informatics (INDIN)* (pp. 529–535). doi: 10.1109/INDIN.2018.8472083.

3. Diep, D., Alexakos, C., & Wagner, T. (2007). An ontology-based interoperability framework for distributed manufacturing control. In: *IEEE International Conference on Emerging Technologies and Factory Automation, ETFA* (pp. 855–862). doi: 10.1109/EFTA.2007.4416869.

4. Fadel, F. G., Fox, M. S., & Gruninger, M. (2002). A generic enterprise resource ontology. In: *Proceedings of 3rd IEEE Workshop on Enabling Technologies: Infrastructure for Collaborative Enterprises* (pp. 117–128). doi: 10.1109/enabl.1994.330496.

5. Fielding, R. T., & Taylor, R. N. (2002). Principled design of the modern Web architecture. *ACM Transactions on Internet Technology, 2*(2), 115–150. doi: 10.1145/514183.514185.

6. Gudgin, M., Hadley, M., Mendelsohn, N., Moreau, J.-J., Nielsen, H. F., Karmarkar, A., & Lafon, Y. (2007). *SOAP Version 1.2 Part 1: Messaging Framework (Second Edition).* Retrieved July 22, 2019, from https://www.w3.org/TR/soap12-part1/

7. Haldey, M. (2009). *Web Application Description Language: W3C Member Submission 31 August 2009.* Retrieved from https://www.w3.org/Submission/wadl/

8. Kalogeras, A. P., Gialelis, J. V, Alexakos, C. E., Georgoudakis, M. J., & Koubias, S. A. (2006). Vertical integration of enterprise industrial systems utilizing web services. *IEEE Transactions on Industrial Informatics, 2*(2), 120–128. doi: 10.1109/TII.2006.875507.

9. Lemaignan, S., Siadat, A., Dantan, J. Y., & Semenenko, A. (2006). MASON: A proposal for an ontology of manufacturing domain. In: *IEEE Workshop on Distributed Intelligent Systems: Collective Intelligence and Its Applications (DIS'06)* (pp. 195–200). doi: 10.1109/DIS.2006.48.

10. Nach, H., & Lejeune, A. (2008). Implementing ERP in SMEs: Towards an ontology supporting managerial decisions. In: *2008 International MCETECH Conference on e-Technologies (mcetech 2008)* (pp. 223–226). doi: 10.1109/MCETECH.2008.11.

11. OWL – Semantic Web Standards. (n.d.). Retrieved July 22, 2019, from https://www.w3.org/OWL/

12. Sauter, T. (2005). Integration aspects in automation – a technology survey. In: *2005 IEEE Conference on Emerging Technologies and Factory Automation* (Vol. 2, pp. 9–263). doi: 10.1109/ETFA.2005.1612688.

13. Web Services Glossary § Web service, W3C. (2004). Retrieved July 21, 2019, from https://www.w3.org/TR/2004/NOTE-ws-gloss-20040211/#webservice

14. Zoubeidi, M., Kazar, O., Mesbahi, N., & Benharzallah, S. (2014). Toward an architecture for the semantic integration in enterprise resource planning. In: *2014 International Workshop on Advanced Information Systems for Enterprises, IWAISE 2014* (pp. 45–50). doi: 10.1109/IWAISE.2014.10.

Sensorless Control of Commutation Winding Low-Power Brushless DC Motor Based on the Use of Back-EMF

V. Enin [1], A. Stepanov [2]

Chair "Electrical engineering and industrial electronical", Bauman Moscow State Technical University, Moscow, Russian Federation
E-mail: [1] enin@bmstu.ru, [2] stepanov.bmstu@gmail.com

Abstract. The method of sensorless control of switching of windings of three-section BLDC motor with permanent magnets based on calculation of back-EMF of rotation is proposed. After converting the equations of the three-section BLDC motor to a two-phase system, the switching moments of the windings are determined. Switching moments are calculated using a function representing the ratio of back-EMF rotations computed for a two-phase system. In these moments back-EMF of the turned off and turned on sections are equal. Using this function, signals are generated to control the transistors of inverter. We consider a BLDC motor with a trapezoidal back-EMF of rotation, which is approximated by a piecewise linear function and an inscribed ellipse. Modeling of three-section BLDC using the proposed method of sensorless control of switching windings confirmed the effectiveness of the method and the possibility of its use in a wide range of rotor speeds.

Keywords: brushless DC motor, sensorless control, back–EMF, approximation, simulation.

INTRODUCTION

In a number of areas of technology and industry: instrumentation, control systems and navigation of aircrafts, because of its compactness, reliability and low prices, sensorless electrical drive, in particular to brushless DC motors, find incrasing use. The works [1–7] are devoted to design and control of the electric drive systems with brushless motors. The widespread use of BLDC in the industry is associated with the development of power electronics and semiconductor technologies, which led to the creation of a new element base of intelligent integrated circuits. Such integrated circuits contain not only power electronic components (diodes, transistors), but also power element control devices – drivers. The keys are traditionally controlled by signals from the rotor position sensor (SPR). The use of the rotor position sensor complicates the design of the motor, increases the price and reduces its reliability, since the operation of the sensor is influenced by external environmental conditions: temperature, humidity, vibration, smoke, radiation. The other approach is based on intensively investigated in recent time methods of sensorless control of commutation of the BLDC motors. Most of the research on the development of sensorless control of switching windings of BLDC motors

is based on the calculation of the back-EMF of rotation or flux coupling of the motor windings, which are calculated by switching signals for the inverter. When using back-EMF, which is calculated from the voltage at the terminals of the electric motor and the current in the motor windings, the rotor position is determined by the intersection of zero back-EMF rotation [8]. Switching is performed after passing the back-EMF rotation through zero. The error of determining the moment of switching of the sections of the plug can result in unreliable operation, especially at high speeds of rotation of the rotor. In this regard, a number of works are devoted to the development of methods for correcting the error of switching moments of motor sections. In [8] the method of back-EMF rotation is developed for non-ideal back-EMF and an adaptive method of compensation of switching errors based on the analysis of back-EMF at the time of switching on and off the section. Paper [9] proposed a method for improving the accuracy of the switching points using the method of least squares. Sensorless control for brushless DC monor based on the line-to-line back-EMF is proposed in paper [10]. In works [11–12] methods of compensation of an error of determination of the moments of switching of windings taking into account not ideality of back-EMF of rotation are offered. Methods based on the analysis of the back-EMF of rotation have the disadvantage, namely, the back-EMF of rotation depends on speed of rotation of the rotor, which complicates the determination of the moments of switching in a wide range of speeds of rotation of the rotor. In [13–16], a function (called the G-function) is used to determine the commutation point, which is the ratio of the back-EMF of the sections calculated from the current and voltage of the sections. The commutation points are calculated on the basis this function. Impulses are formed, when denominator of the G-function takes the value of zero heresy. The resulting signal contains noise and a high-frequency component generated by the operation of diodes, which is eliminated by the low-frequency filter. The disadvantage of sensorless control methods based on the calculation of back-EMF is the problem of calculation of switching signals at low speed and at a stationary rotor. The strategy of sensorless control at start-up of BLDC at perturbation by loading is proposed in paper [17].

Method improved sensorless control based on a simple compensation algorithm using zero-crossing point signals is proposed in [18]. In paper [19], the analysis of the third harmonic of the back-EMF is used for determining the position of the rotor.

In [20] a method of sensorless control of a two-section brushless DC motor (BLDC) was developed, based on the analysis of a function that does not depend on the speed of rotation and forms pulses at the equality of the back-EMF of rotation of the first and second sections. These pulses are used for switching sections. Despite the large number of works on sensorless control, the problem of reliability and accuracy of determining the switching points, as well as the problem of starting the engine are relevant and require further research.

This paper proposes a method for sensorless switching control of windings of a three-section brushless DC motor. The case of 120 degree switching and connection of windings by a star with an isolated common point is considered. Calculation of switching points is made by converting the equations of electrical equilibrium to a fixed coordinate system α, β.

MATHEMATICAL MODEL OF THREE-SECTION BRUSHLESS DC ELECTRIC MOTOR

The power supply circuit of the windings of a three-section DC brushless motor by an electronic switch on field-effect transistors [1] is shown in Fig. 1. The equations in phase coordinates for the BLDC sections with permanent magnets taking into account of the sections have the form (the case of nonsalient rotor is considered):

$$Ri_a + L\frac{di_a}{dt} + e_a(t) = u_{an}(t), \tag{1}$$

$$Ri_b + L\frac{di_b}{dt} + e_b(t) = u_{bn}(t), \tag{2}$$

$$Ri_c + L\frac{di_c}{dt} + e_c(t) = u_{cn}(t), \tag{3}$$

where R is the active resistance of the winding section of the stator; L is inductance of winding section; u_{an}, u_{bn}, u_{cn} are phase voltage on the windings; i_a, i_b, i_c are currents in the windings of the stator sections; e_a, e_b, e_c – back-EMF of the windings of the stator.

When connecting with a star without a neutral line $i_a + i_b + i_c = 0$. Voltage of winding, if neutral line has not been extracted, is calculated with a use of virtual neutral line. For function back-EMF approximated by the sinusoidal function $e_a + e_b + e_c \approx 0$ is also assumed. Then voltage of winding are equal to

$$u_{an} = (2u_{ab} + u_{bc})/3, \ u_{bn} = (-u_{ab} + u_{bc})/3, \ u_{cn} = (-u_{ab} - 2u_{bc})/3.$$
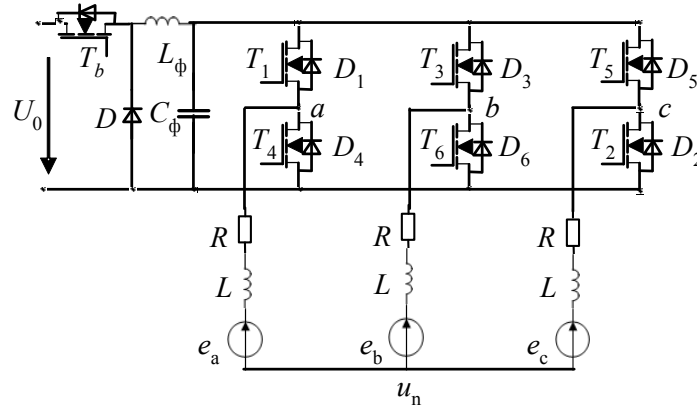
Figure 1. Brushless DC motor drive system

Let us pass from the equations in phase coordinates (1)–(3) to the mathematical model of the machine in a fixed coordinate system α, β on the basis of the transformation

$$u_\alpha = \frac{2}{\sqrt{6}}u_a - \frac{1}{\sqrt{6}}u_b - \frac{1}{\sqrt{6}}u_c, \tag{4}$$

$$u_\beta = \frac{1}{\sqrt{2}}u_b - \frac{1}{\sqrt{2}}u_c. \tag{5}$$

The inverse transition from the coordinates of the state in a fixed coordinate system to phase voltages or currents is based on the inverse transformation

$$u_a = \frac{2}{\sqrt{6}}u_\alpha, \tag{6}$$

$$u_b = -\frac{1}{\sqrt{6}}u_\alpha + \frac{1}{\sqrt{2}}u_\beta, \tag{7}$$

$$u_c = -\frac{1}{\sqrt{6}}u_\alpha - \frac{1}{\sqrt{2}}u_\beta. \tag{8}$$

Transforming the system (1)–(3) with use of (4)–(8), we obtain

$$Ri_\alpha + L\frac{di_\alpha}{dt} + e_\alpha(t) = u_\alpha,$$

$$Ri_\beta + L\frac{di_\beta}{dt} + e_\beta(t) = u_\beta,,$$

where $e_\alpha(t)$, $e_\beta(t)$ are back-EMF sections in the system α, β.

Calculate the back-EMF $e_\alpha(t)$, $e_\beta(t)$ can be as follows

$$e_{ab}(t) = u_a - u_b - R(i_a - i_b) - L\left(\frac{di_a}{dt} - \frac{di_b}{dt}\right),$$

$$e_{bc}(t) = u_b - u_c - R(i_b - i_c) - L\left(\frac{di_b}{dt} - \frac{di_c}{dt}\right),$$

$$e_{ca}(t) = u_c - u_a - R(i_c - i_a) - L\left(\frac{di_c}{dt} - \frac{di_a}{dt}\right),$$

then

$$e_\alpha(t) = \frac{1}{\sqrt{6}}(e_{ab}(t) - e_{ca}(t)),$$

$$e_\beta(t) = \frac{1}{\sqrt{2}}(e_{bc}(t)).$$

Electromagnetic torque in the stationary coordinate system α, β, equal to

$$T = \frac{e_\alpha i_\alpha + e_\beta i_\beta}{\omega_m}$$

where ω_m is the angular velocity of the rotor.

Next, we consider the 120 degree switching sections of the rotor windings, in which two sections operate simultaneously, and one of the sections is disconnected from the source.

Trapezoidal function $\Phi' = d\Phi/d\theta$ (Φ is magnetic flux, $\theta = p\omega_m$ electric angle, ω_m is rotor rotation angle, p is number pair pole) is approximated by piecewise linear function with inscribed ellipse Fig. 2. The approximating function is a continuous function with a continuous derivative, which is its advantage in the simulation and calculation of the back-EMF rotation. The ellipse is described by the equation

$$\frac{\theta^2}{a^2} + \frac{(\Phi' - \Phi'_c)^2}{b^2} = 1,$$

where a, b are the large and small axis of the ellips

$$\Phi'_b = \Phi'_{max} - h.$$

For Fig. 2 denoted by θ_p the period of trapezoidal, function. On the intervals $[-\theta_p/4, \theta_1]$, $[\theta_2, \theta_p/4]$ the dependence is approximated by a linear function, on the interval $[\theta_1, \theta_2]$ the dependence is approximated with an ellipse. Given: Φ'_{max} − maximum value, Φ'_b - value at the boundary of the interval of the function $\Phi'(\theta)$. The angle of inclination of the line at intervals $[-\theta_p/4, \theta_1]$, $[\theta_2, \theta_p/4]$ is determined by the formula $v = \pm (\Phi'_b)/\theta_1$.
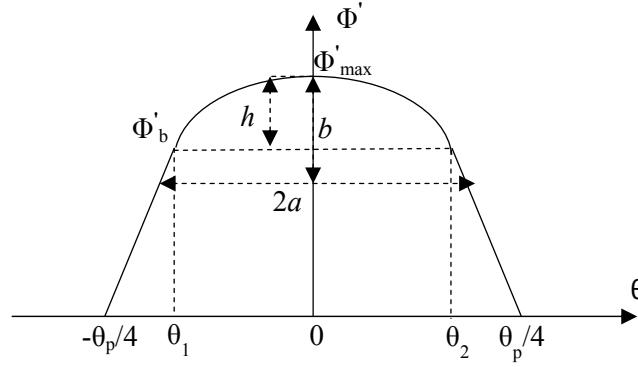
Figure 2. Approximation of the dependence of the back-EMF on the angle of rotation of the rotor

At the point θ_1, the line is tangent to the ellipse, then it must hold

$$v = -\frac{\theta_1 b^2}{a^2(b-h)}.$$

It must also hold

$$(b-h)^2 = b^2\left(1 - \frac{\theta_1^2}{a^2}\right).$$

Then parameters a, b will be equal to

$$b = d1/d2, \tag{9}$$

$$d_1 = h^2 + vh\theta_1, \quad d_2 = v\theta_1 + 2h,$$

$$a = \sqrt{\frac{h_1}{h_2}}, \tag{10}$$

$$h_1 = \theta_1 b^2, \quad h_2 = v(b-h).$$

Setting the angle θ function $\Phi'(\theta)$ on the interval $[\theta_1, \theta_2]$ is calculated by the formula

$$\Phi'(\theta) = \Phi'_{max} - b + \sqrt{b^2(1 - \theta^2/a^2)}, \tag{11}$$

The dependence of the back-EMF sections in relative units expressed using the function $\Phi'(\theta)$ is shown in Fig. 3.

The chosen approximation of the function $\Phi'(\theta)$ is essentially a spline function. On the intervals $[-\theta_p/4, \theta_1]$ and $[\theta_2, \theta_p/4]$ this function $\Phi'(\theta)$ is a linear function of the electrical angle, and the interval $[\theta_1, \theta_2]$ is a nonlinear function of the angle θ. An inscribed ellipse determines the nonlinear function, the parameters are calculated by formulas (9) – (11). The choice of parameters Φ'_b, Φ'_{max}, θ_p, θ_1, θ_2 affects the value of the switching interval and the switching moments of the windings in which the back-EMF of the switched-off and switched-on phase coincides.

The value $h = \Phi'_{max} - \Phi'_b$, $\theta \in [\theta_1, \theta_2]$ determines how much the amplitude of the phase back-EMF differs from the constant. Also, the choice of these parameters can improve the accuracy of the approximation of the magnetic flux and, accordingly, the function $\Phi'(\theta)$ from the electric angle θ. The most widespread in practice is 120^0 degree switching, in which the winding is connected to the source at an interval of 120^0 electric degrees, then disconnected

from the source at an interval of 60^0 electric degrees. The proposed method of approximation will more accurately describe for different types of BLDC the dependence of the back-EMF on the electric angle θ and thus increase the accuracy of determining the switching points.
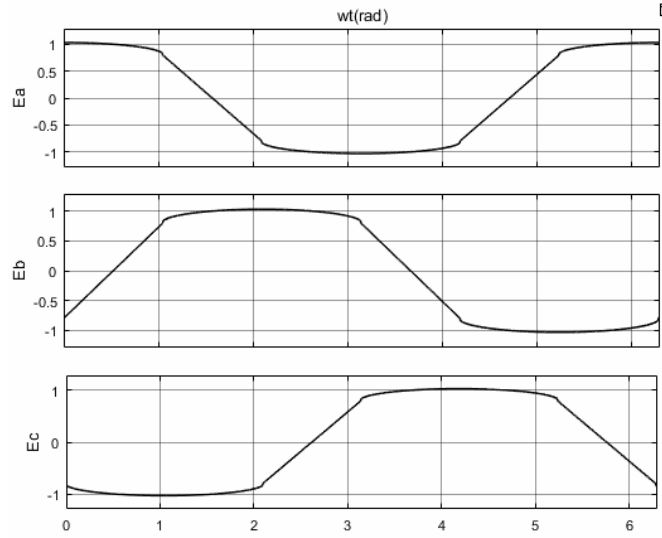
Figure 3. The system is three-phase back-EMF

SENSORLESS COMMUNICATION SECTIONS OF THE BLDC MOTOR IN THE TWO PHASE COORDINATES

Now we consider on 120-degree commutation. The section connected to the source will be called active and back-EMF denoted $e_w(t)$. For section disable, back-EMF is denoted by $e_{on}(t)$. The back-EMF of the section to be switched on at the next switching, is denoted $e_{off}(t)$. Then, the transition to a fixed coordinate system α, β, can be made as follows

$$e_\alpha(t) = \frac{2}{\sqrt{6}} e_w(t) - \frac{1}{\sqrt{6}} e_{on}(t) - \frac{1}{\sqrt{6}} e_{off}(t), \tag{12}$$

$$e_\beta(t) = \frac{1}{\sqrt{2}} e_{on}(t) - \frac{1}{\sqrt{2}} e_{off}(t). \tag{13}$$

When switching sections of the stator windings taking into account (12), (13) we will use a function that represents the ratio of the back-EMF sections of the stator in a fixed coordinate system α, β

$$H(t) = \frac{e_\alpha(t)}{e_\beta(t)}. \tag{14}$$

At the time of switching the back-EMF of the switched section must be equal to the back-EMF of the switched section, at this point the function $H(t)$ (14) takes an infinite value. Then, by setting some threshold value H_t, switching will be performed when the modulo function $H(t)$ exceeds the threshold value. Then the included section with the back-EMF $e_{on}(t)$ is disconnected from the source, and the section disconnected with the back-EMF $e_{off}(t)$ is connected to the output of the voltage source. The next miscomputation the interval is accepted. The pulses generated by the function (14) determine switching moments.

Back-EMF $e_\alpha(t)$, $e_\beta(t)$ contains high-frequency noise generated by PWM, pulses during operation of the inverter keys, which can lead to the erroneous determination of synchronization points. Using a low-pass filter reduces the impact of these factors. The accuracy of the switching moment also depends on the value of the threshold H_t and rotor speed ω_m, sampling rate Δt_d. Increasing the threshold H_t for the formation of the switching signal of the sections increases the accuracy of determining the switching moment, but if the threshold is too large and the rotor speed is high, it can lead to the omission of the synchronization point and disruption of the stable operation of the motor. The calculation of switching moments has the advantage because the ratio of the backi-EMF does not depend on the rotor speed and can be used in a wide range of speeds.

SIMULATION AND EXPERIMENT

To substantiate and study the effectiveness of the proposed algorithm of sensorless control of the valve motor, a simulation of a contactless low-power electric motor of the DLBC type is carried out. The motor is an electric machine with a three-section winding on the stator and a multi-pole rotor with permanent magnets. The number of pairs of poles is 4. The active resistance and inductance of the stator sections are respectively $R = 6.0$ Ohms, $L = 0.00042$ H. The supply voltage of a constant source is 27 V. The sections of the stator windings are connected into a star. The functional scheme of sensorless switching control of the three-section winding is shown in Fig. 4.
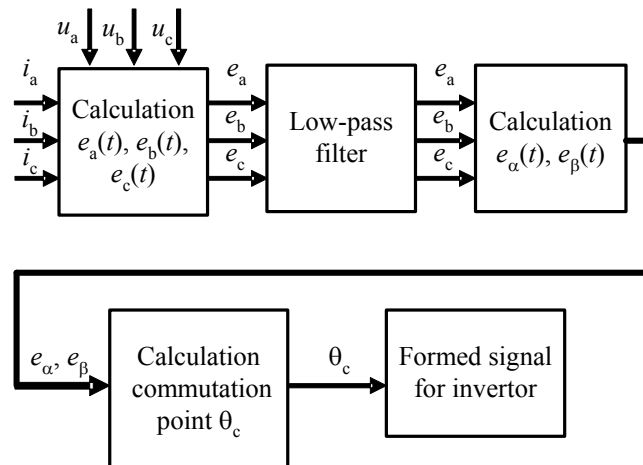
Figure 4. The block diagram for the switching control of the windings BLDC

When the rotor rotates, back-EMF is induced in the stator windings. The back-EMF is calculated from the voltages u_a, u_b, u_c, supplied to the section and section currents i_a, i_b , i_c. Switching of windings is made at equality of back-EMF of rotation of the switched-off and switched-on phase, (120 degree switching is considered). In case of dependence of the back-EMF on time, calculated from the phase voltages and current sections, as a result of the operation of the keys of the power semiconductor invertor pulses occur.

After calculating the back–EMF, these pulses are smoothed by a low-pass filter. By phase back-EMF $e_a(t)$, $e_b(t)$, $e_c(t)$ are calculated back-EMF in a fixed coordinate system $e_\alpha(t)$, $e_\beta(t)$. Back-EMF in a fixed coordinate system are used to determine the switching moments of the windings.

The start-up of BLDC with the subsequent transition to sensorless control of switching of windings was investigated. A direct start of the motor under load was made when switching

signals were supplied in the form of a periodic sequence of rectangular pulses. The pulse period was selected according to the motor parameters. The transition to sensorless control is possible by increasing the motor speed to a value at which the counter-EMF can be isolated from the noisy signal. The time of transition after start-up to sensorless control was set.

Fig. 5 shows the rotation speed, torque and rotation angle of the rotor, the transition to sensorless control was made at $t = 0.01$ s, while the speed after the start increased by ≈ 100 rpm. Fig. 6 shows phase currents.
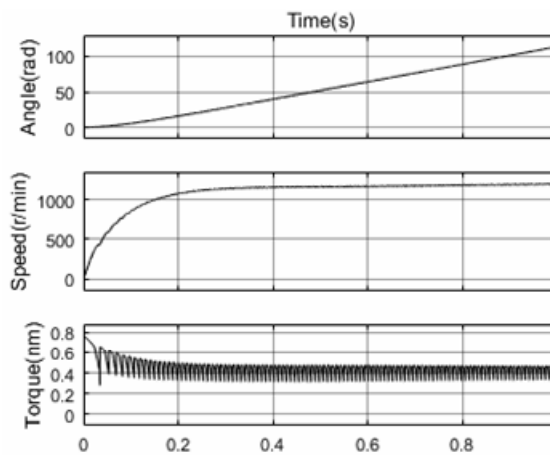
Figure 5. Start and transition to sensorless control
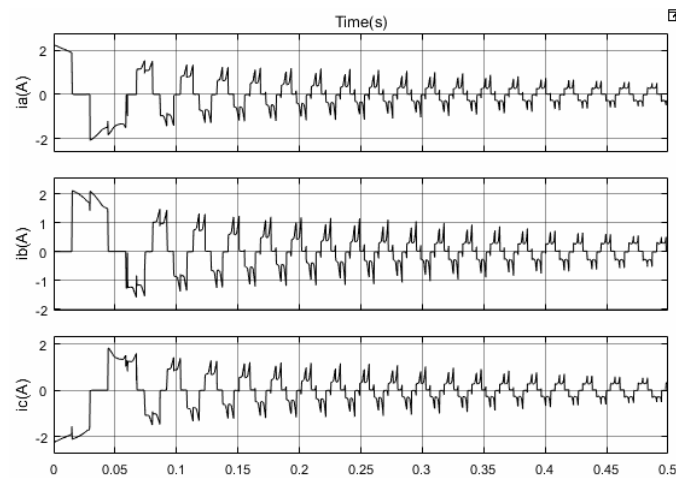
Figure 6. Phase currents in motor windings at start-up and transition to sensorless control

CONCLUSION

This paper proposed a new algorithm for sensorless determination of switching angles three-section brushless DC permanent magnet motor and control power semiconductor invertor. The sensorless control algorithm is based on the transformation of the three-section motor equations to a two-phase system in a fixed coordinate system α, β.

Communication points are determined by a use calculating the back-EMF rotation in a fixed system α, β. The back-EMF are described trapezoidal functions which consists of the piecewise linear functions and the inscribed ellipse. The start–up problem is solved by direct starting of the motor and transition to sensorless control after some delay equal to several periods.

The advantage of the proposed algorithm is the independence of the ratio of the back-EMF sections of the rotor speed, which allows the use of the proposed method in a wide range of speeds.

REFERENCES

1. Arakelyan, A.K., & Afanas'ev, A.A. (2006). Ventil'nyye elektricheskiye mashiny v sistemakh reguliruyemogo elektroprivoda [The rectifier of the electric machine in the systems of electric drive]. In 2 volumes. Moscow : Higher school. (In Russian).

2. Tsatsenkin, V. K. (1991). Bezreduktornyy avtomatizirovannyy elektroprivod s ventil'nymi dvigatelyami [Direct drive automated electric drive with brushless DC motors]. Moscow : MPEI. (In Russian).

3. Belkovsky, A. P., & Tsatsenkin, V. K. (2010). Pretsizionnyy elektroprivod s ventil'nymi dvigatelyami [Precision electric drive with brushless DC motors]. Moscow : MPEI. (In Russian).

4. Zimin, E. N., Katsevich, V. L., & Kozyrev, S. K. (1981). Elektroprivody postoyannogo toka s ventil'nymi preobrazovatelyami [DC electric drives with power converters]. Moscow : Energoizdat. (In Russian).

5. Baranov, M. V., Brodovskiy, V. N., Zimin, A. V., Karzanov, B. N. (2006). Elektricheskiye sledyashchiye privody s momentnym upravleniyem ispolnitel'nymi dvigatelyami [Electric servo actuators with torque in the controlled engines]. Moscow : Bauman Moscow State Technical University. (In Russian).

6. Soloviev, V.A. (2004). Nepreryvnoye tokovoye upravleniye ventil'nymi dvigatelyami [Continuous current control of electric drive]. Moscow : Kosygin MSTU. (In Russian).

7. Ovchinnikov, E., & Lebedev, N. A. (1979). *Beskontaktnyye dvigateli postoyannogo toka [Brushless DC motors]*. Leningrad : Nauka. (In Russian).

8. Halvaei Niasar, A., Vahedi, A., & Moghbelli, H. (2008). A novel position sensorless control of a four-switch, brushless DC motor drive without phase shifter. *IEEE Transactions on Power Electronics, 23,* 3079–3087. doi: 10.1109/tpel.2008.2002084.

9. Guo, R. C., Mu, Z., & Li, J. D. (2017). Research on position sensorless control system of high-speed brushless DC motor. In: *9th International Conference on Intelligent Human-Machine Systems and Cybernetics, 2017* (pp. 62–65). IEEE. doi: 10.1109/IHMSC.2017.21.

10. Liu, G., Cui, C., Wang, K., Han, B., & Zheng, S. (2016). Sensorless control for high-speed brushless DC motor based on the line-to-line back EMF. *IEEE Transactions on Power Electronics, 31,* 4669–4683. doi: 10.1109/TPEL.2014.2328655.

11. Li, H., Zheng, S., & Ren, H. (2017). Self-correction of commutation point for high-speed sensorless BLDC motor with low inductance and nonideal back EMF. *IEEE Transactions on Power Electronics, 32,* 642–651. doi: 10.1109/TPEL.2016.2524632.

12. Li, W., Fang, J., Li, H., & Tang, J. (2016). Position sensorless control without phase shifter for high-speed BLDC motor with low inductance and nonideal back EMF. IEEE Transactions on Power Electronics, 31, 1354–1366. doi: 10.1109/TPEL.2015.2413593.

13. Su, G., McKeever, J. (2004). Low-cost sensorless control of brushless DC motor using a frequency-independent phase shifter. *IEEE Transaction on Power Electronics, 19,* 296–302. doi: 10.1109/TPEL.2003.823174.

14. Chlandy, R., Kosh, C. (2008). Flatness-Based tracking of an electromagnetic VVT actuator with disturbance observer feedforward compensation. *IEEE Transaction on Control System Technology, 16,* 652–663. doi: 10.1109/TCST.2007.912121.

15. Chen, S., Zxou, X., Bai, G., Wang, K., Zhu, L. (2018). Adaptive commutation error compensation strategy based on a flux linkage function for sensorless brushless DC motor drives in a wide speed range. *IEEE Transaction on Power Electronics, 33,* 3752–3764. doi: 10.1109/TPEL.2017.2765355.

16. Chen, S., Liu, G., Zhu, L. (2017). Sensorless control strategy of a 315 kW high-speed BLDC motor based on a speed-independent flux linkage function. *IEEE Transactions on Industrial Electronics, 64,* 8607–8617. doi: 10.1109/TIE.2017.2698373.

17. Liu, G., Chen, S., Zhen, S., Song, X. (2017). Sensorless low-current start-up strategy of 100-kW BLDC motor with small inductance. *IEEE Transactions on Industrial Informatics, 13,* 1131–1140. doi: 10.1109/TII.2016.2607158.

18. Park, J. S., Lee, K. L., Lee, S. G., Kim, W.H. (2019). Unbalanced ZCP compensation method for position sensorless BLDC motor. *IEEE Transactions on Power Electronics, 34,* 3020–3024. doi: 10.1109/TPEL.2018.2868828.

19. Song, X., Han, B., Zheng, S., Fang, J. (2018). High-precision sensorless drive for high-speed BLDC motors based on the virtual third harmonic back-EMF. *IEEE transactions on Power Electronics, 33,* 1528–1540. doi: 10.1109/TPEL.2017.2688478.

20. Enin, V. N., Stepanov, A. V. (2018). The commutation of BLDC motors in sensorless control via EMF of rotation. *Herald of the Bauman Moscow State Technical University, 2018,* 6(123), 87–101. doi: 10.18698/0236-3933-2018-6-87-101. (in Russian).

Solving the Problem of Automated 2D Images Compositional Characteristics Evaluation

F. F. Gazimzyanov [1], M. A. Al Akkad [2]

Computer Science Department, Kalashnikov Izhevsk State Technical University, Izhevsk, Russian Federation
E-mail: [2] aimanakkad@yandex.ru

Abstract. This paper contains an overview of the progress achieved by researchers in solving the problem of evaluating 2D images compositional characteristics. A review of methods potentially suitable for solving such a problem is given, the selected method is justified, and the adaptation of the selected method to a specific task is given. A mathematical model adapted to work with existing models using a new method called Adjusting the Structural Skeleton Coefficients is presented. The structure of the training samples and the special aspects of data collection are described. Data analysis and sorting is performed using a developed genetic algorithm, and the choice of the method is justified. The obtained results are analyzed, and visualization of the compositional parameters of simple scenes, for different groups of respondents identified during data sorting and analysis, is introduced. Finally, the overall results of the research are presented, concluding that they coincide with the suggestion of Arnheim about perception.

Keywords: Structural Skeleton, Image Analysis, Computer Vision, Perception, Genetic Algorithms

1. INTRODUCTION

A general concept of an automated system for evaluating the compositional characteristics of 2D images was developed based on the work of Rudolf Arnheim. A mathematical model [1] for the first chapter of Arnheim's book "Balance" [2] was proposed, which allows obtaining the compositional characteristics of objects located inside the "structural skeleton" of the image.

For the accurate operation of the system, *pF* (perceptive force) coefficients of the structural skeleton should be customized with the peculiarities of human perception. There are no exact values by which a graph of such function could be plotted in the book of Rudolf Arnheim except the value at which the object stands at the source of the structural skeleton. So the system should be configured with human perception data [3].

There are several methods for solving this problem: 1) *Least square method:* The developed mathematical model can be expressed as an equation, and the survey will provide statistics. The least squares method can be applied similarly to the equalization on elements given by Linnik Yu. V. [4] in chapter VIII pp. 203-211. 2) *Gradient descent:* The method is also seen to be usable, since the developed mathematical model of the structural skeleton can be presented as a complex function. The acceptable solutions set of this function can be investi-

gated and we can find the required minimum, at which the parameters of the equation of the structural skeleton would be adjusted in accordance with the human perception [5]. 3) *Artificial neural networks:* It is worth to note that this approach is universal, but maybe redundant in some cases. However, it can be used to solve the problem of selecting coefficients for sources of perceptive forces of the structural skeleton [6, 12]. 4) *The genetic algorithm*: Genetic algorithms and such approaches are used in the training of neural networks, and also they can be an independent optimization method. In this case, we are talking about an independent method. It is also important to note that, despite the fact that genetic algorithms work similar to the gradient descent, they do not require a strict definition of the mathematical model.

To offer machines the ability of aesthetic quality assessment of images a lot of research still need to be made. For assessing photos quality, high-level features were designed [15], the consensus on visual quality was learned for image management [16], for automated albuming and retrieval multidimensional image value assessment and rating was used [17], several visual quality assessment algorithms were investigated [18], an interesting study about aesthetic visual quality assessment of paintings was carried out [11].

2. ADJUSTMENT OF THE MATHEMATICAL MODEL COEFFICIENTS

The genetic approach was selected because it provides a convenient isolated layer of abstraction over existing methods. Moreover, it allows operating with atomic units and fairly simple concepts from genetics to control the learning process. Empirical results of efficiency show incomparably higher efficiency than random solution search [7]. However, of course, such an approach will lose speed in any analytical solution, such as LSM (Least square method) or unconstrained optimization.

2.1. Adjusting the Structural Skeleton Coefficients Method

The principle of DNA functioning, genes transfer from parents to children and directed development of genetic systems is described by Richard Dawkins in his book "The Selfish Gene" [8, pp. 60–94].

The author defines the gene as a carrier of certain genetic information, a feature that, however, has not definite physical boundaries in the sequence of the chromosome. However, in our case we operate with atomic numerical parameters, in the same way they are defined in the computer memory. Therefore, it will be more convenient to identify the concepts of a gene and a cistron, chromosomes regions bounded by certain sequences that designate the beginning and end of a cistron [8, p. 69]. Then accordingly the chromosome is a sequence of genes. A genotype is a specific set of chromosomes, and the concept of a phenotype can be reduced to a combination of genotype and environmental factors.

Now we will apply all this to the tuning of the developed system. Let's turn to the formula:

$$pF_{scene} = \begin{cases} |pF_{dots}| \in [0; e] & | \quad pF_{seg}(pF_{s1}, pF_{s2}...pF_{sN}) \times 2 \\ |pF_{dots}| \notin [0; e] & | \quad pF_{seg}(pF_{s1}, pF_{s2}...pF_{sN}) + pF_{dots}(pF_{d1}, pF_{d2}...pF_{dM}) \end{cases}, \quad (1)$$

where e – the error value at which we consider the influence of point sources of structural plan is equal to zero, pF_{dots} – the influence of point sources of structural plan for the object, pF_{seg} – the influence of line sources of structural plan. While pF_{sN} and pF_{dM} are the settlement functions of the value of the impact of perceptual forces of a certain line or point source of the structural plan on object.

Each pF_s and pF_d can be represented in the context of the genetic algorithm context as a chromosome. In turn, the x parameters from formulas

$$pF_{segs} = \frac{\sum_1^N pF_{sN}\left(d_N, x_{1N}, x_{2N}, \ldots, x_{VN}\right)}{N}, \qquad (2)$$

$$pF_{dots} = \frac{\sum_1^M pF_{dM}\left(d_M, x_{1M}, x_{2M}, \ldots, x_{WM}\right)}{M}, \qquad (3)$$

can be defined as genes, where d is the distance to the center of mass of the object within the structural plan and x is the parameter of the source structural plan function pF. The function is constructed by Akima's spline interpolation [14].

The entire structural skeleton is identical to the genotype.

When we make a set of some initial "genes" or "DNA" for our mathematical model of the structural skeleton, and create "parents", we may get "successors" - models with different variations of pF functions of the structural skeleton. To determine their quality, we need a *fitness* function. We can use formula 1, as well as the polling data and then compare the results of the human estimation and pF_{scene} function. This difference will determine the quality of a certain genes combination. We can get the total difference for all the scenes data from the learning sample derived from the polls. Together with the genotype, the *fitness* function forms a phenotype.

Let's present all of this in a more formal way:

$$gene = x \qquad (4)$$

$$chromosome = \{gene_1, gene_2, \ldots, gene_n\} \qquad (5)$$

$$genotype = \{chromosome_1, chromosome_2, \ldots, chromosome_n\} \qquad (6)$$

$$phenotype = \{genotype, fitness\} \qquad (7)$$

$$fitness = \sum_{n=0}^N | pf_{scene^n}\left(genotype\right) - hE_{scene^n} |, \qquad (8)$$

where *gene,* is the x values of the supporting points of the pF function graph in formulas 2 and 3. While *chromosome, genotype, phenotype, fitness* function, and $pf_{scene^n}\left(genotype\right)$ are the score of a particular scene in formula 1 that were used in the genes of the genotype as the parameters of the pF functions, and hE_{scene^n} is the human estimate.

2.2. Software Implementation

For the software implementation of this method the Jenetics library was selected [7, pp. 60–94]. This library is well documented, developed using the Java Stream API, which allows the full use of hyper-threading JVM, and provides a high level of compatibility with already developed systems that implemented flow control, and allows the use of popular patterns during development [13]. As a format for the declarative description, JSON was chosen[1,2].

---

[1] XML Specifications Page, http://www.xml.com
[2] JSON Specifications Page, http://www.json.org/json-ru.html

One of the minuses is that the library provides immutable entities that may confuse the user who is not familiar with the Builder and Factory patterns [9, p. 89].

3. RESPONDENTS DATA ANALYSIS METHOD

A survey was conducted for obtaining the data. People were asked to rate graphic compositions of the simple geometric objects, like in the first chapter of Rudolf Arnheim book. Amount of 76 compositions was presented in certain forms.

They were printed on A4 sheets in order to identify people's perception of the scenes as accurate as possible, the thing that different sizes and dimensions of computer screens don't offer. For the use of the obtained data, they need to be analyzed to highlight the main trends in the evaluation of certain compositions and to find (or not to find) any patterns among the responses of the questioned people. Obtaining an average estimate is uninformative, since the standard deviation in the estimates was very large. If we look at the distribution of human estimates for each scene, the spectrum of answers, it will be obvious that often in the scenes there are tendencies to different answers, for example, 2 and 5, and finding an average just does not allow to see these features.

This approach allows to obtain interesting learning samples, but if we assume that there are certain taste groups with similar inclinations in the evaluation, which may intersect, finding the mode also will not ensure the representation of all existing conformities. It should be noted that the array of data obtained from interviews can be represented as a three-dimensional plane, a two-dimensional table, where the value in each cell can be interpreted as a height. If we assume that people have common aspirations in the perception of these scenes, smoothing the plane by reversing the rows of a table can group data and allow us to see the necessary dependencies that will allow to adjust the system.

Despite the fact that there is an analytical approach to the problem of smoothing surfaces using sufficient conditions of smoothness [10, p. 71], we have already well configured the system for optimization of a genetic algorithm. Because we haven't the task to obtain the fastest algorithm, we try to sort the data with directional selection. In this case, each chromosome will contain a single gene – ID of a specific line. In addition, all chromosomes must contain a unique set of gene-identifiers, a table row must not be repeated. The Jenetics library [7] provides tools for working with such tasks by using ordered sets and selectors, which leads the enumeration process to recombination, not to crossing-over. The codec allows to obtain the set of identifiers arranged in a certain order from a genotype. We can then build a new version of the table based on this set. The fitness function can work in several ways: we can calculate a sum of absolute differences of the vertical neighboring elements or go through the table by a vertical window, calculating the sum of the average values for each neighboring element. In each case, the smaller result will mean the smoothest surface, and so the people's answers are likely to be grouped by common trends.

The software implementation of such sorting does not differ from the implementation of the optimization of a genetic algorithm mentioned above in section 2.2. "Software implementation". A special type of genes *EnumGene<Integer>* was used, and *PartiallyMatchedCrossover* was used for the crossover, which ensures that each gene will only occur on the chromosome once.

3.1. Results of Respondents Data Analysis

We have analyzed the survey data above mentioned in section 3, which was collected by Google Sheets service as shown in Figure 1, and adjusted using the Jenetics library, and we've

discovered that the most scenes had a tendency to one or two estimates, and only a few did not have a tendency and the answers was evenly distributed. The map built by the modes, is depicted on Figure 3. The result is consistent with Arnheim's experiments described in his book that is shown on Figure 2: the more "stable" areas are the right-hand side of the square, as well as the lower sources of the structural skeleton. The lower right corner is the most stable.
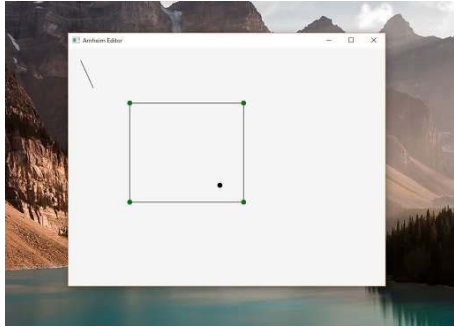

Figure 1. The software environment visual interface
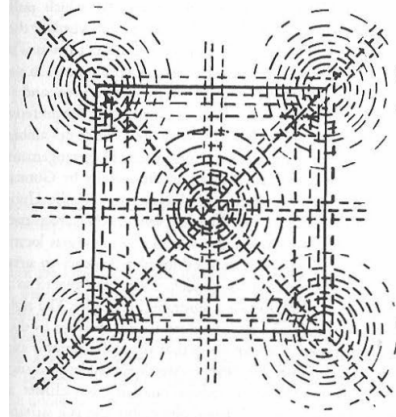

Figure 2. Arnheim's structural skeleton ([2], pp. 13)
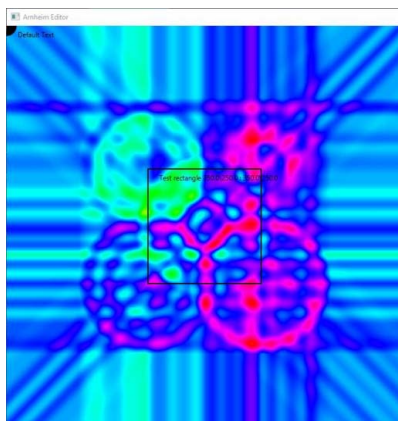

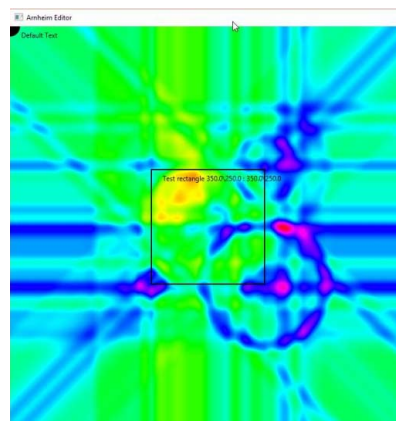**Figure 3.** *pF* map for the modes by all estimates

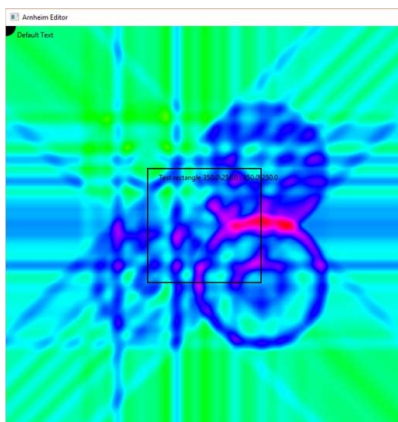**Figure 4.** *pF* map for modes on negative evaluations

Figure 5. *pF* map for modes on neutral evaluations
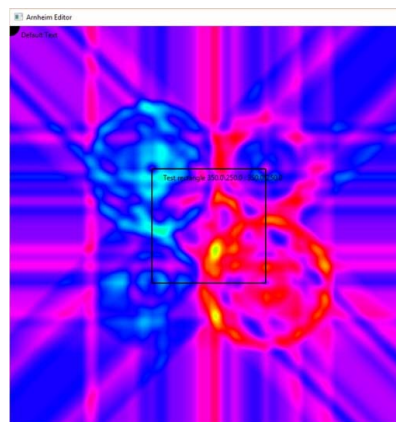
Figure 6. *pF* map for modes on positive evaluations

Also, we can see the predominance in the right and lower parts inside the structural skeleton relatively to the vertical line of symmetry. The visual assumption of the area for the visual center is also shifted to the right lower part. Also results of sorting of all answers are given, with the help of the vertical sum of differences (Figures 4, 5, 6). In the sorted data visually it is possible to allocate groups of people who are inclined to negative (adolescence female artists) and to positive (no clear pattern in this group) estimates.

Also middle-aged men without artistic skills have tendency to more moderate, average estimates. The sorting by the genetic algorithm based on the average value of the estimate in the groups is not informative because of the small number of surveys. Perhaps, more large-scale surveys and additional information about respondents will make it possible to identify the dependencies on average, but the identification of the tendencies seems to be more effective.

If we hold more accurate multivariate analysis, which would allow us to group the results of surveys in a different plane, it would be possible to identify certain "tastes" among people, according to which the system can be configured. This will solve the problem of subjectivity of such systems and methodologies.

4. THE OBTAINED RESULTS AND CONCLUSIONS

We have chosen genetic algorithm as an optimization method and it is an appropriate choice for the research. Besides the overall simplicity of the approach, it turned out to be universal for adjusting the coefficients of the mathematical model, and for sorting data. Analysis of the theoretical values of the mathematical model confirmed that it was a correct representation for the methodology described in Arnheim's book. There is an obvious similarity between the visualized results in his book and the obtained map. Data analysis showed that operating on the mean values in this subject area was not informative.

Finding the mode of the survey's results showed a better representation of the distribution of estimates. Analysis of the responses made it possible to conclude that there were certain trends in people's responses, so the results were sorted by the developed method. System setting according to the survey data and visualization of that field showed that the principles described by Arnheim, manifested even in the analysis of small groups. Created system is ready for more serious data analysis and extension of mathematical models and software tools that will provide more accurate research results.

ACKNOWLEDGMENT

REFERENCES

1. Al Akkad, M. A. & Gazimzyanov, F. (2019). Avtomatizirovannaya sistema otsenki kompozitsionnykh kharakteristik 2D-izobrazheniya: matematicheskaya model' [Automated system for evaluating 2D-image compositional characteristics: mathematical model]. *Intellektual'nye sistemy v proizvodstve [Intelligent Systems in Manufacturing],* 15(2), 105–108. doi: 10.22213/2410-9304-2017-2-105-108 (in Russian).

2. Arnheim, R. (2012). *Iskusstvo i vizual'noe vospriyatie [Art and visual perception].* Moscow, Russia : Arkhitektura-S, 392 pp. (in Russian).

3. Al Akkad, M. A., & Gazimzyanov, F. F. (2019). Avtomatizirovannaya sistema otsenki kompozitsionnykh kharakteristik 2D-izobrazheniya: nastroyka matematicheskoy modeli [Automated system for evaluating 2D-Image compositional characteristics: configuring the mathematical model]. *Intellektual'nye sistemy v proizvodstve [Intelligent Systems in Manufacturing],* 17(1), 26–33. doi: 10.22213/2410-9304-2019-1-26-33. (in Russian).

4. Linnik, Yu. V. (1962). *Metod naimen'shikh kvadratov i osnovy matematiko-statisticheskoi teorii obrabotki nablyudenii [Ordinary least squares and mathematical statistical theory of observational processing basics. 2nd edition].* Moscow, Russia : Gos. izd-vo fiz.-mat. lit. [State publishing house of physical and mathematical literature], 349 pp. (in Russian).

5. Akulich, I. L. (1986*). Matematicheskoe programmirovanie v primerakh i zadachakh [Mathematical programming in examples and exercises].* Moscow, Russia : Vysshaya Shkola [Higher School Publ. House], 319 pp. (in Russian).

6. Korobeinikov, A. V. (2013). *Programmirovanie neironnykh setei [Neural network programming].* Izhevsk, Russia : Publ. House of Izhevsk State Technical University, 44 pp. (in Russian).

7. Wilhelmstötter, F. (2017). *Jenetics library user's manual.* Jenetics. Retrieved from: http://jenetics.io/manual/manual-3.8.0.pdf.

8. Dawkins, R. (2013). *Egoistichnyi gen* [Egoistic gene]. Moscow, Russia : Corpus Publ., 512 pp. (in Russian).

9. Gamma, E., Khelm, R., Dzhonson, R., & Vlissides, D. (2016). *Priemy ob"ektno-orientirovannogo proektirovaniya. Patterny proektirovaniya [Object-oriented design techniques. Design Patterns].* St. Petersburg, Russia : Piter Publ., 366 pp. (in Russian).

10. Poznyak, E. G., & Shishkin, E. V. (1990). *Differentsial'naya geometriya: pervoe znakomstvo [Differential geometry: first acquaintance].* Moscow, Russia: Publ. house of Moscow State University, 384 pp. (in Russian).

11. Li, C., & Chen, T. (2009). Aesthetic visual quality assessment of paintings. *IEEE Journal of Selected Topics in Signal Processing, 3*(2), 236-252. doi: 10.1109/JSTSP.2009.2015077.

12. Zeiler, M. D., & Fergus, R. (2014). Visualizing and understanding convolutional networks. In: *European Conference on Computer Vision,* pp. 818-833. arXiv: 1311.2901.

13. Eckel, B. (2006). *Thinking in Java.* Prentice Hall, 4th edition. 1150 pp.

14. Akima, H. (1970). A new method of interpolation and smooth curve fitting based on local procedures. *Journal of the ACM, 17,* 589–602. doi: 10.1145/321607.321609.

15. Ke, Y., Tang, X., & Jing F. (2006). The design of high-level features for photo quality assessment. In: *IEEE Computer Society Conference on Computer Vision and Pattern Recognition (CVPR'06), 1,* 419–426. doi: 10.1109/CVPR.2006.303.

16. Datta, R., Li, J., & Wang, J. Z. (2007). Learning the consensus on visual quality for next-generation image management. In: *Proceedings of the ACM International Conference on Multimedia* (pp. 533–536). doi: 10.1145/1291233.1291364.

17. Loui, A., Wood, M. D., Scalise, A., & Birkelund, J. (2008). Multidimensional image value assessment and rating for automated albuming and retrieval. In: *15th IEEE International Conference on Image Processing* (pp. 97–100). doi: 10.1109/ICIP.2008.4711700.

18. Moorthy, A. K. & Bovik, A. C. (2011). Visual quality assessment algorithms: what does the future hold? *Multimedia Tools and Applications, 51,* 675–696. doi: 10.1007/s11042-010-0640-x.

The Investigation of Trajectory Control for an Anthropomorphic Manipulator Attached to a Vehicle

I. N. Ibrahim [1], M. A. Al Akkad [2]

[1] Mechatronics Department, Kalashnikov Izhevsk State Technical University, Izhevsk, Russian Federation
E-mail: ibrncfe@gmail.com
[2] Computer Science Department, Kalashnikov Izhevsk State Technical University, Izhevsk, Russian Federation
E-mail: aimanakkad@yandex.ru

Abstract. This paper concentrates on deriving an inverse kinematics solution of a manipulator attached to an aerial vehicle for real-time applications. Analyzing the vehicle's movement itself is not considered. The kinematics solution using Denavit-Hartenberg model was introduced. Adopting the resulted forward kinematics equations of the manipulator, the trajectory planning problem turns into an optimization task. For solving constrained complicated nonlinear functions, shuffled frog leaping search algorithm is suggested to get a global online solution of the design configurations with a weighted objective function subject to some constraints. It is a constrained metaheuristic and population-based approach. Moreover, it is able to solve the inverse kinematics problem considering the mobile platform, in addition to avoiding singularities, since it does not demand the inversion of a Jacobian matrix. Simulation experiments have been carried out for the trajectory planning of a six degree of freedom aerial manipulator, and the obtained results confirmed the feasibility and effectiveness of the suggested method.

Keywords: Inverse Kinematics, Metaheuristics Methods, Evolutionary Algorithms, Optimization Techniques, Shuffled Frog Leaping Algorithm

1. INTRODUCTION

Metaheuristic optimization algorithms are an encouraging alternative to traditional numerical solution methods of inverse kinematics (IK), when working in real-time and precision is required. Furthermore, the linear and dynamic programming techniques usually fail to reach local optimum in solving NP-hard problems with a large number of variables and non-linear objective functions. This paper focuses on population-based heuristic search methods for optimization problems and on memetic algorithms (MAs), where memes propagate themselves in the meme pool by leaping from brain to brain via a process that can be called imitation. This idea can be applied to a robotic agent to use MAs in resolving its movement in the workspace. The solution can be achieved by minimizing an objective function allowing the end-effector to follow the optimal path to avoid singularities and obstacles. A special type of optimization algorithm was developed and deployed for the solving the IK of a humanlike manipulator.

Jacobian-based solutions are identified to scale inadequately with the high number of degrees of freedom [1], in addition to singularities existence. A comparative study of several methods based on the Jacobian matrix [2], clarified that the modified Levenberg-Marquardt method is much better for a large set of random configurations, but may lose convergence compared to Jacobian transpose and pseudocode inverse methods. For solving real-time IK without using the Jacobian matrix, numerical and analytical mathematical tools based on the end-effector position were proposed, but without mentioning the solution time consumption [3]. A similar method for (2n+1) DoF hyper-redundant manipulator arm was also applied [4]. Two methods were combined as a real-time IK solver for a human-like arm manipulator based on closed-form analytical equations for a given position [5]. On-line adaptive strategy based on Lyapunov stability theory, radial basis function network (RBFN) and quadratic programming was proposed, but it requires complex hardware resources [6], the simulation was done for the end-effector position in addition to avoid obstacles and was conducted on the 7-DoF PA-10 robot manipulator. A kinematic and time-optimal trajectory planning was considered for redundant robots, two approaches were presented, joint space decomposition and numerical null-space method for a given pose [7], and were tested by 7-DoF industrial robots, but demanded high time consumption for solving the IK problem. Differential evolution (DE) was explained and proved as one of the most powerful and versatile global numerical optimizers for non-differential and multimodal problems [8], and requires less time and has more robustness in solving the IK problem. Quadratic programming, branching, and a weighted multi-objective function that gave a short-time response of seconds were used [9], while comparative research of four different heuristic optimization algorithms GA, PSO, QPSO and GSA for 4-DoF manipulator in order to reach the target as a position was presented [10]. It was proved that Quantum PSO is the best with average execution time of 1.65 seconds. The performance of many PSO variants was investigated to resolve two DoF IK problems for a given position [11], proving that PSO-VG is the fastest which took less average convergence iterations of 740 for 15 particles. A fitness function was derived and minimized to resolve the pose IK problem based on PSO for multiple DoF up to 180 [12], concluding that the runtime and iterations are 4.22 seconds and 118 respectively for a 9-DoF. A hybrid method called DEMPSO based on DE and Modified PSO algorithms was developed in order to minimize the solution time for the pose, moreover a comparative study for several swarm intelligent optimization algorithms as ABC and ACO algorithms were presented [13]. DEMPSO results showed great advantage concerning execution time for reaching the position similar to the performance of DE for the orientation aim. The simulation was conducted with population size 30 for 10-DoF serial-parallel robot. Comparison of three evolutionary algorithms as GA, PSO, and DE was made [14]. A comparative study of IK solvers for a mobile manipulator using DE algorithm was presented [15], concluding that hybrid DE and biogeography-based optimization called HBBO provides good results but a higher computational cost for weighted fitness function and pose target. In contrast, DE proved to be superior to PSO, CS, and TLBO, additionally verified that the PSO algorithm does not solve the IK problems correctly. A developed methodology was applied on a six-bar mechanism [16], using DE with the geometric centroid of precision positions technique (GCCP). DE was used to improve the design of a fuzzy controller for a wall-following hexapod robot [17]. A modified self-adaptive DE was proposed [18], in order to improve the static force of humanoids robot, showing robust, safe, reliable performance compared with other metaheuristics. An approximation tool for an industrial robot inverse model based on an adaptive neural model optimized by advanced DE was presented [19]. An optimal joint trajectory planning method was proposed using forward kinematics of 7-DoF free-floating space robot based on DE method [20], depicting the general aspect of equality and inequality constraints which govern each joint in the manipulator. Shuf-

fled frog-leaping algorithm SFLA was introduced which is a population-based collaborative search metaphor inspired by natural memes [21]. The effectiveness, suitability, and global optimal resolving have been demonstrated in addition to the short processing time. MSFLA for a high dimensional continuous function optimization was proposed [22]. This method yields strong robustness and best convergence. A comparative study for PSO, SFLA, MSFLA, and MSFLA-EO, designated that MSFLA is better than others, and was assumed for obtaining the optimum preventive maintenance scheduling of generating units in power systems [23]. A comparative study among five evolutionary-based optimization algorithms GA, MA, PSW, ACO, and SFLA was presented [24], showing that SFLA is the best concerning the processing time for solving the F8 function.

In this work, in order to solve the IK of a mobile manipulator the MSFLA algorithm is proposed, which is accurate and has fast convergence in discovering the solution [25], and as an extension of our work in [26][27][28][29]. Initially, we define an objective function to minimize the error between the desired and the actual end-effector pose. The objective function takes into account the minimal movement between the previous and the actual joint configurations. To overcome the constrained problems, we use a penalty function to penalize all those manipulator configurations that violate the allowed joint boundary. Hence, the proposed approach estimates the feasible manipulator configuration needed to reach the desired end-effector pose.

2. MANIPULATOR KINEMATICS

The data in Table 1 represent link parameters of the manipulator's arm-part based on Denavit-Hartenberg (DH) convention in two forms: standard and modified. Whereas the standard simulation form of LabView Robotics module was used, in order to validate the design. Where θ, a, d and α are the joint angle, link length, link offset and link twist between joints. While T_i is the homogeneous transformation matrix between the frames that is a function of θ while the other three parameters are constant. The initial values of θ_i form an input to the IK-solver and are important to define the positions of joints of the manipulator in its initial state. Joints must have a constant offset distance and a variable rotation angle.

Table 1. Link parameters of the manipulator's arm-part.

Standard Denavit Hartenberg				
α_i	a_i [cm]	d_i [cm]	θ_i	Initial Value of θ_i
$-\pi/2$	6.4	0	θ_1	0
0	30.2	0	θ_2	$-\pi/2$
$\pi/2$	0	0	θ_3	$\pi/2$
$\pi/2$	0	23.5	θ_4	0
$-\pi/2$	5.3	0	θ_5	$\pi/2$
0	5.6	-2	θ_6	0

The position of all links of the manipulator's arm-part can be specified with a set of 6 joint variables from the shoulder's joints till wrist's joints as shown in Figure 1. This set of variables is often referred to as a 6×1 joint vector [25]. The space of all joint variables is re-

ferred to as the joint-space $\Theta = \left[\theta_1, \theta_2, \ldots, \theta_6\right]^T$. Here we have been concerned with computing the Cartesian space representation from the knowledge of the joint-space information. Hence the homogeneous transformations of the links were used ${}^{i-1}_i T$. If the robot's joint-position sensors are estimated by servo-mechanisms, the Cartesian position and orientation of the hand-part can be computed by ${}^0_7 T$ [25].
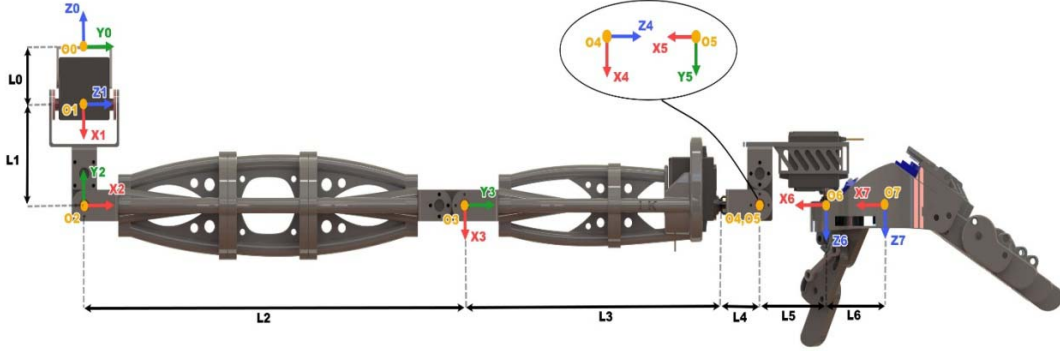
Figure 1. Sketch of the outer shape of the manipulator including its joints and links. It has seven links and six revolute joints in arm-part while the last part is considered as an end-effector of the manipulator and contains 5 fingers. Each joint represents a single DOF

3. PROPOSED OPTIMIZATION TECHNIQUES FOR SOLVING KINEMATICS

The evolutionary optimization algorithms can solve the complicated nonlinear equations completely and efficiently. The solution of the IK for the manipulator is a very difficult problem to obtain by traditional approaches. Besides, the suggested strategies do not require the inversion of any Jacobian matrix, and then it avoids singularities configurations. In this paper, to optimize this problem, the MSFL algorithms is used. This optimization technique is based on the forward kinematics equations, which always produces a solution in cooperation with an objective function. Hence, the general aspect of the problem can be expressed as minimizing $J(\Theta)$, constrained by $\Theta_{\min} \leq \Theta \leq \Theta_{\max}$. Furthermore, the objective function could be defined as the weighted sum of the errors as follows:

$$J(\Theta) = \sigma P_{error}(\Theta) + \varepsilon O_{error}(\Theta) = \sigma \left\| P_G - P_E(\Theta) \right\| + \varepsilon \left\| O_G - O_E(\Theta) \right\|,$$

where $P_{error}(\Theta)$ and $O_{error}(\Theta)$ represent the position and orientation errors respectively and could be computed as a difference in distance between the target and current position, in this work we used an Euclidean formula as a representation of distance. While the parameters σ and ε are the weights of the position and the orientation, respectively. Let $G = (P_G, O_G)$ be a given target end-effector pose while $E(\Theta) = (P_E(\Theta), O_E(\Theta))$ is the current end-effector pose in the workspace corresponding to configuration $\Theta = \left[\theta_1, \theta_2, \ldots, \theta_6\right]^T$ which can be calculated using forward kinematics, where P refers to the 3D position vector of pose while O refers to the vector of Roll-Pitch-Yaw Euler angles of pose (in radians), respectively. Which the optimization algorithms are exploring directly in the configuration space of the manipulator. Each individual $\Theta_i = \left[\theta_{i,1}, \theta_{i,2} \ldots \theta_{i,j} \ldots \theta_{i,6}\right]^T$ represents an ith candidate set of joint angles. At each iteration, we evaluate each candidate configuration Θ_i by passing it

through the forward kinematics module and measuring the position and orientation error between where the end-effector would be at configuration Θ_i and the target end-effector pose. In order to enforce joint limits, each dimension j of element Θ_i should be limited to searching in the range of valid joint angles $\Theta_i \in [\Theta_{min}, \Theta_{max}]$. This can be realized by clamping each dimension j within these bounds at each iteration immediately after it is updated.

4. MODIFIED SHUFFLED FROG-LEAPING ALGORITHM

The SFLA algorithm is inspired by the memetic evolution of frogs exploring food in a lake, which consolidates the benefits of the genetic-based MAs and by the social behavior-based particle swarm optimization [21]. SFLA incorporates: firstly, the evolution process on each memeplex that embraces different cultures of frogs, where the culture stimulates a fitness value, and serves as a local search within memeplex analogous to PSO algorithm, which imitates the social behavior of the leaping action of frogs searching for food. Secondly the influence by the ideas of other frogs from other memeplexes throughout the shuffling rule. This animates the cooperation process which it implies an adaptation idea and improves the success rate of discovering the solution in the optimization puzzle. In this process, a modification was applied to the frog-leaping action that enhances the exploration manner in the space [22][23]. The randomization strategy in the evolution process offers the algorithm the ability to discover the local best solution within search space stochastically in addition to the communication process that possibly finds a global optimum solution in shorter time. The local search and the shuffling processes continue until the defined convergence criteria are satisfied. The pseudocode of the algorithm is presented in Algorithm 1.

Algorithm 1. The pseudo-code of the Shuffled Frog-Leaping Algorithm

---

Initialization:
Population $\leftarrow \{\Theta_1, \Theta_2, \ldots, \Theta_i, \ldots, \Theta_{NP}\}$;

$m \leftarrow number \quad of \quad memeplexes$;

$n \leftarrow quantity \quad of \quad frogs \quad in \quad each \quad memeplex$;

$l \leftarrow 1, iN$

while (*convergence criteria is satisfied Or until met iN*) *do*

    Rank Step: Evaluate each frog Θ_i using a fitness function;

    Partition Step:
    Construct an array U of frogs and their fitness's values;
    Sort the array U in descending order based on the fitness column;
    Construct ($Y^k; k = 1, \ldots, m$) memeplexes each including n frogs;

    Evaluation Step:
    for $\ell \leftarrow 1, iM$ *do*
        for $k \leftarrow 1, m$ *do*
        Determine the worst and best frogs position based on their fitness's values;
        Improve the worst frog position using a leaping distance;
        end for
    end for
    Shuffle Memeplexes Step: combine the evolved memeplexes;
    Check Convergence: Update the population best frog's position Θ_g;
    $\ell \leftarrow \ell + 1$;
end while

The MSFLA meta-heuristic strategy is summarized in the following steps:

a. Initialization: construct the population NP of frogs randomly similar to the first step in DE algorithm, then Select m, and n, where m is the number of memeplexes and n is the number of frogs in each memeplex. The total amount of frogs NP can be calculated as $NP = m.n$, additionally, the ith frog is expressed as a vector with a dimension equal to the configuration space as follows: $\Theta_i = (\theta_{i,1}, \theta_{i,2}, \ldots, \theta_{i,6})$; $i = 1, 2, \ldots, NP$.

b. Rank: compute the performance value f_i for each frog Θ_i. Sort the NP frogs in a descending order according to their fitness. Save them in an array: $U = \{f_i, \Theta_i; i = 1, 2, \ldots, NP\}$, so that $i = 1$ denotes the frog with the best performance value and could save it as a Θ_g in each iteration while the algorithm is running.

c. Partition: partition array U into m memeplexes $Y_1, Y_2, \ldots, Y_m$, each including n frogs, such that: $Y^k = [\Theta_i^k, f_i^k \mid \Theta_i^k = \Theta_{(k+m(i-1))}, f_i^k = f_{(k+m(i-1))}, i = 1, \ldots, n]; k = 1, \ldots, m$. In this process, the first frog goes to the first memeplex, the second frog goes to the second memeplex, frog m goes to the mth memeplex, and frog $m+1$ goes back to the first memeplex, etc.

d. Memetic Evaluation: evolve each memeplex $Y^k; k = 1, \ldots, m$ according to the frog-leaping algorithm as follow. Within each memeplex, the frogs with the best and the worst fitness values are defined as Θ_b and Θ_w. The frog with the global best fitness is defined as Θ_g, then, an improvement process is applied only to the frog with worst fitness in each cycle. Hence, the position of the frog with the worst fitness is modified which emulates the leaping process as follows: leaping distance $D = C_L \operatorname{rand}(0,1)[\Theta_b - \Theta_w]$, then new position $\Theta_w = \Theta_w + D$; $D \in]-D_{max}, D_{max}[$. Where, $\operatorname{rand}(0,1)$ is a random number between 0 and 1, D_{max} is the maximum allowed change in a frog's position and C_L is the modification of the algorithm which it is a constant indicates the amount of frog-leaping in each memeplex. The evaluation process, for all memeplexes, is repeated by an adaptable number of iterations iM, until no improvement becomes possible.

e. Shuffle Memeplexes: shuffle frogs and replace all memeplexes $Y^k; k = 1, \ldots, m$ into U, such that $U = \{f_i, \Theta_i; i = 1, 2, \ldots, NP\}$ similar to the initialization phase, afterwards sort U in order to decrease the performance value, update the population best frog's position Θ_g.

f. Check convergence: if the convergence criteria is satisfied then stop otherwise return to the partition step and continue for a specific quantity of iterations iN.

After each iteration the first frog in the sorted list represents a global solution. The number of iterations iM specifies the search depth within memeplexes while iN governs the solution producing process.

5. SIMULATION RESULTS

The IK of a redundant manipulator with six joints to follow a destination pose was solved. The manipulator's joints correspond to the variable $\theta_j : j = 1, 2, \ldots, 6$ are constrained. In the IK experiments, the desired end-effector pose for the manipulator's arm-part was determined by this vector $G = (P_G, O_G) = (x, y, z, roll, pitch, yaw) = (-20, 3, 40, 0, 10, 15)$. The parameters of the objective function were adjusted as follows $\varepsilon = 1 - \sigma = 0.7$, so there is a balance between position and orientation to be optimized. In case of MSFLA, the parameters of

the algorithm were introduced in Table 2, and a summary of the results of utilizing the algorithm for multiple scenarios was introduced in Table 3. These experiments are carried out to show all possibilities of the MSFL algorithm with variations in the number of iterations and in the population size. The purpose is to show the relationship between error and execution time with relation to iterations and population then to adapt the algorithm to take more optimum solution. An execution time of 729 ms for a human-like robotic arm with 6 joints is good for this type of Metaheuristic algorithm to make a comparison with those methods and algorithms used by other researchers that were mentioned above in the introduction.

Figure 2 shows the values of the objective function.

Table 2. Setting of the MSFL Algorithm.

m	Number of memeplexes	3
n	Number of frogs within memeplexes	NP/m
C_L	Amount of Leaping	1.3

Table 3. Inverse Kinematics Results of MSFL Algorithm

Tests	Population	Iterations		$J(\Theta)$	Total Error	Execution Time [ms]	Reaching Target $(x, y, z, roll, pitch, yaw)$
		iN	iM				
1	20	30	10	11.618	29.71	729	$(-15.7365, 5.43, 52.57, 6.63, 12.66, 16.164)$
2	30	30	10	7.6614	12.08	1045	$(-21.183, 2.915, 50.77, -0.201, 10.01, 14.85)$
3	40	30	15	10.5382	19.21	1685	$(-25.08, 8.56, 46.818, -6.2, 9.6, 5.4251)$
4	40	40	30	18.4625	18.46	4526	$(-25.23, 8.34, 47.59, -2.53, 8.62, 14.13)$
5	60	40	30	8.2925	8.292	6645	$(-24.46, 0.0421, 44.59, 1.65, 11.116, 14.05)$
6	80	50	40	11.024	11.02	13540	$(-26.998, 3.594, 42.87, -0.068, 9.81, 15.67)$
7	100	60	60	29.774	29.77	24191	$(-20.03, 30.039, 39.971, -7.71, 3.679, -0.72)$
8	130	70	60	0.1511	0.649	46282	$(-20.09, 2.99, 40.004, 0.208, 9.64, 14.89)$
9	170	60	50	0.6168	2.168	40459	$(-20.151, 2.84, 40.09, 0.89, 10.36, 16.15)$
10	200	90	40	0.1139	0.298	57362	$(-19.927, 3.0072, 39.98, -0.134, 10.105, 14.89)$
11	200	100	60	0.0729	0.378	92779	$(-20.002, 2.998, 39.99, -0.137, 10.151, 14.92)$
12	200	120	80	2.7672	5.8164	150246	$(-20.48, 4.153, 40.49, 0.807, 4.087, 13.787)$
13	200	200	100	2.6713	1.9339	318481	$(-19.27, 2.235, 41.94, -0.979, 10.88, 11.48)$
14	250	90	40	0.003	0.016	69818	$(-19.99, 3.00023, 39.99, 0.0049, 10.006, 14.99)$
15	250	140	80	1.266	6.553	215027	$(-20, 3, 40, -7.01976e - 10, 10, 15)$
16	250	140	100	4.647e-9	1.05e-8	260325	$(-20.09, 2.97, 40.0008, -1.687, 6.689, 13.57)$
17	300	140	80	1.01e-9	3.33e-9	255989	$(-20, 3, 40, 1.16487e - 9, 10, 15)$
18	500	90	40	5.49e-10	9.9e-10	136888	$(-20, 3, 40, -1.66261e - 11, 10, 15)$
19	500	200	100	3.02e-15	1.56e-14	681646	$(-20, 3, 40, 3.22962e - 15, 10, 15)$
20	1000	30	45	0.0968	0.025	95197	$(-20.031, 3.04, 40.04, -0.0037, 10.96, 14.876)$

The position and orientation of the manipulator's end-effector after applying the solutions to validate the IK solver are presented in Figure 3 and Figure 4, while the joints' positions of the manipulator in Figure 5.
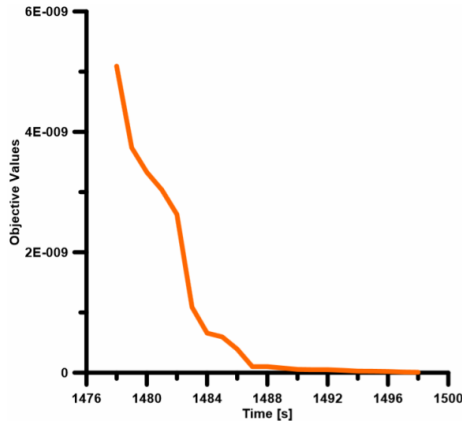
Figure 2. The values of the objective function after applying IK-MSFLA solver
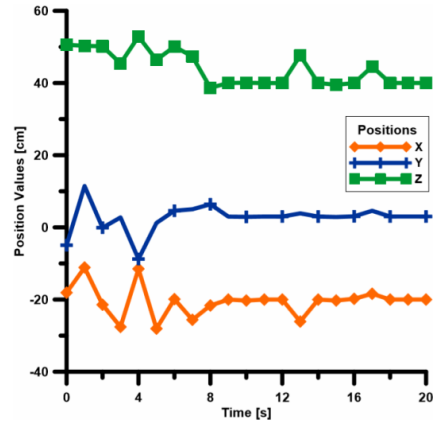
Figure 3. The position of end-effector for the manipulator after applying the solutions to validate IK-MSFLA solver
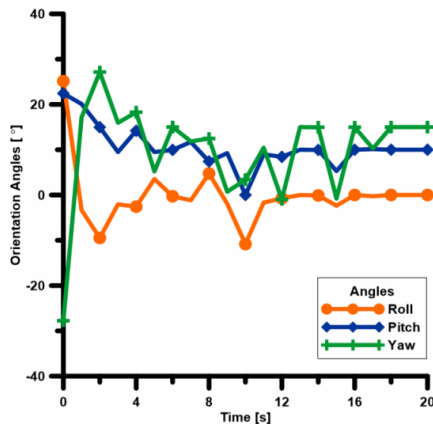
Figure 4. The orientation of the manipulator's end-effector after applying the solutions to validate IK-MSFLA solver
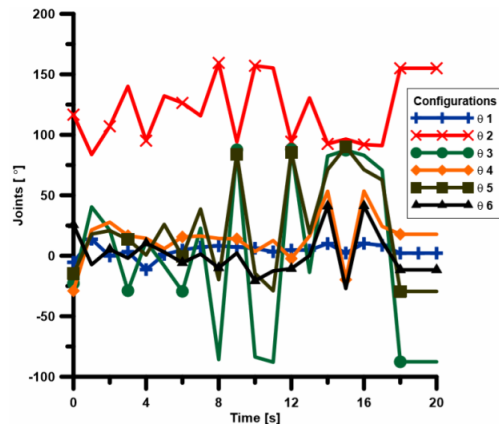
Figure 5. The joints' positions of the manipulator after applying the solutions to validate IK-MSFLA solver

Preliminary tests have been carried out in the laboratory for investigating the performance of the algorithms in addition to analyzing the response, stability, robustness, and smooth motion of the manipulator. The experiments consisted of the execution of various trajectories with the manipulator as shown in Figure 6.

Figure 6. Inverse kinematics tests of a human-like manipulator prototype. It is a lightweight manipulator of 1.1 kg, it has a range of 85 cm in the workspace and a maximal payload of 0.2 kg. The length of the robot in the stretching state is 1.04 m

Figure 7 presents the real-time data from the manipulator plus the platform.
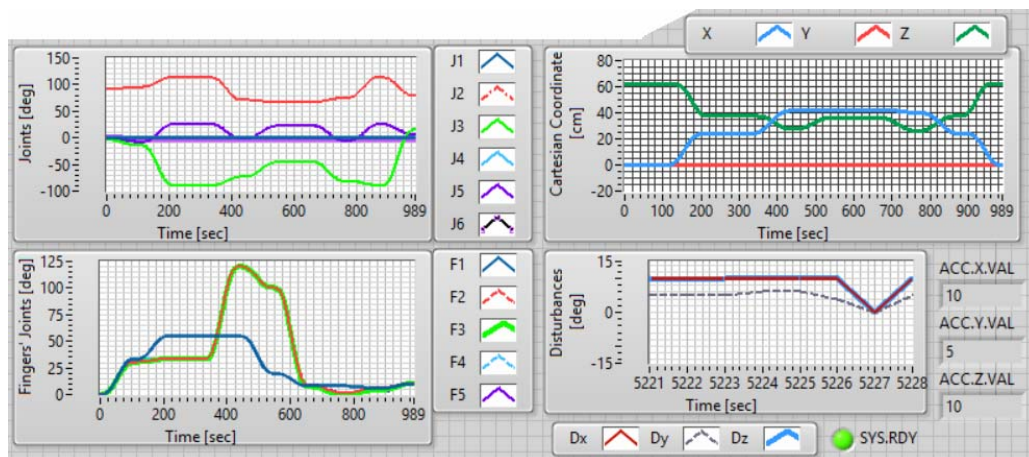
Figure 7. Real-time measurements from the manipulator and the platform, there are configurations of the joints' manipulator, coordinates of the hand, configurations of the fingers and finally the disturbances

6. CONCLUSION

In comparison with other researchers work, the inverse kinematics of a human-like six joints manipulator to follow a certain pose was solved. The modified shuffled frog-leaping algorithm was used and the parameters of the objective function to be optimized were adjusted to have balance between position and orientation. It was obvious that the execution time depends on both the population size and the iterations. The population size achieves the diversity feature, which allows the algorithm to explore more solutions in the workspace while the high iteration gives a solution much closer to the target. The IK solver was validated. Each new solution is considered as a global solution within its iteration, and it grants the algorithm the ability to explore new global solution. Therefore, it is important to alter the settings of the DE algorithm to get a solution based on the objective function in shorter time. The adaptation of the algorithm parameters nearby the setting point may improve the solution to be more fitting but with longer convergence time. The obtained results confirmed the feasibility and effectiveness of the suggested method.

REFERENCES

1. Buss, S. R. (2004). Introduction to inverse kinematics with jacobian transpose, pseudoinverse and damped least squares methods. IEEE Journal of Robotics and Automation, 17(1-19), 16.

2. Dulęba, I., & Opałka, M. (2013). A comparison of Jacobian-based methods of inverse kinematics for serial robot manipulators. International Journal of Applied Mathematics and Computer Science, 23(2), 373-382.

3. Wang, X., Zhang, D., & Zhao, C. (2017). The inverse kinematics of a 7R 6-degree-of-freedom robot with non-spherical wrist. Advances in Mechanical Engineering, 9(8), 1687814017714985.

4. Ananthanarayanan, H., & Ordóñez, R. (2015). Real-time Inverse Kinematics of (2n+ 1) DOF hyper-redundant manipulator arm via a combined numerical and analytical approach. Mechanism and Machine Theory, 91, 209-226.

5. Tolani, D., & Badler, N. I. (1996). Real-time inverse kinematics of the human arm. Presence: Teleoperators & Virtual Environments, 5(4), 393-401.

6. Toshani, H., & Farrokhi, M. (2014). Real-time inverse kinematics of redundant manipulators using neural networks and quadratic programming: a Lyapunov-based approach. Robotics and Autonomous Systems, 62(6), 766-781.

7. Reiter, A., Müller, A., & Gattringer, H. (2016, October). Inverse kinematics in minimum-time trajectory planning for kinematically redundant manipulators. In Industrial Electronics Society, IECON 2016-42nd Annual Conference of the IEEE(pp. 6873-6878). IEEE.

8. Geitle, M. (2017). Improving differential evolution using inductive programming (Master's thesis).

9. Bodily, D. M., Allen, T. F., & Killpack, M. D. (2017, May). Motion planning for mobile robots using inverse kinematics branching. In Robotics and Automation (ICRA), 2017 IEEE International Conference on (pp. 5043-5050). IEEE.

10. Ayyıldız, M., & Çetinkaya, K. (2016). Comparison of four different heuristic optimization algorithms for the inverse kinematics solution of a real 4-DOF serial robot manipulator. Neural Computing and Applications, 27(4), 825-836.

11. Rokbani, N., & Alimi, A. M. (2013). Inverse kinematics using particle swarm optimization, a statistical analysis. Procedia Engineering, 64, 1602-1611.

12. Collinsm, T. J., & Shen, W. M. (2017, April). Particle swarm optimization for high-DOF inverse kinematics. In Control, Automation and Robotics (ICCAR), 2017 3rd International Conference on (pp. 1-6). IEEE.

13. Mao, B., Xie, Z., Wang, Y., Handroos, H., Wu, H., & Shi, S. (2017). A hybrid differential evolution and particle swarm optimization algorithm for numerical kinematics solution of remote maintenance manipulators. Fusion Engineering and Design, 124, 587-590.

14. Kachitvichyanukul, V. (2012). Comparison of three evolutionary algorithms: GA, PSO, and DE. Industrial Engineering and Management Systems, 11(3), 215-223.

15. López-Franco, C., Hernández-Barragán, J., Alanis, A. Y., Arana-Daniel, N., & López-Franco, M. (2018). Inverse kinematics of mobile manipulators based on differential evolution. International Journal of Advanced Robotic Systems, 15(1), 1729881417752738.

16. Shiakolas, P. S., Koladiya, D., & Kebrle, J. (2005). On the optimum synthesis of six-bar linkages using differential evolution and the geometric centroid of precision positions technique. Mechanism and Machine Theory, 40(3), 319-335.

17. Juang, C. F., Chen, Y. H., & Jhan, Y. H. (2015). Wall-following control of a hexapod robot using a data-driven fuzzy controller learned through differential evolution. IEEE Transactions on Industrial electronics, 62(1), 611-619.

18. Pierezan, J., Freire, R. Z., Weihmann, L., Reynoso-Meza, G., & dos Santos Coelho, L. (2017). Static force capability optimization of humanoids robots based on modified self-adaptive differential evolution. Computers & Operations Research, 84, 205-215.

19. Ngoc Son, N., Anh, H. P. H., & Thanh Nam, N. (2016). Robot manipulator identification based on adaptive multiple-input and multiple-output neural model optimized by advanced differential evolution algorithm. International Journal of Advanced Robotic Systems, 14(1), 1729881416677695.

20. Wang, M., Luo, J., Fang, J., & Yuan, J. (2018). Optimal Trajectory Planning of Free-Floating Space Manipulator Using Differential Evolution Algorithm. Advances in Space Research.

21. Eusuff, M., Lansey, K., & Pasha, F. (2006). Shuffled frog-leaping algorithm: a memetic meta-heuristic for discrete optimization. Engineering optimization, 38(2), 129-154.

22. Li, X., Luo, J., Chen, M. R., & Wang, N. (2012). An improved shuffled frog-leaping algorithm with extremal optimisation for continuous optimisation. Information Sciences, 192, 143-151.

23. Samuel, G. G., & Rajan, C. C. A. (2014). A modified shuffled frog-leaping algorithm for long-term generation maintenance scheduling. In Proceedings of the Third International Conference on Soft Computing for Problem Solving (pp. 11-24). Springer, New Delhi.

24. Afzalan, E., Taghikhani, M. A., & Sedighizadeh, M. (2012). Optimal placement and sizing of DG in radial distribution networks using SFLA. International Journal of Energy Engineering, 2(3), 73-77.

25. Ibrahim I.N. (2018). Ultra Light-Weight Robotic Manipulator. Bulletin of Kalashnikov ISTU. - 2018. - Vol. 21. - N. 1 - P. 12-18. doi: 10.22213/2413-1172-2018-1-12-18 (in Russian).

26. Ibrahim, I. N., & Al Akkad, M. A. (2017). Studying the Disturbances of Robotic Arm Movement in Space Using the Compound-Pendulum Method. Bulletin of Kalashnikov ISTU, 20(2), 156-159.

27. Ibrahim, I. N., Al Akkad, M. A., & Abramov, I. V. (2017, June). Attitude and altitude stabilization of a microcopter equipped with a robotic arm. In Control and Communications (SIBCON), 2017 International Siberian Conference on (pp. 1-8). IEEE.

28. Ibrahim, I. N., Al Akkad, M. A., & Abramov, I. V. (2018, May). Exploring Ackermann and LQR stability control of stochastic state-space model of hexacopter equipped with robotic arm. In Journal of Physics: Conference Series (Vol. 1015, No. 3, p. 032160). IOP Publishing.

29. Ibrahim, I. N., Akkad, M. A. A., & Abramov, I. V. (2018, March). UAV efficient PID and LQR controllers design based on its stochastic state space dynamics model including disturbances. In Electronic and Networking Technologies (MWENT), 2018 Moscow Workshop on (pp. 1-9). IEEE.

Comparative Analysis of Digital Underwater Video Image Color Balance Correction Algorithms

S. N. Kirillov, P. N. Skonnikov, A. A. Baukov

Department of Radio control and Communications, RSREU, Ryazan, Russia
E-mail: skonnikovpn@yandex.ru

Abstract. Digital video image color balance correction algorithms are analyzed. The procedure of selecting the objects presented in a video sequence is proposed to be used in order to make a comparative analysis of color information: hue and saturation in HSL model, and chroma as well. The indices of color balance correction quality are substantiated. To carry out full-reference assessment, the groups of video sequences were chosen where various underwater vehicles filmed inside and outside the water can be found. The selection of underwater vehicles in images was made; the parameters of color information of the vehicles selected were estimated in the following video images: reference, source (underwater) and processed with the help of color balance correction algorithms under consideration. A comparative analysis of color correction methods for video recordings taken in aquatic environment was carried out in order to identify the best algorithm according to the criterion of the closest color information of objects presented in an underwater video image to color information of corresponding objects not being distorted by aquatic environment. The results of the comparison have shown that the usage of Gray World Assumption algorithm leads to an improvement in hue up to 6.12 times with saturation loss of 8.8 %, and the usage of White Patch Retinex algorithm – up to 4.43 times with a loss of saturation of 22.4 %.

Keywords: video processing, color balance, aquatic environment, object selection, hue, saturation, chroma

INTRODUCTION

Currently, the work aimed at studying water basin bottom relief, surveying sunken objects, laying and maintaining gas and oil pipelines is actively carried out, scientific research of ocean and sea depths is also conducted. To implement these works, underwater mobile robotic devices are used, generally, with installed digital color video cameras, which make it possible to observe and record scenes at various depths, as well as to control the actions performed.

The quality of underwater video images is significantly influenced by scattering and absorption of light in aquatic environment [1–3]. The degree of light absorption depends on wavelength, as well as on impurities concentration and type. Thus, minimum absorption in the waters of the World Ocean is observed in the range between 470…570 nm [2]. The process of light absorption leads to a reduction in the range of transmitted colors, and, consequently, to distortions in the hue of objects presented in video images taken in an aqueous medium [2]. Distortions of this type significantly reduce the quality of video data, worsen the perception of

underwater scene by the operator controlling the device. In addition, these factors make it difficult to detect and recognize the objects located on an oozy bottom. Therefore, to observe underwater scenes with the help of mobile robotic vehicles, an enhanced vision system improving the quality of video image by color balance correction is needed.

At present, various types of corresponding color correction algorithms are known, the results of which are different [4–11], therefore, it seems relevant to perform a comparative analysis of these approaches. The purpose of the analysis is to identify the best algorithm according to the criterion described below for the best approximation of color information of the objects presented in the video image taken in aquatic environment to color information of these objects not distorted by environment.

ALGORITHMS UNDER COMPARISON

Currently, Bradford's color correction method [4] is known, in which XYZ color space [12, 13] of an original image (X_S, Y_S, Z_S) is linearly converted to the color (X_D, Y_D, Z_D) of a processed image using the points of equal energy or reference white (X_{WS}, Y_{WS}, Z_{WS}) and (X_{WD}, Y_{WD}, Z_{WD}) of source and processed frames, respectively [4]. One of the problems solved in this method is to estimate a reference white point (X_{WS}, Y_{WS}, Z_{WS}). The solutions to this problem are determined by various color balance correction algorithms based on Bradford method: White Patch Retinex (WPR) [5, 6], Gray World Assumption (GW) [5, 7, 8] and Principal Component Analysis (PCA) [9–11, 14].

The basic idea of WPR algorithm is the assumption that the white area presented in a video scene reflects maximum possible light source for each range [5]. Therefore, in this algorithm, the vector of maximum values of pixel intensities in each channel (R, G and B) is taken as a reference white point, and the brightest pixels of each range are excluded from consideration.

GW algorithm assumes that the average color of scene is gray [5]. In accordance with this assumption, a reference white point is calculated by averaging the values of pixel intensities in each range, after excluding the brightest and darkest pixels.

PCA color correction algorithm is based on the principal component method [9–11, 14]. Colors in RGB space form three-element vectors. In the algorithm considered, at the initial stage, these color vectors are arranged according to the norm of projection onto image average color vector. A reference white point represents a vector of dominant direction in the set of selected color vectors, which is calculated using the principal component analysis method [14].

EXPERIMENT DESCRIPTION

General principles of comparison

The goal of applying color balance correction algorithms in enhanced vision systems for underwater mobile robotic vehicles is to bring the colors of objects presented in the frame closer to more "natural" ones. Here, "natural" colors are the colors not being distorted by aquatic environment. To assess the quality of color balance correction in order to reduce the influence of aquatic environment, it is appropriate to use reference color parameters of objects of interest, where color parameters of these objects are used as a reference under normal conditions, that is, in daylight out of water.

For the experiment, the groups of videos containing four different underwater vehicles were chosen [15-17]. Three of them, having a bright yellow color, were presented in video recordings taken both underwater and out of water. The fourth apparatus is a priori known to have white color; therefore, in this group, only video records obtained in aquatic environment are used. In the video recordings selected, objects move and change their spatial orientation as the result of which underwater vehicles and their individual elements have different lighting. In addition, scenes with different background color are used for underwater video recordings.

To exclude background and extraneous objects from the analysis, an automated selection of the object of interest is performed. Then for the selected object the average values of color parameters are calculated. In this case, averaging is performed over the pixels of the object selected and over the frames. Further, these parameters calculated for reference, source and processed video are used to compare color balance correction algorithms.

Hue, saturation and chroma have been chosen as the analyzed color parameters. Hue and saturation are used when presenting colors in HSI (HSV) and HSL models [18-20]. However, despite widespread use of these color spaces, the use of saturation as a measure of colorfulness can lead to incorrect results in dark areas of an image. Therefore, for additional consideration of colorfulness, chroma values of the object selected are also calculated.

Comparison procedure

When analyzing the quality of color balance correction, images representing the frames of the chosen videos are used: reference image I_{ref}, original image I_{source} to be corrected for color balance, and the results of processing using PCA I_{PCA}, WPR I_{WPR}, GW I_{GW} algorithms. The image data is initially presented as a component of red, green, and blue $I = \{R, G, B\}$. The color of the object of interest is calculated in the same way for all images I_{ref}, I_{source}, I_{PCA}, I_{WPR}, I_{GW}.

On the first stage of a comparison procedure of the algorithms indicated, the image is transferred to HSL color space. For each pixel $i = \{r, g, b\}$ of image I, a transformation is performed, as a result of which pixel i is represented as components of hue, saturation and lightness $i = \{h, s, l\}$, respectively [18, 19]. In addition, chroma values are calculated [18, 19]:

$$c = \max(r, g, b) - \min(r, g, b). \tag{1}$$

On the second stage, the object of interest is selected, that is, a mask M is formed, m pixels of which are defined as follows:

$$
\begin{cases}
m = 1, & \text{if} \begin{cases} h \in [H_{min}, H_{max}]; \\ s \in [S_{min}, S_{max}]; \\ l \in [L_{min}, L_{max}]; \end{cases} \\
m = 0, & \text{otherwise.}
\end{cases} \tag{2}
$$

where H_{min}, H_{max}, S_{min}, S_{max}, L_{min}, L_{max} are lower and upper thresholds of the channels of hue H, saturation S and lightness L, chosen experimentally for each video record. In order not to take into account excessively illuminated or darkened areas of the object, where values h and s may turn out to be incorrect, lightness thresholds were chosen not equal to the limits of dynamic range of channel L, i.e. $L_{min} > 0$, $L_{max} < 1$.

In Fig. 1 frames I_{ref} of video recordings of various scenes and selected objects for clarity being presented in the form of element wise multiplication result $I_{ref} \cdot M$ are shown.

Figure 1. Frames of source video recordings of various scenes (on the left)
and the results of objects selection (on the right)

On the third stage, color parameters of the objects selected are averaged by pixels and frames. The average hue value of the selected object is determined by the formula

$$\bar{H} = \sum_{N_f}\sum_{N_p} h \cdot m \Big/ \sum_{N_f}\sum_{N_p} m, \qquad (3)$$

where N_p is the total number of pixels in a frame, N_f is the number of frames in a video. For other color parameters, the calculation is performed in the same way. This operation is performed for all video recordings: reference, source and processed by PCA, WPR, GW algorithms. Thus, at this stage, the parameters of average hue $\bar{H}_{ref}$, $\bar{H}_{source}$, $\bar{H}_{PCA}$, $\bar{H}_{WPR}$, $\bar{H}_{GW}$, average saturation $\bar{S}_{ref}$, $\bar{S}_{source}$, $\bar{S}_{PCA}$, $\bar{S}_{WPR}$, $\bar{S}_{GW}$ and average chroma $\bar{C}_{ref}$, $\bar{C}_{source}$, $\bar{C}_{PCA}$, $\bar{C}_{WPR}$, $\bar{C}_{GW}$ are determined.

Fig. 2 as an example shows the frame of an original video and the results of the image processed by the algorithms considered. This image shows only the selected objects, since only the pixels of these objects are taken into account when analyzing the algorithms.
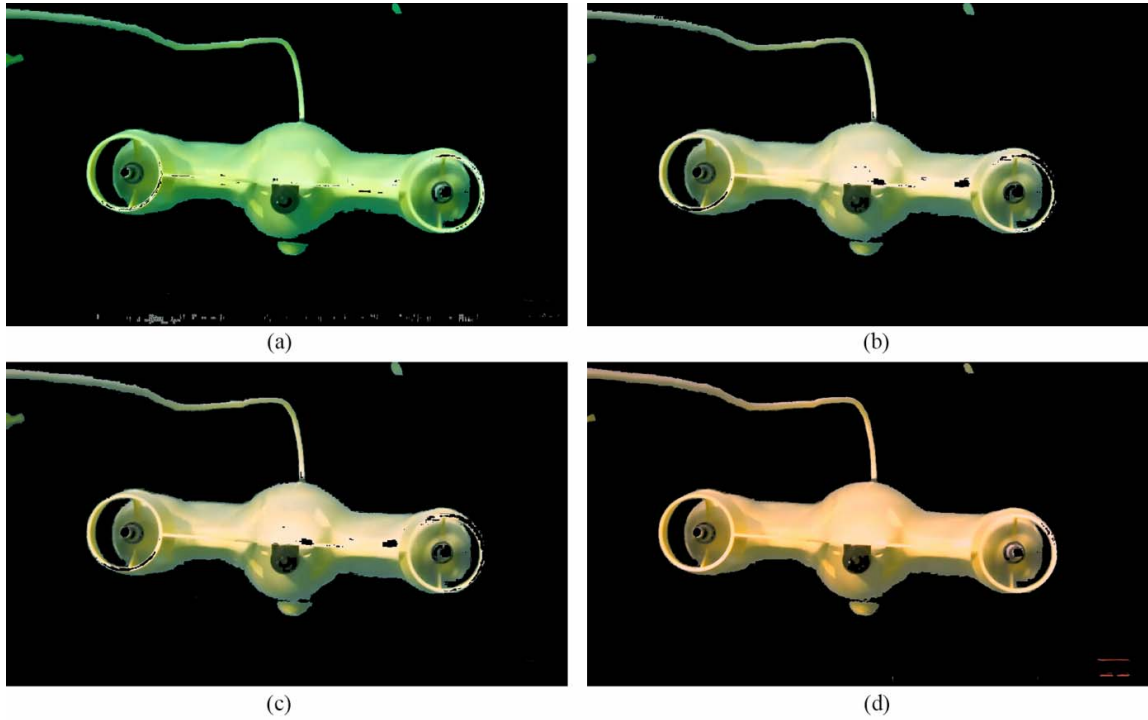

Figure 2. The selected object on the source image (a) and on the images processed using PCA (b), WPR (c), and GW (d) algorithms

The values of color averaged parameters of the object in this frame (at $N_f = 1$) were: $\bar{H}_{source} = 0.31$, $\bar{H}_{PCA} = 0.24$, $\bar{H}_{WPR} = 0.21$, $\bar{H}_{GW} = 0.11$, $\bar{S}_{source} = 0.56$, $\bar{S}_{PCA} = 0.4$, $\bar{S}_{WPR} = 0.43$, $\bar{S}_{GW} = 0.62$.

For the scenes with yellow objects, parameters $\bar{H}$, $\bar{S}$ and $\bar{C}$ themselves are not indicators of improved color balance. The difference $\Delta\bar{H} = \bar{H} - \bar{H}_{ref}$ is used as a measure of hue proximity to reference values. Here $\bar{H}$ is seen as one of the values $\bar{H}_{source}$, $\bar{H}_{PCA}$, $\bar{H}_{WPR}$, $\bar{H}_{GW}$. The measure of video image hue improvement due to the application of an algorithm is determined as a ratio $G_H = \Delta\bar{H}_{source}/\Delta\bar{H}$ by the criterion of approaching a reference value. Saturation and chroma gain are calculated as ratios $G_S = \bar{S}/\bar{S}_{ref}$, $G_C = \bar{C}/\bar{C}_{ref}$, respectively. Improvement in color balance correction quality corresponds to the increase in value $|G_H|$ and the approximation of values G_S and G_C – to a unity.

A group of videos containing a white underwater vehicle was analyzed in a slightly different way. Firstly, hue values were not taken into account, since this parameter does not make sense for a white object. Secondly, since for a white object $\bar{S}_{ref} = 0$ and $\bar{H}_{ref} = 0$, an indicator showing the quality of color balance correction algorithms application are the coefficients of decreasing saturation $R_S = \bar{S}_{source}/\bar{S}$ and chroma $R_C = \bar{C}_{source}/\bar{C}$. Accordingly, in this case the larger the values of R_S and R_C, the better the algorithm for color balance correction is.

EXPERIMENTAL RESULTS

Table 1 shows mean values of hue $\bar{H}$, saturation $\bar{S}$ and chroma $\bar{C}$ of selected objects, as well as coefficients G_H, G_S, G_C calculated on their basis.

Table 1. Averaged color parameters of selected objects and indicators of color balance improvement for scenes with yellow objects

Scene	Video	$\bar{H}$	$\bar{S}$	$\bar{C}$	G_H	G_S	G_C
1	Reference	0.125	0.584	85	–	1	1
	Original	0.308	0.576	82	1	0.987	0.9639
	PCA	0.263	0.345	48.8	1.33	0.592	0.574
	WPR	0.254	0.339	41.3	1.42	0.58	0.486
	GW	0.095	0.754	91	−6.12	1.291	1.07
2	Reference	0.109	0.633	118.1	–	1	1
	Original	0.259	0.283	56	1	0.448	0.475
	PCA	0.237	0.267	55.3	1.14	0.42	0.468
	WPR	0.236	0.267	55.3	1.14	0.42	0.468
	GW	0.236	0.267	55.3	1.14	0.42	0.468
3	Reference	0.128	0.765	147	–	1	1
	Original	0.424	0.756	101.6	1	0.989	0.69
	PCA	0.199	0.57	87.7	4.2	0.746	0.596
	WPR	0.195	0.594	89.3	4.43	0.776	0.607
	GW	0.177	0.698	108.7	6.12	0.912	0.739

Analysis of this table shows that all color balance correction algorithms considered improve the hue $\left(|G_H|>1\right)$, but hue colorfulness is distorted. In this case, PCA and WPR algorithms reduce saturation and chroma, and GW algorithm provides the least distortion of these parameters. However, when using this algorithm, the object as a result of processing may be oversaturated ($G_S>1$, $G_C>1$). The value $G_H<-1$ for GW algorithm shows that an overshoot occurs, i.e., as a result of processing the hue approaches the reference, but the hue change is larger than necessary: $\left|\Delta\bar{H}_{source}\right|<\left|\bar{H}_{source}-\bar{H}_{GW}\right|<\left|2\Delta\bar{H}_{source}\right|$.

Values of $\bar{S}$, $\bar{C}$ parameters and R_S, R_C quality indicators for a white object are given in Table 2.

Table 2. Averaged parameters of colorfulness of selected objects and indicators of its reduction for scenes with white objects

Video	$\bar{S}$	$\bar{C}$	R_S	R_C
Original	0.259	42.2	1	1
PCA	0.211	31.3	1.23	1.35
WPR	0.194	28.7	1.33	1.47
GW	0.977	113.1	0.27	0.37

From the analysis of Table 2 it can be seen that PCA and WPR algorithms reduce saturation and chroma of an object having a white color, that is, improve the image. GW algorithm, in contrast, leads to a false "coloring" of an object.

CONCLUSION

The results of color parameter analysis of the underwater objects highlighted in video have shown that GW algorithm provides the best approximation to the standard. However, this algorithm in some cases leads to the overshoot of all considered parameters and false staining of less saturated objects. The improvement in hue as a result of applying GW algorithm reaches 6.12 times with a saturation loss of 8.8 %.

For tasks in which the overshoot of color parameters and false staining are not allowed, among the considered color balance correction algorithms, WPR algorithm has the best quality indicators. The improvement in hue in this case reaches 4.43 times with the loss in saturation of 22.4 %.

REFERENCES

1. Dolin, L. S., & Levin, I. M. (1991). *Spravochnik po teorii podvodnogo videniya [Handbook of underwater vision theory]*. Leningrad: Gidrometeoizdat (in Russian).

2. Fisenko, T. Yu., & Fisenko, V. T. (2012). Issledovanie i razrabotka metodov uluchsheniya podvodnykh izobrazheniy [Research and development of improving underwater images methods]. In: *Sbornik trudov X Mezhdunarodnoy konferentsii "Prikladnaya optika – 2012" [Proceedings of the X International Conference "Applied Optics - 2012"]* (pp. 294 – 298). (in Russian).

3. Kirillov, S. N., & Kostkin, I. V. (2016). Besprovodnaya sistema vysokoskorostnoy podvodnoy opticheskoy svyazi dlya peredachi videodannykh s borta podvodnogo apparata v rezhime real'nogo vremeni [Wireless system of high-speed underwater optical communication for real time transmission of video data]. *Radiotekhnika [Radioengineering], 11,* 80–89 (in Russian).

4. Lindbloom, B. *Chromatic adaptation.* Retrieved from http://www.brucelindbloom.com/index.html?Eqn_ChromAdapt.html.

5. Ebner, M. (2007). *Color constancy.* Chichester, West Sussex: John Wiley & Sons.

6. Cardei, V. C., & Funt, B. (1999). Committee-based color constancy. In: *Proceedings of the IS&T/SID Seventh Color Imaging Conference: Color Science, Systems and Applications* (pp. 311–313).

7. Buchsbaum, G. (1980). A spatial processor model for object colour perception. *Journal of the Franklin Institute, 310*(1), 337–350.

8. Judd, D. B. (1960). Appraisal of Land's work on two-primary color projections. *Journal of the Optical Society of America, 50*(3), 254–268.

9. Hotelling, H. (1933). Analysis of a complex of statistical variables into principal components. *Journal of Educational Psychology, 24,* 417–441, and 498–520.

10. Jolliffe, I. T. (2002). Principal component analysis. Series: Springer Series in Statistics, 2nd ed., Springer, NY, XXIX.

11. Cheng, D., Prasad, D. K., & Brown, M. S. (2014). Illuminant estimation for color constancy: Why spatial-domain methods work and the role of the color distribution. *Journal of the Optical Society of America A, 5,* 1049–1058.

12. Gonzalez, R. C., & Woods, R. E. (2012). *Tsifrovaya obrabotka izobrazheniy [Digital Image Processing].* Moscow: Tekhnosfera (in Russian).

13. Smith, T., & Guild, J. (1931–32). The C.I.E. colorimetric standards and their use. *Transactions of the Optical Society, 33*(3), 73–134. doi:10.1088/1475-4878/33/3/301.

14. Abdi, H., & Williams, L.J. (2010). Principal component analysis. *Wiley Interdisciplinary Reviews: Computational Statistics, 2*(4), 433–459. doi:10.1002/wics.101.

15. *Silverlit remote control submarine Spycam Aqua running video.* Retrieved from https://www.youtube.com/watch?v=eiB2iviEq2Q.

16. *5 AMAZING Underwater Drones.* Retrieved from https://www.youtube.com/watch?v=KekgdyGACdY.

17. Herkewitz, W. *Ocean Drones Plumb New Depths*. Retrieved from https://www.nytimes.com/2013/11/12/ science/earth/ocean-drones-plumb-new-depths.html?smid=yt-nytimes.

18. Oleari, C. (2016). *Standard colorimetry: definitions, algorithms and software*. Chichester, West Sussex: John Wiley & Sons.

19. Malacara, D. (2011). *Color vision and colorimetry: theory and applications*. 2nd ed. Bellingham, Washington USA: Society of Photo-Optical Instrumentation Engineers (SPIE) Press.

20. Gonsales, R. C., Woods, R. E., & Eddins, S. L. (2006). *Tsifrovaya obrabotka izobrazhenij v srede MATLAB [Digital image processing using MATLAB]*. Moscow: Tekhnosfera (in Russian).

Towards a Web-Based Framework for Computer-Aided Manufacturing

Andrei Lobov [1,2], Antti Martikkala [1], Prasun Biswas [1]

[1] Automation Technology and Mechanical Engineering, Tampere University, Tampere, Finland
E-mail: {andrei.lobov, antti.martikkala, prasun.biswas}@tuni.fi
[2] Mechanical and Industrial Engineering, Norwegian University of Science and Technology, Trondheim, Norway
E-mail: andrei.lobov@ntnu.no

Abstract. Computer-aided manufacturing (CAM) helps to see how manufacturing processes could be executed checking if desired products can be made and at what cost. Usually, a 3D model of a targeted product is used as one of the inputs for CAM. Although actively used for some application domains and despite of well-developed CAM technologies and tools frameworks, further acceptance of CAM is hindered by, on one hand, a restricted access and, on another, knowledge needed to use CAM tools and methods. This article outlines a concept for web-based integration framework architecture for CAM. It defines main stakeholders and their roles in efficient product development and virtual commissioning.

Keywords: Computer-aided Manufacturing, Digital manufacturing, web tools, virtual commissioning

INTRODUCTION

With the development of Internet technologies and global connectivity of people the access to knowledge has simplified. The Wikipedia can be seen as an example of collective knowledge documenting and sharing. Those articles can be now accessed almost globally. Despite the questioning the quality or reliability of Wikipedia as a source of information, it is seen as "a valuable jumping off point for research" [1]. The Wikipedia, as any other encyclopedia, has limited ways to share the knowledge, as these mostly use text and images to systemically organize and describe selected concepts or phenomena in the articles. For the articles published on the Wikipedia, some basic animation and references to videos can be also added to further simplify presentation and comprehending of study materials.

The advent of Internet technologies pushed the capabilities of knowledge sharing further than just a passive perception from the paper or the screen. The study process can be organized now interactively. For example, massive open online courses or MOOC can integrate many people on the same platform with the tools helping to automate testing of students' knowledge (e.g. quizzes) and sometimes to interact with other students. The W3Schools [2], helping people to learn and apply web development standards, allows direct execution of code examples in a web browser to demonstrate their behavior. At the end, the leaner does not have to have any sophisticated tools, as a web browser could be enough.

Development of web technologies has affected also different engineering disciplines. In particular, for product design Computer-aided design (CAD) can be in principle and already done online. For instance, Onshape Product Design Platform [3] offers an interface to use CAD and related engineering APIs.

Industrial Internet can be defined as the application of Internet-based protocols and web technologies for industrial applications. The industrial applications differ from general 'office' applications in terms of requirements for reliability, availability and deterministic execution guaranteeing response times within certain time interval satisfying the needs of application. The use of Internet-inspired protocols can be found already at the production floor. For instance, EtherCAT [4], Ethernet/IP [5] and PROFINET [6] can be seen as examples of protocols, which appearance could be attributed to the success of the Internet.

This article describes a web-based framework that can support Computer-aided Manufacturing, so that engineers, on one hand, could benefit from integration of data at the different stages of product design and manufacturing, and, on the other, make it possible to integrate manufacturing system runtime data.

The rest of the paper is organized as follows. Next section describes the state of the art identifying the gaps and potential development directions. The state of the art is followed by a proposal of architecture for the framework to integrate engineering and runtime data. The fourth section contains the discussion followed by the conclusion and future work.

STATE OF THE ART

The problem of integration of various data can be approached in different ways. In [7], authors develop digital manufacturing toolbox aiming to assist, in particular, manufacturing SMEs, which may struggle to have sufficient resources for research, development and innovation (RDI) activates. That work defines digital manufacturing as tailored, case-specific integration of various technologies for the Production automation, Digital scanning and measurement, Manufacturing design and production simulation, Robotics, and, last, but not least additive manufacturing. Referred work does not suggest the use of web technologies rather proposing a selection of the tools via a process of discussion, preparatory work, tool process, delivery and customer care promoting a supervision of an expert from a particular organization.

Authors of [8] developed a system capable of monitoring main parameters of the CNC (Computer Numerical Control) equipment including the assessment of the consequences of the equipment failure. The proposed server/client architecture and the use of, for instance, "MS SQL Server2008 R2B" shows that the solution is build using Internet-based technologies integrating specific modules with Ethernet and Modbus protocols.

Prevention of confidentiality breach that could lead to the loss of Intellectual Property is discussed in [9]. As there are many cyber-physical or networked embedded systems start to serve the machine accessible with common internet protocols, these systems can be vulnerable points for hacker attacks. The authors of [9] look to the problem in a broader context rather than "simple" hacking of communication networks. They also consider, for example, dynamic response of a machine (e.g. 3D printer) in terms of vibrations produced that could be potential leakage of sensitive information about the work done by the machine. [10] has further elaborated various information leakage channels that in addition to vibration may include acoustic, power and magnetic side-channels. The mission is the development of information leakage-aware CAM tool.

Development of the Internet gave rise also to the new principles of software management. Online software package managers give developers a possibility to dynamically upload re-

quired libraries from the Internet. One of such managers is the package installer for Python (pip)[1]. In [11] a Python-based 3-axis CNC plotter has been developed. The authors highlighted in their work among other things that their solution is following the principles of "open source, easy to understand, requiring basic programming knowledge, thereby making it easily amendable for the user" and "hardware which is less expensive and a setup which is less complex." In other words, both software and hardware for the CNC plotter are easy to develop and manage.

In [12] researchers have benefited from Open NX, "a collection of APIs that allows *user* to create custom applications for NX through an open architecture using well-known programming languages"[2], developing CAM assistant program helping with tool-path planning and selection of cutting tools depending on materials in use. Same as in the abovementioned example of Python-based solution, here also the principle of developing own add-ons for a commercial tool is supported with openness of interface, dedicated APIs for known programming languages.

[13] have made a literature review for STEP-NC aiming to help with data integration between CAD-CAPP (Computer-aided Process Planning)-CAM-CNC. ISO 14649 (STEP NC), which is entitled as "Industrial automation systems and integration", format aims to provide bi-directional data flow between the manufacturing tools. It is according to [13] at the early stage with respect to its inclusion and active use with manufacturing systems. [14] proposes to use graph-based methods and algorithms to support data representation and analysis. Different types of graphs can be employed for corresponding problems ranging from product and process representative models to support of overall decision making and design of assembly lines. In [15], Visual C++ was used to develop "simple and affordable CAPP system". Here the simplicity and affordability can be attributed to the use of open formats, such as, for example, DXF (Drawing eXchange Format) originally developed for AutoCAD that can be also opened by many CAD applications.

[16] highlights the role of the Industrial Internet in integration of CAD-CAE (Computer-aided Engineering)-CAPP-CAM allowing worldwide integration at the same time assuring product quality. Machines and the factories are seen as the nodes in the Industrial Internet in reference to the Industry 4.0 concept having web-based highly-automated smart factories. Such an integration may require end-to-end digitalization [17] supporting gradual development of production automation as a whole involving various information systems, such as Manufacturing Execution Systems (MES) and Enterprise Resource Planning (ERP). Furthermore, cloud-based architectures can be employed for the task of integration to develop so called cloud manufacturing environment [0]. In such an environment, the manufacturing services can be seen as independent entities capable of own decision making as these interact with the users.

In [19], a generic architecture for controlling Smart Manufacturing System (SMS) is described. The architecture includes a possibility for making new task plans, performing data analytics, diagnosis of disturbances to determine resilience strategy. The integration of SMS in the view of the authors should be supported via the use of cyber-physical systems (i.e. embedded networked systems) and revised concept of agents that may include "combinations of humans, cyber-, physical- and cyber-physical technologies" [19].

Another approach for integration can be found in [20] that outlined a Semantic Web Services framework, where different actors, e.g. device vendors, equipment vendors, system integrators, standardization institutions and customers cooperate using a common language –

---

[1] https://pypi.org/project/pip/
[2] https://docs.plm.automation.siemens.com/tdoc/nx/10/nx_api

the Web Ontology Language (OWL)[1] – for building a manufacturing system. The ontologies can be organized into three main categories that of Product, Process and Resource (that also includes, for instance, equipment) [21]. The Process ontology can be seen as a pivotal point to join product and resource ontologies, i.e. to match product needs and skills/capabilities provided by resources.

PROPOSED ARCHITECTURE

Following the "triangle" of Product, Process, Resource outlined in the previous section, that can be extended for Computer-aided Manufacturing integrating necessary services and tools for going from the design of a product to its manufacturing. Fig. 1 presents overall integration framework, where the product and its needs can be depicted via the use of CAD applications, production equipment (manufacturing resources) should be considered via the CAM tools. These to be joined with valid process models, ideally supported by CAPP applications.

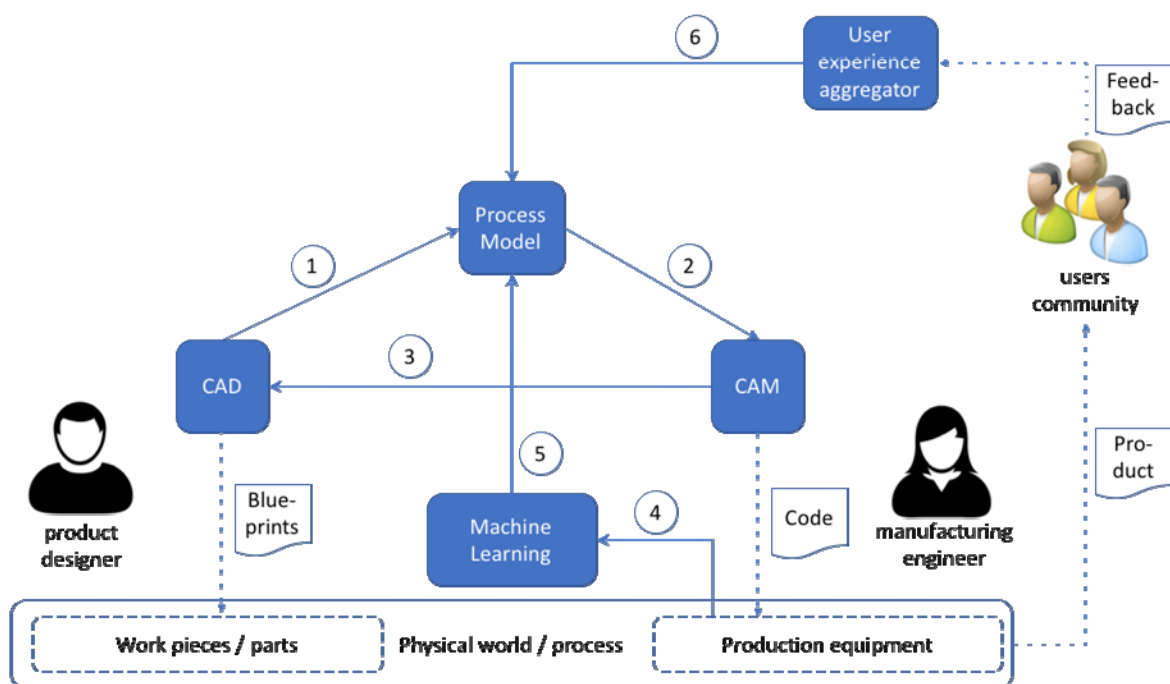**Figure 1.** Integration Framework for Computer-aided Manufacturing

The process model block can be seen as a central element, because any inconsistencies during production process would signify that the loop (1)-(2)-(3) (the "triangle") has some deficiencies that have to be corrected. Thus, the analysis of possible corrective measures should start from the process model block.

---

[1] https://www.w3.org/OWL/

In Fig. 1 the numbers on the edges are used to refine given relationships. The refinements are summarized in Table 1.

Table 1. Relations description in the proposed framework

Relation #	Description
1	Product designer inputs the CAD model representing a part or a workpiece to the CAPP application for generating production plan taking into account the structure of a product, requirements and materials it is made of. Selection of materials can be automated based on the requirements the final product / workpiece should meet.
2	The process plan is input for the CAM tool that refines it in accordance to the available equipment at the production floor.
3	As there could be some inconsistences noticed, these can be reported back to the product designer by manufacturing engineer in order to try to find if there are possibilities to change the design to meet product required and be able to manufacture the product.
4	As the product is being manufactured, the production equipment can report real-time process data to learn on actual manufacturing system behavior.
5	The aggregated data from the actual process is used to fine tune process models. Thus, an earlier feedback to the product designer could be possible based on manufacturing site data.
6	As the products reach their final (or next stage) customers, there should be a possibility to learn on customer's feedback, which is again fed to the process model, i.e. it is not the task of designer or manufacturing engineer to analyze how the manufacturing site is doing as a whole, but through the (adjusted) process models it should become evident which particular requirement is not met or needs further improvement.
Blueprints	Workpieces / products / parts blueprints are generated with CAD tools and ideally should accompany products through different stages of product lifecycle.
Code	Code for equipment (e.g. G-code for CNC machines) generated to produce corresponding products.
Product	Actual product that goes out of given manufacturing system to its customers.
Feedback	Customers' feedback is collected. It could be ranging from human-made reports to automated feedback collected via the IoT instruments connected to the product.

As the feedback received from users, it is processed in terms of process model and manufacturing resources before reaching product designer (e.g. CAD engineer). Thus, the designer is faced not only with direct customer feedback (which is important to know in any case), but also with the implications of the feedback for the other phases of product development and manufacturing.

Integration of abovementioned elements can happen via web technologies and, in particular, following Service-oriented Architecture (SOA). The SOA provides well-defined interfaces such as for example Web Service Description Language (WSDL), which possible application is described in [20]. Having common language representing services and its capabilities makes it possible for a computer to automatically find and integrate required modules for the application. Another approach for service definition is based on RESTful Web Services[1], where the resource identification is based on the notion URI, i.e. Uniform Resource Identifier (everything in a way can be seen as a web resource, having dedicated unique address) with basic set of operations to create, read, update, delete (CRUD) online resources using HTTP (HyperText Transfer Protocol)[2] methods PUT, GET, POST and DELETE.

---

[1] https://docs.oracle.com/javaee/6/tutorial/doc/gijqy.html

[2] https://tools.ietf.org/html/rfc2068

DISCUSSION

There are already available ad hoc demonstrators for various steps outlined in Table 1. However, complete integration is still a challenging task partially due to the lack of agreement for common standards and protocols. Further development of Internet technologies is seen as a key to find a solution based on most commonly used communication protocols and knowledge representation formats. Similar, as for the growing share of Ethernet-based protocols for industrial automation, the same trend can help stabilizing web-based integration technologies for CAM.

Web-based integration framework for CAM can help developing and validating new products in SMEs having simple access to available and affordable modules and tools that may be already packaged for some widely-used (web) programming languages such as JavaScript (Node.js) or Python[1].

In addition to the stakeholders explicitly listed in Fig. 1, there are developers of those open source modules and tools supporting CAD, CAM, machine learning and process definition algorithms. There probably would exist a gap in a quality and usability for some of the "free" modules. However, those are seen to diminish as the standards for service definition and descriptions will be further elaborated.

CONCLUSION AND FUTURE WORK

In this paper, we argue that web-based framework can be a solution for making wider use of Computer-aided Manufacturing. The web standards and technologies being extensively used, tested and developed for a large community of users are possible to apply in domain of manufacturing at different levels of the enterprise ranging from a production floor up to the ERP systems supporting strategic decision making. There are already first successful *ad hoc* applications available, although the challenge remains for finding widely acceptable solution. Such a solution is envisioned to appear as winning web standards for communication and knowledge representation get further developed and accepted.

REFERENCES

1. *Reliability of Wikipedia.* Retrieved July, 2019, from the Wikipedia website: https://en.wikipedia.org/wiki/Reliability_of_Wikipedia

2. *W3Schools.com: The World's Largest Web Developer Site.* Retrieved July, 2019, from: https://www.w3schools.com

3. *Onshape Product Design Platform.* Retrieved July, 2019, from: https://www.onshape.com

4. *EtherCAT Technology Group.* Retrieved July, 2019, from: https://www.ethercat.org/default.htm

5. *Ethernet/IP.* Retrieved July, 2019, from ODVA website: https://www.odva.org/Technology-Standards/EtherNet-IP/Overview

6. *PROFINET Specification.* Retrieved from PROFIBUS and PROFINET International website, July, 2019: https://www.profibus.com/download/profinet-specification

7. Kaartinen, H., Pieskä, S., & Vähäsöyrinki, J. (2016). Digital manufacturing toolbox for supporting the manufacturing SMEs. In: *2016 7th IEEE International Conference on Cognitive Infocommunications (CogInfoCom)* (pp. 000071-000076). Wroclaw, Poland: IEEE. doi: 10.1109/CogInfoCom.2016.7804527

8. Holopov, V., Kushnir, A., Kurnasov, E., Ganichev, A., & Romanov, A. Development of digital production engineering monitoring system based on equipment state index. In: *2017 IEEE Conference of Russian*

---

[1] https://github.com/aewallin/opencamlib

Young Researchers in Electrical and Electronic Engineering (EIConRus) (pp. 863-868). St. Petersburg, Russia: IEEE. doi: 10.1109/EIConRus.2017.7910692

9. Chhetri, S. R., Faezi, S., & Faruque, M. A. A. (2017). Fix the leak! an information leakage aware secured cyber-physical manufacturing system. In: *Design, Automation & Test in Europe Conference & Exhibition (DATE), 2017* (pp. 1408-1413). Lausanne, Switzerland: IEEE. doi: 10.23919/DATE.2017.7927213

10. Chhetri, S. R., Faezi, S., & Al Faruque, M. A. (2018). Information leakage-aware computer-aided cyber-physical manufacturing. In: *IEEE Transactions on Information Forensics and Security, 13,* 2333-2344. doi: 10.1109/TIFS.2018.2818659

11. Shivakumar, T., Sravan, M. S., & Selvajyothi, K. (2016). Python based 3-Axis CNC plotter. In: *2016 IEEE International Conference on Power and Energy (PECon)* (pp. 823-827). Melaka, Malaysia: IEEE. doi: 10.1109/PECON.2016.7951672

12. Chung, C., & Ma, T. (2017). Implementation of CAM programming with machinability database. In: *2017 IEEE/SICE International Symposium on System Integration (SII)* (pp. 236-240). Taipei, Taiwan: IEEE. doi: 10.1109/SII.2017.8279218

13. Ubaid, A. M., & Dweiri, F. T. (2018). Sustainable systems integration by means of STEP-NC: Literature review. In: *2018 Advances in Science and Engineering Technology International Conferences (ASET)* (pp.1-8). Abu Dhabi, United Arab Emirates: IEEE. doi: 10.1109/ICASET.2018.8376883

14. Weise, J., Benkhardt, S., & Mostaghim, S. (2018). A survey on graph-based systems in manufacturing processes. In: *2018 IEEE Symposium Series on Computational Intelligence (SSCI)* (pp. 112-119). Bangalore, India: IEEE. doi: 10.1109/SSCI.2018.8628683

15. Karim, M. S. A., & Tai Tiong, C. (2019). Development of a simple and affordable computer aided process planning (CAPP). In: *2019 Advances in Science and Engineering Technology International Conferences (ASET)* (pp. 1-4). Dubai, United Arab Emirates: IEEE. doi: 10.1109/ICASET.2019.8714443

16. Zhu, C., Zhao, S., & Li, S. (2018). A study of small complicated axisymmetric parts manufacturing in industry 4.0. In: *2018 5th International Conference on Industrial Engineering and Applications (ICIEA)* (pp. 158-162). Singapore, Singapore: IEEE. doi: 10.1109/IEA.2018.8387088

17. Oleynik, A. V., Kuznetsova, L. V., & Petrov, V. E. (2018). Digital transformation of machine-building production. In: *2018 IEEE International Conference "Quality Management, Transport and Information Security, Information Technologies" (IT&QM&IS)* (pp. 704-708). St. Petersburg, Russia: IEEE. doi: 10.1109/ITMQIS.2018.8524977

18. Lou, P., Zhu, C., Yan, J., Zhang, X., & J. Hu. (2018). The emergence of cooperative behaviors under the incentive mechanism of profit allocation in a cloud manufacturing environment. In: *2018 3rd International Conference on Information Systems Engineering (ICISE)* (pp. 147-151). Shanghai, China: IEEE. doi: 10.1109/ICISE.2018.00035

19. Romero, D., Jones, A. T., & Wuest, T. (2018). A new architecture for controlling smart manufacturing systems. In: *2018 International Conference on Intelligent Systems (IS)* (pp. 421-427). Funchal - Madeira, Portugal: IEEE. doi: 10.1109/IS.2018.8710540

20. Lobov, A., Lopez, F. U., Herrera, V. V., Puttonen, J. & Lastra, J. L. M. (2008). Semantic Web Services framework for manufacturing industries. In: *2008 IEEE International Conference on Robotics and Biomimetics* (pp. 2104-2108). Bangkok, Thailand: IEEE. doi: 10.1109/ROBIO.2009.4913327

21. Ferrer, B. R., Mohammed, W. M., Lobov, A., Galera, A. M., & Lastra, J. L. M. (2017). Including human tasks as semantic resources in manufacturing ontology models. In: *IECON 2017 - 43rd Annual Conference of the IEEE Industrial Electronics Society* (pp. 3466-3473). Beijing, China: IEEE. doi: 10.1109/IECON.2017.8216587

An Affordable Deep Learning Based Solution to Support Pick and Place Robotic Tasks

M. Mahmoodpour [1], A. Lobov[1,2], S. Hayati [3], A. Pastukhov [4]

[1] Automation Technology and Mechanical Engineering, Tampere University, Tampere, Finland
E-mail: {mehdi.mahmoodpour, andrei.lobov}@tuni.fi
[2] Dept. of Mechanical and Industrial Engineering, Norwegian University of Science and Technology, Trondheim, Norway
E-mail: andrei.lobov@ntnu.no
[3] Software Development Department, Elektrobit Automotive GmbH, Oulu, Finland
E-mail: saboktakin.hayati@elektrobit.com
[4] International Research Centre "Biotechnologies of the Third Millennium", ITMO University, Saint-Petersburg, Russia
E-mail: artem.pastukhov1984@gmail.com

Abstract. In the current competitive market, the lack of financial resources is a major challenge for Small and Medium Enterprises (SMEs). As a result, SMEs seek low-cost technologies to be employed in their enterprises. Moreover, robotics together with vision systems have become an indispensable part of the current production systems regarding their capabilities to improve the productivity and performance of manufacturing processes. The aim of this paper is to describe an affordable solution for the pick and place robot operation using computer vision technology. The application is designed to identify, pick and place the objects with different arrangements on the palette. For the fulfillment of the vision system, the latest deep learning techniques and image processing software is used to detect the parts. Moreover, the proposed application is dynamic and scalable, created for different use cases so that the operation for various parts with diverse shapes can be handled. The application is tested and validated at the Tampere University Robotic Laboratory (Robolab).

INTRODUCTION

In the current manufacturing enterprises, rapid reconfiguration and quick response to the frequent changes is a critical demand in order to meet the customers' expectations [1]. The inclusion of advanced technologies can help firms to respond to this demand and support the benefits of the enterprise more effectively. On the other hand, since the SMEs have budget constraints to spend in technological infrastructure, they look for solutions that need less financial investment and can fit with their current infrastructure seamlessly. Nevertheless, the advancement of technology has brought low-cost modern technologies in existence over recent years, which allows SMEs to stay in the market and grow more quickly. The other ad-

vantage associated with affordable technologies is that more people are able to launch their startups easily and contribute to the economic growth of the global market.

From the first day the robots were employed in the manufacturing industries, they have made major changes to the production management in industrial sectors with high accuracy and reliability demand. Especially in today's fast-paced production environments, robots play a pivotal role in the industrial automation domain due to their remarkable performance in boosting the efficiency and quality of manufacturing processes as well as lowering the operation costs. As a result, SMEs have become a target for robotic technologies vendors helping them to utilize robots in their manufacturing operations. Thus, robot vendors have introduced the new generation of robots that can fit into small spaces of small manufacturers premises. Collaborative robots or "cobots" are good examples that have enabled SMEs to take advantage of robotic to improve their productivity. Moreover, the adoption of robotic vision systems has been acknowledged by industry sector in recent years. Over the past years, there has been a considerable improvement in the performance of vision technologies while the cost of using such technologies has dropped dramatically. Furthermore, the integration of vision technology with robotic operations can significantly increase the productivity of robots. According to above-mentioned issues, robotic applications including vision technology should be enough affordable for SMEs so that they can leverage the benefits come with this technology without being concerned to allocate a significant financial budget. Also, the smooth integration of machine vision technology with the current robotic operations of SMEs is another crucial aspect that should be taken into consideration. In this context, any machine vision solution should be developed in a way that the commissioning and installing can be carried out simply and quickly by the field operators of SMEs without special skills. Furthermore, the machine vision module should be standalone and easy to maintain. In addition, particularly for pick and place operation, the machine vision module should be flexible enough so that can be reconfigured quickly to support pick and place operation of the wide range of parts with different configurations for multiple use cases.

In this paper, we have focused on low-cost vision systems for SMEs to implement the pick and place robotic operations. The proposed modular and dynamic application allows the SMEs to integrate the solution to their robotic manipulators smoothly without the need to make major changes in current systems. The hardware we used, as computation resource to accomplish our solution, is Raspberry Pi 3, a single-board computer that represents excellent value for a small cost.

The rest of the article is organized as follows. First, the literature review of computer vision systems and techniques is carried out. Next, the state-of-the-art computer vision for robotics is provided. Then, the methodology of research is discussed, followed by the implementation and results with the verification of the proposed solution. Finally, the last section concludes the paper and presents the future direction of research.

COMPUTER VISION SYSTEMS / TECHNIQUES

The computer vision is defined as "extracting descriptions of the world from pictures or sequences of pictures" [12]. In general, any computer vision process consists of three main steps: (1) Image acquisition; (2) Image processing; (3) Image analysis and decision-making. In the following, a brief review of each step is provided.

Image acquisition, which is defined as retrieving an image from hardware-based sources such as different kinds of cameras to represent the real-world scene as digital data to be used for further processing [9]. The hardware system for image acquisition uses image sensors to convert ambient light into digital signals, which eventually can be stored and represented as

digital images. Technically, in image processing, digital images are defined as an array of pixels in a two-dimensional matrix, where each pixel represent the intensity value of brightness [13].

Image processing, the acquired image in the first step could be not of sufficiently high quality because of imaging conditions or problems related to the storage of images [9]. As a result, a pre-processing mechanism is required to enhance the quality of captured images; compress the size of the image; perform image restoration, and carry out feature extraction by employing complex algorithms for better human perception and machine interpretation [23]. The image processing process can be defined as an input-output system in which the image processor applies sophisticated operations on the acquired image in order to generate a high-quality image as an output [16]. Typically, this type of image processing which involves primitive operations to enhance the quality of the image is known as low-level processing.

Image analysis and decision-making means the analysis of images and extract information by which the actual decision can be made. Mid-level image processing techniques such as edge detection and segmentation are used to derive features and attributes from the input image. The extracted features allow computer vision system to derive meaningful information from images, and by feeding achieved information to Machine Learning (ML) algorithms and Artificial Intelligence (AI) technology, cognitive insight can be drawn from the input image and proper action can be taken accordingly i.e. high-level image processing. For instance, with the help of mid-level image processing algorithms such as segmentation, the attributes of a scene can be extracted to enable the high-level process system to understand the surrounding environment using AI algorithms for autonomous navigation. Fig. 1 [3] illustrates the steps of a computer vision system discussed.
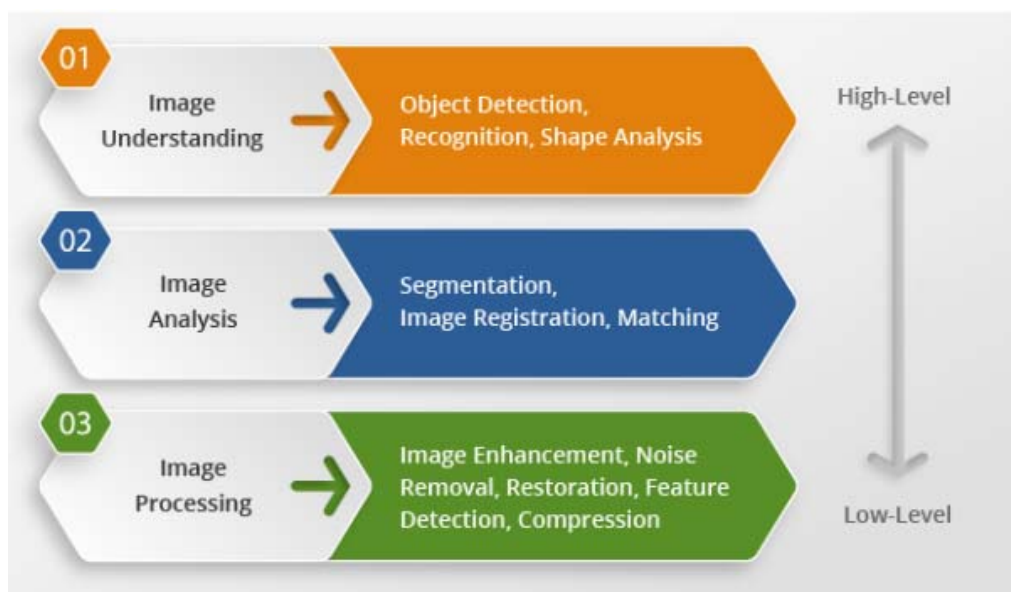

Figure 1. The architecture of a typical computer vision system

ML as a sub-field of AI enables the system to automatically learn from previous data through detecting pattern on data and make a prediction about future data [4]. In this context, computer vision has been influenced by machine learning dramatically over the past 20 years [17]. Machine learning provides powerful techniques for computer vision for adjusting the parameters and using the learned experience to generate, validate and tune the hypothesis [26]. These techniques can be categorized into two major categories: deep learning-based and

traditional machine learning algorithms. Examples of the latter include, random forest (RF) [5], support vector machine (SVM) [18], Hidden Markov model (HMM) [28] and so on. Further, the former category, deep learning, can facilitate feature extraction in the different representation of data by sampling multi-level abstractions of input data, examples include Convolutional Neural Network (CNN) [20] and Recurrent Neural Network (RNN) [22], etc. While there are other deep learning algorithms with a generative approach, such as Generative Adversarial Network (GAN) [14] and Variational Autoencoders (VAE) [24]; they build a model based on simulated observations that extracted from a probability density function [8]. Additionally, deep learning handles large scale datasets such as ImageNet with satisfactory performance [11].

Computer Vision Systems for Robotic Applications

The adoption of computer vision for industrial application and particularly robotics began from the early 1980s [27], thus enabling computers to gain a visual understanding of the surrounding environment through extracting information from digital images of the real world [15]. The development of computer vision technology is growing fast according to emerging low-cost cameras, affordable processing power and evolving vision algorithms [7]. The applications of vision technology for robots in manufacturing processes include identification and locating parts, inspection, assembly, quality control, human-robot collaboration, track the objects, robot navigation and etc. The vision system for robotics can be either scene-related or object-related [2]. The scene-oriented applications involve pathfinding, obstacle avoidance, localization, mapping for mobile robots. On the other hand, object-related vision systems are used to detect objects for different applications such as pick and place, material assembly, quality inspection, machine tending, etc.

In recent years, the usage of deep learning for robot vision applications has become a subject undergoing intense study in robotics realm. The comprehensive survey conducted by authors in [25] reviews the latest achievements and advances in deep learning based robot vision system.

Methodology

As already discussed in the introduction section, any system which aims to enable SMEs to leverage from advanced technologies should be enough affordable. In this study, this essential prerequisite was taken into consideration in order to allow SMEs to employ the designed system in their manufacturing processes. In this context, the hardware and software of the system are chosen in a manner that the entire system is affordable.

Hardware selection: The hardware used to perform system computations, should be capable of carrying out all the tasks defined within the application. Currently, there are a couple of budget computers available in the market. One of the most widely used single-board computers is Raspberry Pi 3 (RP), which can be used for a variety of functions such as automation projects, Internet of Things, educational purposes, industrial applications, etc. Moreover, RP benefits from strong community support, meaning there are many tutorials, resources, and guides provided by contributors all around the world. Also, RP provides a set of general-purpose input/output (GPIO) pins and different ports in order to support the connectivity of a wide range of accessories and peripherals, making it a versatile standalone computer to interact with real-world applications. In particular, for a computer vision application, RP can be equipped with USB webcam or Raspberry Pi camera module making RP capable of handling image acquisition and computer vision algorithms. Furthermore, RP supports all necessary

machine learning and deep learning libraries which are needed to implement a computer vision application.

Software Design: For the software part of the project, as the aim of the research is to enable the integration of vision-system with different robots in a smooth manner, the system is designed in such a way that each module in the system works independently from other modules. This loosely coupled architecture improves the flexibility to the system, thus enabling the development of new modules (e.g. controller for different brands of robots) in an extensible and reusable way. Figure 2 illustrates the designed architecture for the application.
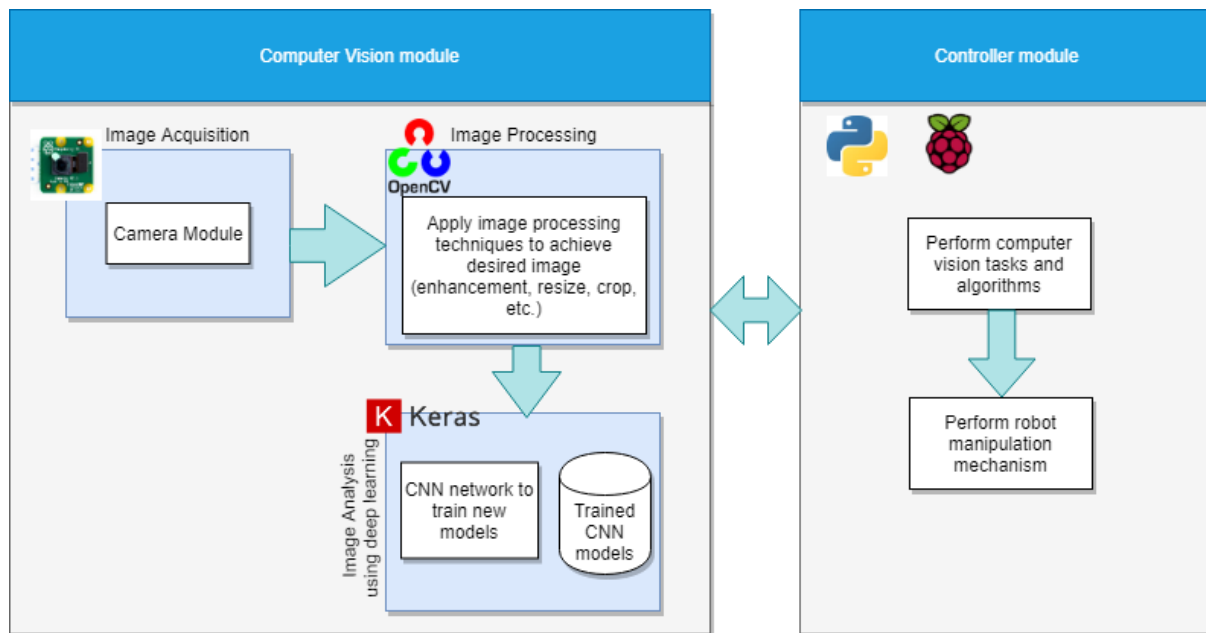

Figure 2. Architectural view of the designed system

As can be seen in the system architecture, the computer vision module uses camera hardware to acquire an image from the external world. Then, the image processing techniques are applied to the acquired image according to the specification of CNN classifier. Next, for the image analysis purpose, the processed image is fed to the CNN network to extract meaningful information from the input image. The controller module interacts with the computer vision system to retrieve the required information in order to carry out the robot manipulation mechanism.

In this study, different tools and libraries are used to perform image processing and deep learning algorithms for the vision part of the project which is discussed briefly in the following.

OpenCV: OpenCV framework [6] is a powerful open source computer vision library which facilitates conducting image processing techniques and algorithms by providing built-in functions. OpenCV is a well-documented library which provides C++, Python, Java and MATLAB interfaces, and supports multiple operating systems such as Windows, Linux, Mac OS, and Android.

Keras: Deep learning techniques have empowered computer vision algorithms significantly. Keras [10] is an open-source high-level neural networks library that allows developing deep learning models for computer vision applications in an easy-to-use manner. It was designed with the aim of enabling fast experimentation with neural networks. Keras has recently integrated into TensorFlow [21], thus allowing using TensorFlow functionalities within Keras

if needed. It is written in Python and runs on CPU and GPU. Moreover, it supports both convolutional networks and recurrent networks, as well as the combinations of the two.

IMPLEMENTATION

In this section, the technical implementation of the proposed methodology for the validation purpose is described.

Vision system hardware: As was stated in the methodology section, Raspberry Pi provides reasonable computing resources with an affordable price. In this study, the Raspberry Pi 3 Model B+ was selected as hardware to perform experiments. Raspberry Pi 3 Model B+ is the latest product in RP 3 series with a 1.4 GHz 64-bit quad-core processor, 1 GB RAM, and support for network communication via Ethernet and wireless LAN. Moreover, the 8-megapixel Raspberry Pi Camera Module v2 was used for image acquisition. All necessary tools and software related to computer vision and deep learning were installed on RP.

Robot setup: The Tampere RoboLab [19] was the place, where all the experiments of study were conducted there. Tampere RoboLab is the learning environment established at Tampere University which aims to provide real-life equipment for pedagogical purposes and particularly robotics education. In this study, for robotic pick and place task, the UR5 robot from Universal Robot in RoboLab was chosen to conduct the experiments in order to validate the solution. The UR5 is a medium size and light-weight collaborative robot (cobot) which widely is used by manufacturers, and particularly SMEs for repetitive tasks such as picking, placing and testing according to its affordable cost compared to other similar products. It can be integrated seamlessly with the working environment through connecting external sensors and actuators as well as other external resources such as, for instance, machine vision system. It supports multiple communication protocols to interact with the external world and remote control such as Modbus and TCP/IP. The communication method we used to control UR5 remotely was TCP/IP socket connection via Ethernet. To do this, the client program needs to run on an external device which in our case is RP and the URScript commands are sent to a server hosted on the robot. We used TCP port 30002 on the robot to send commands over a TCP/IP socket from RP and control the robot remotely. The IP address was configured for both server and client considering that they must be in the same subnet. In this case, RP mounted on the UR5 robot can handle the entire robot control process. Also, to integrate the vision system hardware with the robot, the RP and camera module was mounted on the robot and near to end effector. For this purpose, a plastic holder manufactured by the 3D printer was used to fit the RP and camera on the robot (Figure 3.a).

Using pallets for the pick and place operations results in shorter cycle times according to the repeatability and precision of work. In this regard, a sample indexing table with 32 workpiece positions was used for the experiments. The indexing table (Figure 3.b) is designed specifically for Switch Mode Power Supply (SMPS) transformer coil to handle the pick and place task for soldering operations.

The approach we took for the fulfillment of the vision system to identify objects with different arrangements on the indexing table was based on the implementation of image classification using deep learning. The CNN image classifier allows us to detect the objects on the indexing table for further robotic operations. The image classification model we built using Python and Keras, takes an input (i.e. image) and outputs a class, which in our case the labels are "empty" and "filled". This way, we can classify the given image of every single cell of indexing table using our trained model and predict whether there is a part on cell or not. In order to train our image classifier model, we built a dataset divided into two subsets of images:

- **Empty:** containing the images of empty cells (1000 samples, 28×28 images).
- **Filled:** containing the images of filled cells (1000 samples, 28×28 images).
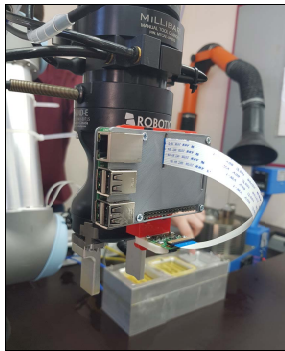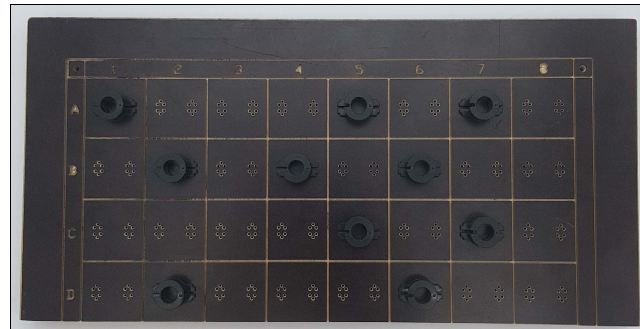
(a)   (b)

Figure 3. Mounting RP on the robot (a); indexing table for SMPS transformer coils (b)

The images were captured in various illumination conditions to build a rich dataset in order to improve the generalization of the trained model. We designed feedforward neural network architecture with backpropagation to train our model. The designed CNN network consists of multiple layers including two convolutional layers, one dense hidden layer and the output layer with two labels. The training was carried out by RP and the trained model was stored on RP for later use in the application.
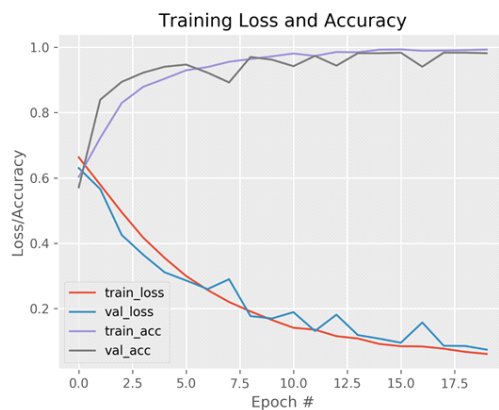

Figure 4. The plot of model accuracy/loss on training

In order to see the training performance of deep learning classifier model, the results are plotted as shown in Figure 3. As can be seen, the accuracy and loss parameters for training and validation converge during the training process, which implies that the model is well generalized and overfitting is handled properly. The network trained for 20 epochs and we achieved 98.91 % testing accuracy. For the training/testing split on data, we dedicated 80 % of the images for training and the rest for testing.

The trained classification model can be loaded in order to enable the application to detect parts. In the following, we explain the details of how the computer vision module works in the system. Figure. 5 illustrates the sequence diagram of the interaction between the different components of the system to accomplish pick and place task using computer vision.

Once the trained CNN model is loaded, the image from the work cell is captured by the camera module. Next, the indexing table is extracted from the captured image using OpenCV edge detection functions such as Canny, Dilate and Erode. Then, we use OpenCV functions to loop over the indexing table image and crop the image of each cell to be examined by image classifier and predict the emptiness or fullness of cell. The results are stored in memory for further use by the robot.
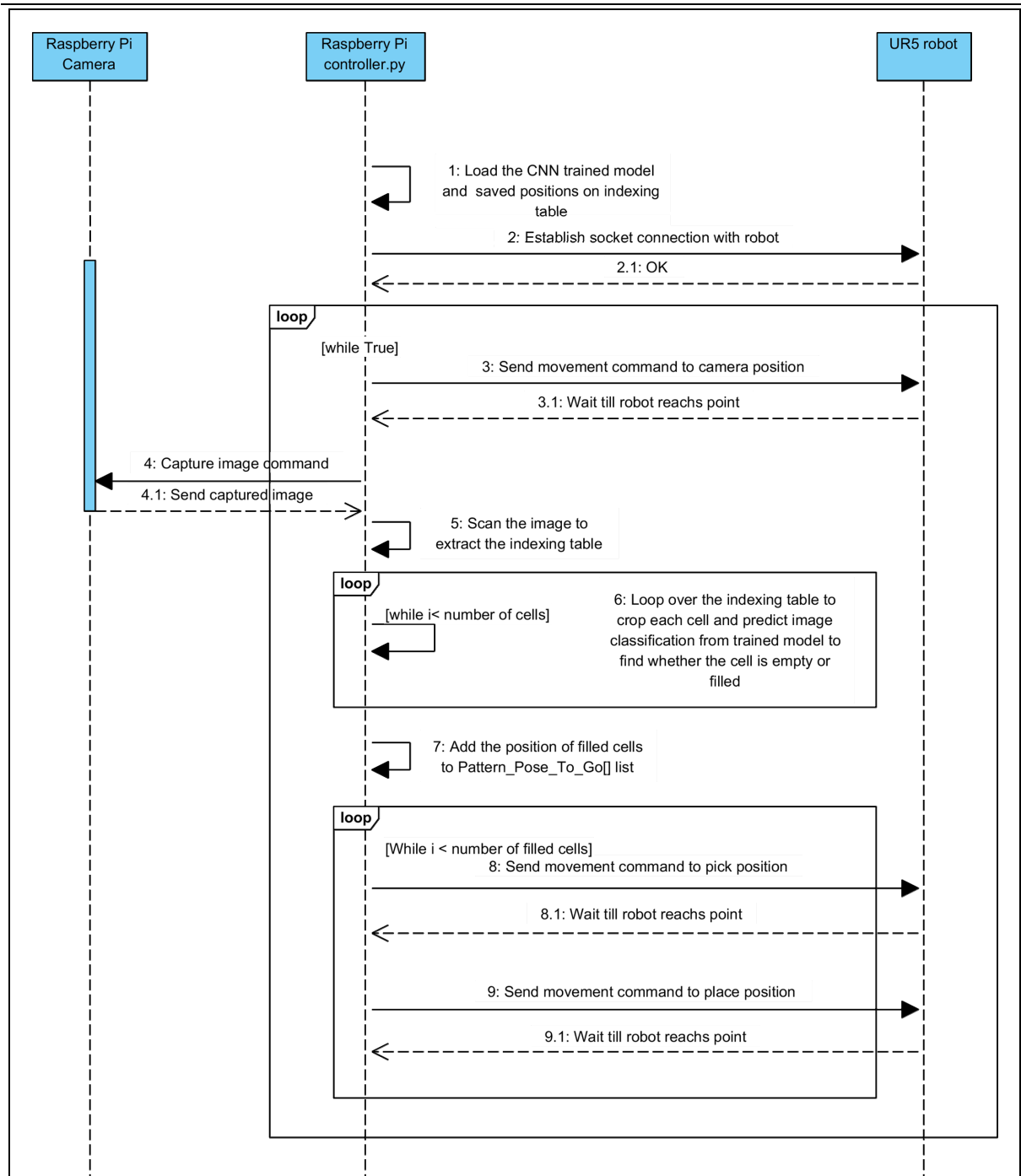
Figure 5. Sequence diagram of system components interactions

For each indexing table, the position of cells is stored in a CSV file using the UR5 palletizing wizard. This file is loaded by application to be used for robot manipulation tasks. Next, according to the results achieved from the computer vision module, a list, containing the position of filled cells is created that the robot should pick the part. Then, RP sends movement commands to robot regarding the created list. The operation continues until the robot reaches all the cells and performs the pick and place task.

RESULTS

The vision system integrated with a robot was examined at Tampere University RobLab. In order to ensure the proper functioning of the designed system, several experiments were carried out with different arrangements of parts on the indexing table. Also, the tests were fulfilled in different illumination conditions to test the performance of the system. The test results were satisfactory and the vision system detected the parts with 100 % accuracy. The performance of the trained classifier was flawless because of having a rich dataset of images for the specific part (i.e. 2000 images in total). However, it should be noted that since there are many parts with different shapes and sizes, building the image dataset for all the parts would be a tedious and time-consuming process. Accordingly, an automated process to create the image dataset is in need to handle this issue.

CONCLUSION

In this paper, we discussed the necessity of allowing the SMEs to leverage the latest technologies in order to be able to compete with larger corporations. In this context, we explained that affordable robotic vision systems could contribute to SMEs' productivity improvement significantly and help them to stay in the market. Moreover, we studied the state-of-the-art technologies and tools in computer vision domain and their usage in robotics. We proposed an affordable solution using Raspberry Pi as a cheap and flexible computer, capable of handling the computational requirements of moderate deep learning applications, which is sufficient for SMEs manufacturing processes. The application was tested and results proved that RP is able to perform adequately for deep learning-based vision system. The proposed application is scalable, created for different use cases so that the pick and place task of various parts with different shapes and sizes can be handled. For the future phase of the research, we plan to implement the solution on other available affordable computers in the market and study the performance benchmarks of each device. Moreover, the implementation of the automated process to create image dataset for training the image classifier model will be taken into consideration.

REFERENCES

1. Abele, E., Meyer, T., Näher, U., Strube, G., & Sykes, R. (Eds.). (2008). *Global production: A handbook for strategy and implementation.* Springer Science & Business Media.

2. Alenyà, G., Foix, S., & Torras, C. (2014). ToF cameras for active vision in robotics. *Sensors and Actuators A: Physical, 218*, 10–22. doi: 10.1016/j.sna.2014.07.014

3. *Application for image processing.* (2019). Retrieved May 14, 2019, from: http://www.smartcoreinc.com/?page_id=2121&ckattempt=1 .

4. Bishop, C. M. (2006). *Pattern recognition and machine learning.* Springer.

5. Bosch, A., Zisserman, A., & Munoz, X. (2007). Image classification using random forests and ferns. In: *2007 IEEE 11th International Conference on Computer Vision* (pp. 1-8). Rio de Janeiro, Brazil: IEEE. doi: 10.1109/ICCV.2007.4409066

6. Bradski, G. (2000). The OpenCV Library. *Dr. Dobb's Journal of Software Tools, 25*(11), 120–126.

7. Bradski, G., & Kaehler, A. (2008). *Learning OpenCV: Computer vision with the OpenCV library.* O'Reilly Media, Inc.

8. Cao, Y, Jia, L., Chen, Y., Lin, N., Yang, C., Zhang, B., Liu, Z., Li, X., & Dai, H. (2019). Recent advances of generative adversarial networks in computer vision. *IEEE Access, 7*, 14985–15006. doi: 10.1109/ACCESS.2018.2886814

9. Chan, T. F., & Shen, J. 2005. *Image processing and analysis: Variational, PDE, wavelet, and stochastic methods.* Siam.

10. Chollet, F., & others. 2015. *Keras*.

11. Deng, J., Dong, W., Socher, R., Li, L.-J., Li, K., & Li Fei-Fei. (2009). ImageNet: a large-scale hierarchical image database. In: *2009 IEEE Conference on Computer Vision and Pattern Recognition* (pp. 248–255). Miami, USA: IEEE. doi: 10.1109/CVPR.2009.5206848

12. Forsyth, D. A., & Ponce, J.. (2003). *Computer vision: A modern approach.* Prentice-Hall.

13. Gonzalez, R. C., & Woods, R. E. (2002). *Digital image processing.* Prentice Hall.

14. Goodfellow, I., Pouget-Abadie, J., Mirza, M., Xu, B., Warde-Farley, D., Ozair S., Courville, A., & Bengio, Y. (2014). Generative adversarial nets. In: *Advances in Neural Information Processing Systems, 27,* 2672–2680.

15. Hartley, R., & Zisserman, A. (2003). *Multiple view geometry in computer vision.* Cambridge university press.

16. Jain, A. K. (1989). *Fundamentals of digital image processing.* Englewood Cliffs, USA: Prentice Hall.

17. Jordan, M. I., & Mitchell, T. M. (2015). Machine learning: Trends, perspectives, and prospects. *Science, 349*(6245), 255–260. doi: 10.1126/science.aaa8415

18. Ko, B. C. Cheong, K.-H., & Nam, J.-Y. (2009). Fire detection based on vision sensor and support vector machines. *Fire Safety Journal, 44*(3), 322–329. doi: 10.1016/j.firesaf.2008.07.006

19. Lanz, M., Pieters, R., & Ghabcheloo, R. (2019). Learning environment for robotics education and industry-academia collaboration. *Procedia Manufacturing 31,* 79–84. doi: 10.1016/j.promfg.2019.03.013

20. LeCun, Y., Kavukcuoglu, K., & Farabet, C. (2010). Convolutional networks and applications in vision. In: *Proceedings of 2010 IEEE International Symposium on Circuits and Systems* (pp. 253–256). Paris, France: IEEE. doi: 10.1109/ISCAS.2010.5537907

21. Abadi, M., Agarwal, A., Barham, P., Brevdo, E., Chen, Zh., Citro, C., Corrado, G. S., et al. (2015). *TensorFlow: Large-scale machine learning on heterogeneous systems.* Retrieved May 14, 2019, from: https://www.tensorflow.org/

22. Mnih, V., Heess, N., Graves, A., & Kavukcuoglu, K. (2014). Recurrent models of visual attention. In: *NIPS'14 Proceedings of the 27th International Conference on Neural Information Processing Systems, 2* (pp. 2204–2212). Montreal, Canada. Retrieved May 14, 2019, from: http://papers.nips.cc/paper/5542-recurrent-models-of-visual-attention.pdf

23. Petrou, M., & Petrou, C. (2010). *Image processing: The fundamentals.* 2nd ed. John Wiley & Sons. doi: 10.1002/9781119994398

24. Pu, Yu., Gan, Z., Henao, R., Yuan, X., Li, Ch., Stevens, A., & Carin, L. (2016). Variational autoencoder for deep learning of images, labels and captions. In: Lee, D. D., Sugiyama, M., Luxburg, U. V. (Eds.). *Advances in Neural Information Processing Systems 29 (NIPS 2016),* 2352–2360.

25. Ruiz-del-Solar, J., Loncomilla, P., & Soto, N. (2018). A survey on deep learning methods for robot vision. *ArXiv, abs/1803.10862.*

26. Sebe, N., Cohen, I., Garg, A., & Huang, T. S. (2005). *Computational imaging and vision: Vol. 29. Machine learning in computer vision.* Springer Science & Business Media. doi: 10.1007/1-4020-3275-7

27. Vernon, D. (1991). *Machine vision: Automated visual inspection and robot vision.* Prentice Hall.

28. Yamato, J., Ohya, J., & Ishii, K. (1992). Recognizing human action in time-sequential images using hidden Markov model. In: *Proceedings 1992 IEEE Computer Society Conference on Computer Vision and Pattern Recognition* (pp. 379–385). Champaign, USA: IEEE. 10.1109/CVPR.1992.223161

Change in the Acoustic and Elastic Properties of the Cylindrical Steel Specimens during the Tensile

O. V. Murav'eva, S. V. Len'kov, A. A. Nagovitsyn, A. F. Basharova

Kalashnikov Izhevsk State Technical University, Izhevsk, Russian Federation
E-mail: pmkk@istu.ru

Abstract. The paper presents the results of an experimental study of the effect of tensile stresses in the elastic and plastic regions on the velocities of longitudinal and transverse waves and the Poisson's ratio for cylindrical samples of steel 40X with different heat treatment. A multiple mirror-shadow method with the use of specialized electromagnetic-acoustic transducers, which provides high accuracy and reliability of measurements due to detuning from the quality of the acoustic contact and the geometry of the sample, as well as the possibility of registering a series of multiple reflections across the sample section, is used. It is shown that the velocities of acoustic waves is minimal, and the Poisson's ratio is maximal for the sample obtained by quenching. The behavior of the curve of the transverse wave velocity change is identical to the transverse deformation of the sample, while the sensitivity of the transverse waves to mechanical stresses is maximal due to the matching with the direction of the applied load. The greatest sensitivity to stress is characteristic of the samples after tempering and normalization. After removal of the load and subsequent «recovery», there is an uneven distribution of the Poisson's ratio along the length of the sample.

INTRODUCTION

During the exploitation, many products made of rolled bars, for example, pumping rods experience tensile loads, are affected by tensile stresses, the occurrence of which leads to the accumulation of damage and critically affects the life service of the product and its characteristics. For testing the stress there are used strain state of products, as a rule, magnetic structuroscopy [1-4] and ultrasonic methods based on the measurement of the characteristics of elastic waves in a tested environment [5-13]. The advantages of acoustic methods based on the measurement of the characteristics of elastic waves in a testing environment include the ability to determine surface and internal stresses, accumulation of micro-damage in the volume of the material; multiparameter of testing in favor of the variety of types of waves used and recorded parameters; efficiency of testing, high resolution capability and the ability to measure directly on the tested objects during operation. Due to the use of elastic waves, it is possible to obtain the most reliable connections with the structural and mechanical parameters of the materials of the products. The method of estimating tensile stresses is based on the phenomenon of acoustoelasticity, which is the quotient between the velocities of ultrasonic

waves and mechanical stresses. The method of acoustoelasticity is standardized as a method of testing of internal mechanical stresses and therefore differs significantly from diagnostic methods that use electromagnetic properties of metals. Also, the exploitation and technological characteristics and deformation behavior of materials are influenced by the Poisson's ratio which associated with the strength and crack resistance and anisotropy of the mechanical properties of the rolled products [14–21].

The aim of the work is to study the effect of the tensile uniaxial load in the elastic and plastic areas, as well as study the effect on the velocity of longitudinal and transverse acoustic waves after loading cylindrical samples of steel 40KH and study Poisson's ratio.

Proposed Approach

As an object of research, there were used samples of 40KH-steel bars according to GOST 4543-71, which used for the manufacture of critical parts of oil-producing equipment – rods-billets of pumping rods and shafts of centrifugal pumps. To evaluate the effect of tensile stresses on the measured characteristics of acoustic waves, samples with a diameter of 14 mm in the state of delivery and subjected to additional heat treatment and mechanical properties of the studied samples are presented in the Table 1. The hardness of the samples was determined using the hardness tester Novotest T-UDZ. The chemical composition of 40KH steel samples was determined by using a portable analyzer of metals and alloys – XMET – 5000: C – 0.4, Cr – 0.8, Si – 0.2, Mn – 0.5.

Table 1. Heat treatment and reference mechanical properties of samples of 40KH-steel

No	Type of the heat treatment	Stress limit, σ_S, MPa	Yield stress, $\sigma_{0.2}$, MPa	Elongation, δ, %	Hardness HB
#1	Delivery condition: heat quenching 860°C, oil, tempering 650°C (improvment)	850	730	19.0	306
#2	Heat quenching, 850°C, oil	1400	1320	8.0	441
#3	Heat quenching, tempering, 570°C	1050	960	17.0	335

To determine the velocities of elastic waves, there was used multiple echo-pulse method with using electromagnetic acoustic (EMA) principle of launching-receiving of acoustic waves which provides high accuracy and reliability of measurements by detuning from the quality of the acoustic contact and the possibility of registering a series of multiple reflections across the sample section [22–24].
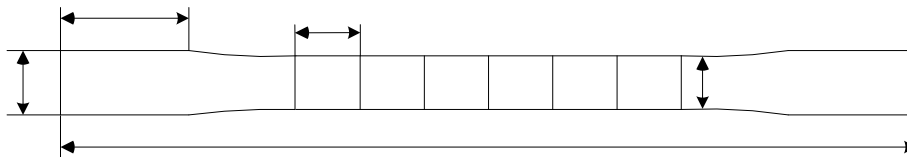

Figure 1. Sample form for investigations and marking for measurement after tensioning

The samples were stretched progressively at intervals of 10 kN until the yield strength was reached by the Instron 300DX test machine. To study the velocities of volume waves, an electromagnetic-acoustic structurescope (SEMA) was used [23-25], which implements the mirror-shadow method on multiple reflections, the functional scheme of which is shown in

Figure 2,a. Polarization of the wave types which was used in the carried coordinate system is shown in Figure 2,b. The axial polarization of the transverse waves U_z corresponds to the direction of loading, the radial polarization of the longitudinal waves U_r is oriented across the tensile load. Launching and receiving of longitudinal and transverse waves were produced in all radial directions along the cross section of the sample there were used specially developed EMA-converters of longitudinal and transverse waves of the split type presented in Figure 3 [26]. For registration and further processing of the received series of multiple reflections the specialized software Prince [27] was used. Typical waveforms of a series of multiple reflections of the transverse wave along the rod diameter and selected fragments of pulses at 7 reflection without load and at a load of 1600 MPa, the fraction of the sample #2 are shown in Figure 4.
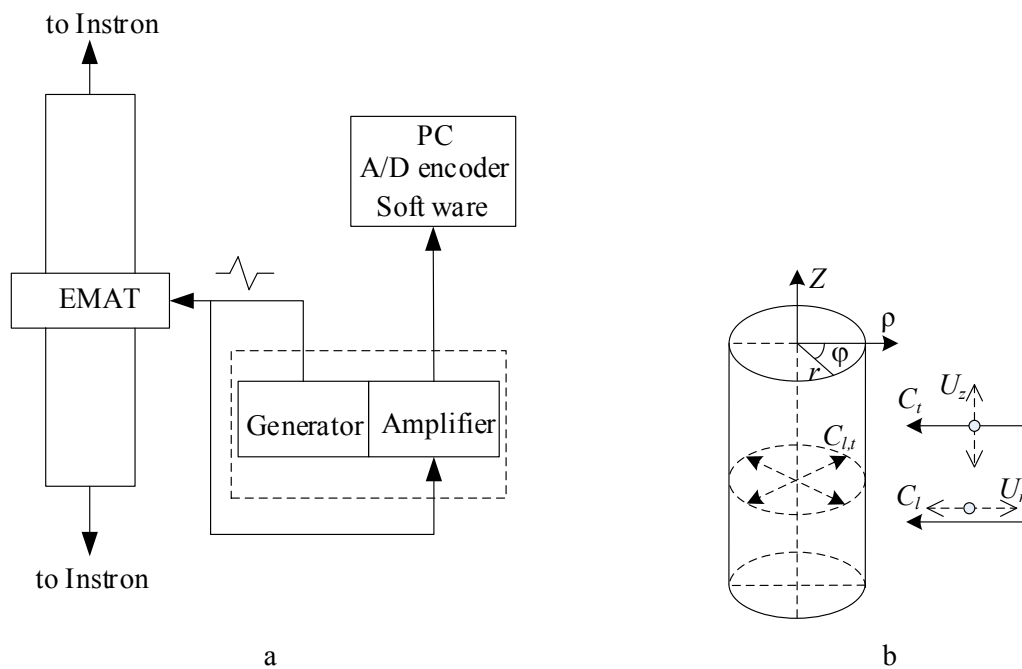

Figure 2. Sample loading and registration scheme (a), carried coordinate system and polarization of the waves used (b)
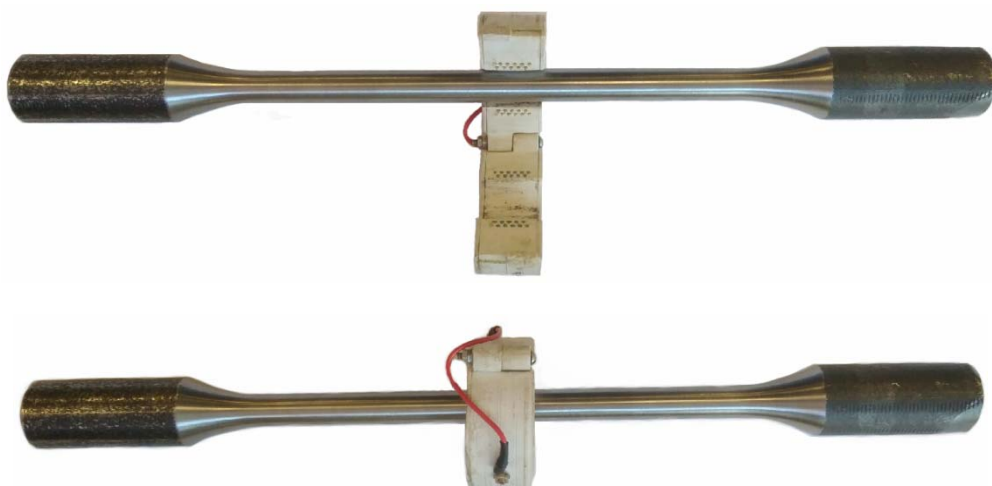

Figure 3. Photo of detachable EMAT of longitudinal waves which is set in the centre of the sample
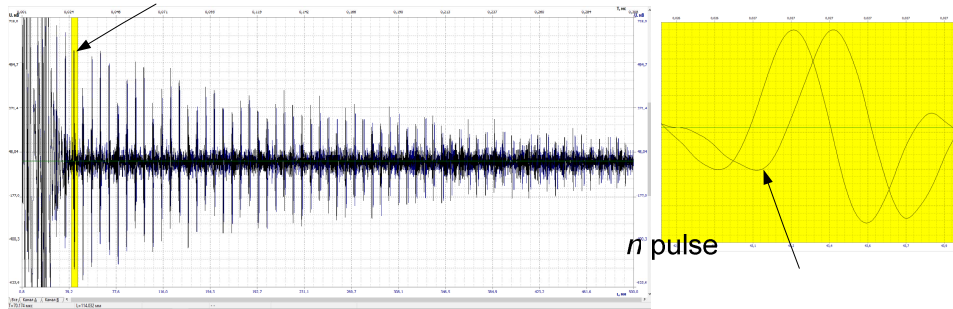
Figure 4. Typical oscillograms of a series of multiple reflections of a transverse wave
along the rod diameter and pulses at 7 reflection without load and at a load of 1600 MPa

The velocities of transverse and longitudinal waves were calculated using the following
formulas:

$$C_{l,t} = \frac{d \cdot n}{\Delta t_n},$$ (1)

where d is the average diameter of the sample at each loading step, Δt_n is the time of the n-th
reflected pulse in the transverse t and longitudinal l waveforms.

The influence of the number of recorded reflections n on the difference of received tense
Δt_n is illustrated in Figure 5. There is a close to linear dependence, in fact the minimum devia-
tions are in the zone of large values n. Significant deviations in the region of small n are due
to the influence of a powerful probing pulse on the measurement accuracy.
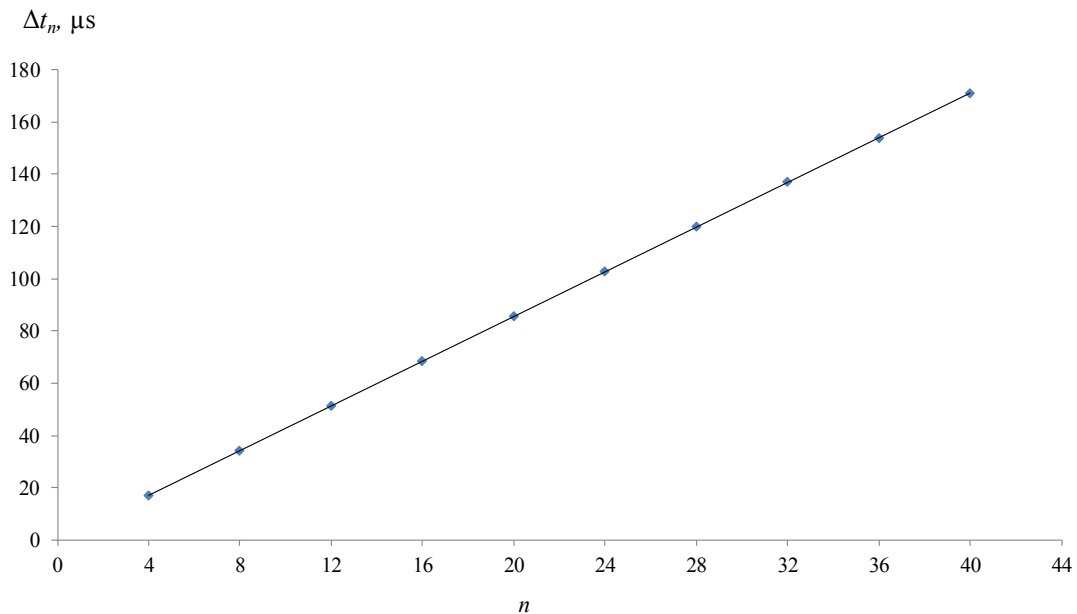

Figure 5. Graph of the dependence between the number of reflections
and the time difference between them

Due to the high sampling rate of the used equipment (100 MHz), the subsequent interpo-
lation of the signal is produced by using specialized software, as well as due to the possibility

79

of measurements on long-range reflections, high accuracy of determining the speed of propagation of acoustic waves (0.5 m/s or 0.01%) with the accuracy of determining the diameter of the sample 50 microns.

The degree of influence of mechanical tensile stresses on the speed of transverse and longitudinal waves can be estimated by the coefficients of acoustoelastic coupling, calculated by the formulas:

$$\beta_{zz}^c = \frac{\Delta C_t}{C_{t0} \cdot \sigma_{zz}}, \tag{2}$$

$$\beta_{zr}^c = \frac{\Delta C_l}{C_{l0} \cdot \sigma_{zz}}, \tag{3}$$

where $\Delta C_{l,t}/C_{l,t(0)}$ is the relative velocity change under loading, σ_{zz} is the applied load.

In the evaluation of the elastic modulus (Poisson's ratio ν) its functional connection is used with the propagation velocity of volumetric (longitudinal and transverse) waves. When a sample is emitted in one section using longitudinal and transverse waves, it is possible to determine the Poisson's ratio regardless of the sample diameter [19]:

$$\nu = \frac{C_l^2 - C_t^2}{2\left(C_l^2 - C_t^2\right)^2} = \frac{1 - 2\gamma^2}{2\left(1 - \gamma^2\right)}, \tag{4}$$

where $\gamma^2 = \dfrac{C_t^2}{C_l^2} = \dfrac{\Delta t_l^2}{\Delta t_t^2}$ – is the ratio of the velocities of the transverse and longitudinal waves, proportional to the ratio of their time propagation.

The proposed method of determining the Poisson's ratio by measuring the difference between the travel times of two types of waves in one section allows to adjust from a number of interfering factors that occur when measuring the absolute values of velocities. Calculations show that the indirect error of the absolute value of the Poisson's ratio does not exceed 0.01 % (that is, up to the fifth significant digit after the decimal point).

RESULTS AND DISCUSSION

The values of longitudinal and transverse wave velocities and Poisson's ratio in 40KH steel samples with different heat treatment options are presented in Table 2. For the sample #2 obtained by quenching, having a martensite structure with a maximum degree of distortion of the crystal lattice, the propagation velocity of longitudinal and transverse waves is minimal, and the Poisson's ratio describing the resistance to transverse deformations is maximal. Subsequent tempering (sample #3), and especially softening treatments such as normalization (sample #1), leading to the most equilibrium ferrite-pearlite structures lead to an increase in the velocity of ultrasonic waves and a decrease in the Poisson's ratio.

Table 2. Longitudinal and transverse wave velocities and Poisson's ratio in the samples under study before loading

Sample number	C_l, m/s	C_t, m/s	ν
#1	5940	3251	0.286
#2	5881	3193	0.291
#3	5918	3232	0.287

It should be noted that the mechanical properties - hardness, strength and yield strength, elongation (Table 1) also correspond to the structural state of the samples and satisfactorily correlate with the propagation velocities of transverse and longitudinal waves. The wave speed decreases with increasing strength and fluidity, hardness of the bars and increases with increasing plasticity, elongation.

The effect of axial tensile stresses on the change in the mean diameter and the relative value of the transverse wave velocities for the samples are illustrated in Figure 6. With increasing tensile load there is a significant linear decrease in the velocity of transverse waves with axial polarization (along the direction of the load). The behavior of the transverse wave velocity change curve is identical to the transverse deformation of the sample. At the same time, the sensitivity of transverse waves to mechanical stresses is maximal due to the coincidence with the direction of the applied load. The greatest sensitivity to stress is characteristic of samples #1 and #3. It should be noted that in the transition from the elastic deformation zone to the plastic deformation zone there is nonlinearity in the behavior of the curve, while the acoustoelasticity coefficients increase. The change in the velocity of radially polarized longitudinal waves is practically unchanged (within the measurement error). The values of acoustoelastic coefficients of transverse waves for the studied samples in the elastic and plastic regions are summarized in Table 3.
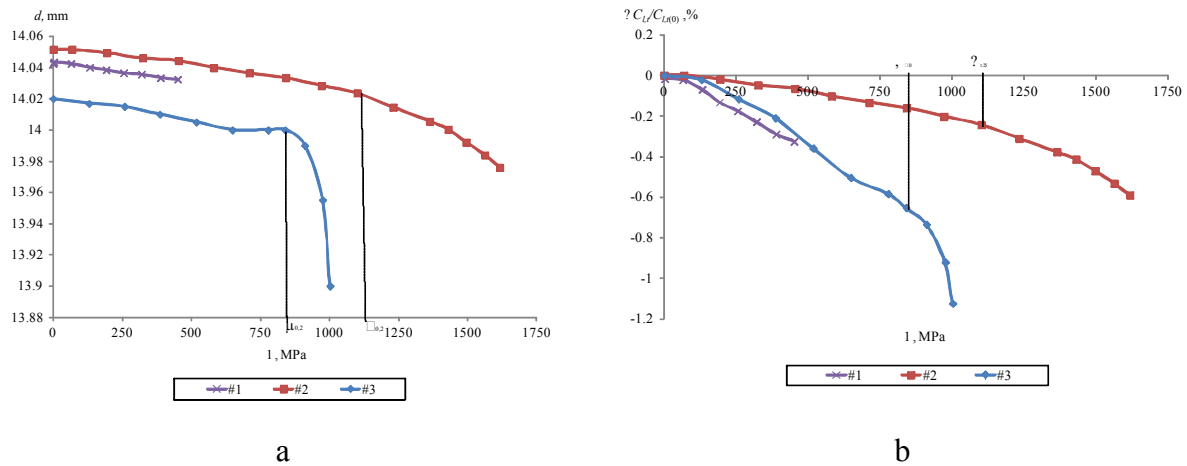

Figure 6. Dependence of diameter of samples (a) and also their relative change of speed of a transverse wave (b) on loading

Table 3. Acoustoelastic velocity coefficients for transverse wave β,1/TPa

Sample number	For	
	Elastic deformation area	Yield area
#1	−6.2	−7.6
#2	−2.2	−6
#3	−5.8	−10,6

Table 4 presents the results of measuring the diameters and velocities of the volume waves at the time of full unloading and some time after the tensile experiment (the process of "recovery" of the sample). There is a slight increase in the diameter for the samples #1 and #2 (within 0.07 %) with an unexpressed yield point in the region. For the sample #3 with a strongly marked yield point, the largest increase in diameter (within 0.5 %) is observed due to stress relief during the "recovery". Note that the velocities of the longitudinal waves do not

change significantly (0.05–0.1%), while the change in the velocity of the transverse waves reaches 0.5 %, and the Poisson's ratio is 1 % for the sample #2.

The curves illustrating the change in the Poisson's ratio with increasing load and its decrease during unloading, as well as its distribution along the length of the studied samples after the process of "recovery" of the sample are shown in Figure 7. There is a linear increase in the Poisson's ratio with an increase in the tensile load, which is least expressed for the #2 sample obtained by quenching, and more expressed for the #1 and #3 samples after normalization and high tempering.

It should be noted that the distribution of the Poisson's ratio along the length of the sample after removal of the load and subsequent "recovery" is sufficiently uneven and reaches 0.5 % for the hardened sample #2 and 0.35 % for samples #1 and #3. The latter indicates a significant uneven distribution of the stress-strain state, especially under plastic deformation.

Table 4. Diameters, velocities of volume waves and Poisson's ratios of the studied samples after load removal and after "recovery"

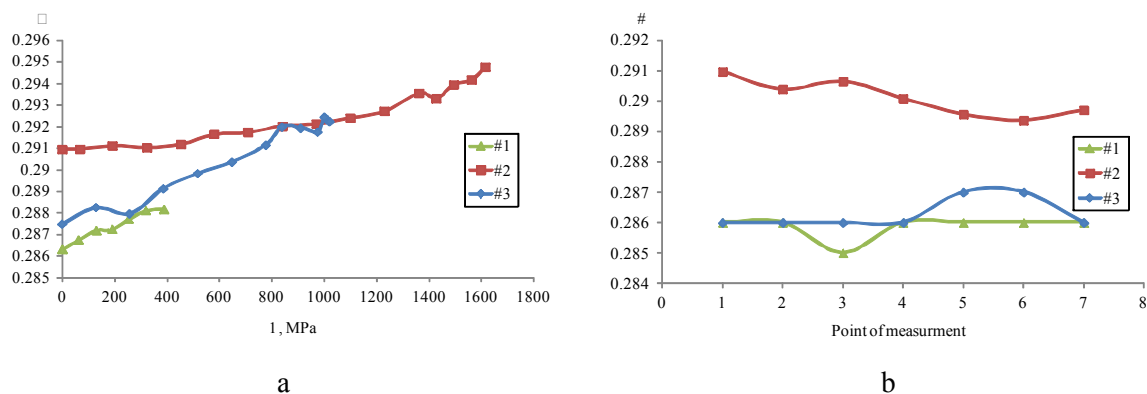| Sample number	at the end of tensioning				after "recovery"			
	d, mm	C_l, m/s	C_t, m/s	ν	d, mm	C_l, m/s	C_t, m/s	ν
#1	14.01	5934	3250	0.286	14.02	5937	3251	0.286
#2	14.00	5880	3183	0.293	14.01	5885	3200	0.290
#3	13.88	5904	3224	0.287	13.95	5910	3235	0.286

Figure 7. The dependence of the Poisson's ratio on the load (a) and its distribution along the length of the test sample after loading (b)

RESULTS

Thus, the developed non-contact EMAT-technology is a thin tool in evaluating the structural and stress-strain state of the bar. The conducted studies have shown the possibility of using the following structural-sensitive factors for the structuroscopy and evaluation of the stress-strain state of steel bars: absolute values of longitudinal and transverse velocities and Poisson's ratio, their change in the process of mechanical loading, and uneven distribution along the length of the sample and acoustoelastic velocity coefficients.

Due to the detuning from the quality of the acoustic contact and the possibility of obtaining a series of multiple reflections, high accuracy, reproducibility and reliability of acoustic structure detection methods are ensured.

It is shown that depending on the type of heat treatment, the velocities of transverse waves vary in the range of 1 %, longitudinal waves – 2 %, and the Poisson's ratio – 1.7 %.

The acoustoelasticity coefficients for transverse wave velocity for the sample in the quenched state were −5.8 1/TPa in the elastic deformation region and −10.6 1/TPa in the yield region.

REFERENCES

1, Gorkunov, E. S., Zadvorkin, S. M., Goruleva, L. S., Makarov, A. V., & Pecherkina, N. L. (2017). Structure and mechanical properties of a high-carbon steel subjected to severe deformation. *The Physics of Metals and Metallography*, *118*, 1006–1014. doi: 10.1134/S0031918X17100076

2. Gupta, B., Uchimoto, T., Ducharne, B., Sebald, G., Miyazaki, T., & Takagi, T. (2019). Magnetic incremental permeability non-destructive evaluation of 12 Cr-Mo-W-V steel creep test samples with varied ageing levels and thermal treatments. *NDT and E International 104*, 42–50. doi: 10.1016/j.ndteint.2019.03.006

3. Hu, B., & Yu, R. (2016). Variations in surface residual compressive stress and magnetic induction intensity of 304 stainless steel *NDT and E International 80*, 1–5. doi: 10.1016/j.ndteint.2016.02.003

4. Ding, S., Tian, G., & Sutthaweekul, R. (2019). Non-destructive hardness prediction for 18CrNiMo7-6 steel based on feature selection and fusion of Magnetic Barkhausen Noise. *NDT and E International 107*, 102138. doi: 10.1016/j.ndteint.2019.102138

5. Ivanova, Y., Partalin, T., & Pashkuleva, D. (2017). Acoustic investigations of the steel samples deformation during the tensile. *Russian Journal of Nondestructive Testing*, *53*(1), 39–50. doi: 10.1134/S1061830917010077

6. Mohammadi, M., & Fesharaki, J. J. (2019). Determination of acoustoelastic/acoustoplastic constants to measure stress in elastic/plastic limits by using LCR wave. *NDT and E International 104*, 69–76. doi: 10.1016/j.ndteint.2019.04.003

7. Zuev, L. B., Barannikova, S. A., Li, Y. V., & Zharmukhambetova, A. (2018). On numerical estimates of the parameters of localized plasticity during metal tension. *Tomsk State University Journal of Mathematics and Mechanics*, *53*, 83–94. doi: 10.17223/19988621/53/8 (in Russian).

8. Gutiérrez-Vargas, G., Ruiz, A., Kim, J.-Y., & Jacobs, L. J. (2018). Characterization of thermal embrittlement in 2507 super duplex stainless steel using nonlinear acoustic effects. *NDT and E International 94*, 101–108. doi: 10.1016/j.ndteint.2017.12.004

9. Wang, W., Xu, C., Zhang, Y., Zhou, Y., Meng, S., & Deng, Y. (2018). An improved ultrasonic method for plane stress measurement using critically refracted longitudinal waves. *NDT and E International 99*, 117–122. doi: 10.1016/j.ndteint.2018.07.006

10. Smirnov, A. N., Knyazkov, V. L., Abakov, N. V., Ozhiganov, E. A., Koneva, N. A., & Popova, N. A. (2018). Acoustic evaluation of the stress-strained state of welded carbon steel joints after different modes of heat input. *Russian Journal of Nondestructive Testing*, *54*(1), 37–43. doi: 10.1134/S1061830918010072

11. Muravev, V. V., & Tapkov, K. A. (2017). Evaluation of strain-stress state of the rails in the production. *Devices and Methods of Measurements, 8*(3), 263–270. doi: 10.21122/2220-9506-2017-8-3-263-270

12. Murav'ev, V. V., Volkova, L. V., Platunov, A. V., Buldakova, I. V., & Gushchina, L. V. (2018). Investigations of the structural and strain-stress state of the rails of current production by the acoustic elasticity method. *Bulletin of Kalashnikov ISTU*, *21*(2), 13–23. doi: 10.22213/2413-1172-2018-2-13-23 (in Russian).

13. Muravev, V. V., Volkova, L. V., Platunov, A. V., & Kulikov, V. A. (2016). An electromagnetic-acoustic method for studying stress-strain states of rails. *Russian Journal of Nondestructive Testing*, *52*(7), 370–376. doi: 10.1134/S1061830916070044

14. Gonchar, A. V., Mishakin, V. V., Klyushnikov, V. A., & Kurashkin, K. V. (2017). Variation of elastic characteristics of metastable austenite steel under cycling straining. Technical Physics. *The Russian Journal of Applied Physics*, *62*(4), 537–541. doi: 10.1134/S1063784217040089

15. Mishakin, V. V., Klyushnikov, V. A., & Gonchar, A. V. (2015). Relation between the deformation energy and the Poisson ratio during cyclic loading of austenitic steel. *Technical Physics. The Russian Journal of Applied Physics*, *60*(5), 665–668. doi: 10.1134/S1063784215050163

16. Babkin, S. E. (2015). The determination of the Poisson ratio for ferromagnetic materials using the EMA method. *Russian Journal of Nondestructive Testing*, *51*(5), 303–307. doi: 10.1134/S1061830915050022

17. Murav'ev, V. V., Murav'eva, O. V., & Volkova, L. V. (2016). Influence of the mechanical anisotropy of thin steel sheets on the parameters of Lamb waves. *Steel in Translation*, *46*(10), 752–756. doi: 10.3103/S0967091216100077

18. Murav'eva, O. V., & Murav'ev, V. V. (2016). Methodological peculiarities of using SH- and Lamb waves when assessing the anisotropy of properties of flats. *Russian Journal of Nondestructive Testing*, *52*(7), 363–369. doi: 10.1134/S1061830916070056

19. Volkova, L. V., Murav'eva, O. V., Murav'ev, V. V., & Buldakova, I. V. (2019). Device and methods for measuring of acoustic anisotropy and the residual stress in the main gas pipelines metal. *Devices and Methods of Measurements*, *10*(1), 42–52. doi: 10.1134/S1061830916070056

20. Tapkov, K.A. (2018). Strain stress modeling of differential hardening rails. *Intelligent Systems in Manufacturing 16*(2), 78–83 (in Russian). doi: 10.22213/2410-9304-2018-2-78-83

21. Muravev, V. V., Volkova, L. V., Platunov, A. V., Buldakova, I. V., & Gushchina, L. V. (2018). Investigations of the structural and strain-stress state of the rails of current production by the acoustic elasticity method. *Bulletin of Kalashnikov ISTU 21*(2), 13–23 (in Russian). doi: 10.22213/2413-1172-2018-2-13-23

22. Murav'eva, O. V., & Zorin, V. A. (2017). The multiple shadow method applied to testing cylindrical objects with Rayleigh waves. *Russian Journal of Nondestructive Testing*, *53*(5), 337–342. doi: 10.1134/S1061830917050059

23. Murav'ev, V. V., Murav'eva, O. V., & Petrov, K. V. (2017). Connection between the properties of 40KH-steel bar stock and the speed of bulk and rayleigh waves. *Russian Journal of Nondestructive Testing*, *53*(8), 560–567. doi: 10.1134/S1061830917080046

24. Muravev V. V., Zlobin D. V., & Platunov A. V. (2017). Device for studies on acoustic-elastic characteristics of thin wires. *Journal of Instrument Engineering*, *60*(6), 572–577. doi: 10.17586/0021-3454-2017-60-6-572-577.

25. Strizhak, V. A., Khasanov, R. R., & Pryakhin, A. V. (2018). Features of excitation of an electromagnetic acoustic transducer under a waveguide method of testing. *Bulletin of Kalashnikov ISTU 21*(2), 159–166 (in Russian). doi: 10.22213/2413-1172-2018-2-159-166

26. Petrov, K. V., & Murav'eva, O. V. Russian Federation Patent for useful model No. 179018 (April 25, 2018).

27. Strizhak, V. A., Pryakhin, A. V., Hasanov R. R., & Efremov, A. B. (2017). Hardware-software complex for rods control by mirror-shadow method using multiple reflections. *Izvestiya vysshikh uchebnykh zavedeniy. Priborostroenie 60*(6), 565–571 (in Russian). doi: 10.17586/0021-3454-2017-60-6-565-571

The Propagation of Symmetric Lamb Wave in the Hollow Cylinder

Yu. V. Myshkin [1, 2], O. V. Murav'eva [1, 3], A. A. Fotina [1], T. S. Chukhlanceva [1]

[1] Department of Instruments and Techniques of Measurement, Testing, Diagnostics, Kalashnikov Izhevsk State Technical University, Izhevsk, Russian Federation
[2] IntroScan Technology JSC, Chaykovsky, Perm Krai, Russian Federation
[3] Udmurt Federal Research Center of Ural Branch of Russian Academy of Sciences, Izhevsk, Russian Federation
E-mail: [1] mubm@yandex.ru

Abstract. The article presents studies of the propagation velocity of the symmetric Lamb wave in a pipe with a diameter of 247 mm and a wall thickness of 8.4 mm. Studies include finite element modeling of the wave propagation process and an experiment using piezoelectric transducers with dry point contact based on sounding 600 mm of pipe at a frequency of 50 kHz. Plots of displacement components at wave propagation in the axial and circumferential directions are obtained, which show the prevalence of the longitudinal component over the vertical shear component from 6 to 30 times. The difference in the wave velocity at its propagation in the axial and circumferential directions was established, which amounted to 290 m/s. The simulation results are in satisfactory agreement with the experimental data.

Keywords: Lamb wave, hollow cylinder, wave velocity, finite element method, dry point contact, guided wave testing, geometric dispersion.

INTRODUCTION

In acoustic waveguide testing, guided waves propagating along the products are used: Pochhammer, Lamb, SH-waves [1–9]. Typically, these types of waves used in the low frequency range, are capable of traveling up to 200 m from the point of excitation, and do not require scanning [5, 9]. Linearly extended objects (rails, rods, pipes, etc.) [1–6] and flat products limited by the environment (plates, sheets, films, etc.) [9–13] can be used as testing products.

From literary sources [5, 8, 9] it is known that from the fundamental modes of guided waves, the symmetric Lamb wave has one and a half times less attenuation compared to the SH wave and three times as compared to the antisymmetric Lamb wave. In addition, the use of the symmetric Lamb wave makes it possible to detect longitudinally oriented defects whose dimensions are comparable to the wavelength, and in the case of using the multiple reflection method, with dimensions by an order of magnitude less than the wavelength. Nevertheless,

the symmetrical Lamb wave is less sensitive to defects in comparison with other types of waves at a given frequency [1–5, 8].

As a rule, Lamb waves are used in the frequency range with a low dispersion of the excited mode. For this, dispersion curves are calculated for the modes of the desired wave types using specialized software [5, 9, 11, 13–15]. Accounting for velocity dispersion allows to decipher the patterns of received signals, conduct thickness measurement of the studied products and limit the frequency range at nondestructive testing. The most commonly used modes for flaw detection of pipelines and plates, S0 and L(0,2) in the region of minimal dispersion, allow detecting corrosion defects, cracks, dents, etc. [10–14, 16, 17]

It is known that the main quantities that determine the dispersion of velocity are the geometric dimensions of the product, properties and parameters of the material structure [9]. Given the uniformity of these properties, the velocity can be calculated quite accurately using dispersion curves. Inhomogeneity in the geometry and properties of the material [18–19] as well as defects lead to an additional change in the propagation velocity of guided waves. As such an inhomogeneity, the cylindrical surface of a hollow cylinder can be considered as a special case of a plate with a curved surface, and the phenomenon of a change in velocity on geometric inhomogeneities is called geometric dispersion.

The main studies in the field of guided wave propagation are related to the influence of bends and complex pipe geometry [15, 20], alternative methods of wave excitation and reception [16, 21–23], their use in tomography systems [17, 24], development of systems for excitation and receiving waves in circumferential direction of the pipe [16, 22–23, 25–28], the possibilities of increasing sensitivity due to wave focusing technique [7, 29], the influence of defects on mode conversion [14, 23, 27], the possibilities of implementing excitation and reception of various modes and types of waves [29–33]. In most works, with the exception of Viktorov's works for a surface wave [34], there is no information on the difference in the propagation velocity of guided waves in the axial and circumferential directions on a cylindrical surface, which can be significant for a small diameter and a large wall thickness of pipe.

The article presents studies of the geometric dispersion of the propagation velocity of the symmetric Lamb wave in a hollow steel cylinder with an external diameter of 247 mm and a wall thickness of 8.4 mm at a frequency of 200 kHz and a sounding base of 300 mm.

DISPERSION CURVES

The main characteristic of guided waves is the velocity dispersion, which can be calculated using the Pochhammer-Chree dispersion equations. Figure 1 shows the dispersion curves calculated for a plate and a hollow cylinder in the Elastic Waveguide Tracer software product. As input parameters for the calculation, the geometric dimensions of the products (plate and pipe), its elastic and physical properties, presented in table 1, were used.

From the presented dependences, one can establish the existence of lower symmetric S0, S1 and antisymmetric A0, A1 modes of the Lamb wave and the horizontally polarized shear wave SH0 in the frequency range up to 300 kHz. In the hollow cylinder at the same frequencies, there must exist longitudinal L(0,1), L(0,2), flexural F(1,m), F(n,1) and torsional T(0,1) waves.

At the operating frequency of 50 kHz of the transducer used in this work, fundamental symmetric S0, antisymmetric A0 Lamb wave, and the horizontally polarized shear wave SH0 are excited. In this case, longitudinal L(0,1), L(0,2), flexural F(1,m), F(n,1) and torsional T(0,1) waves are excited in the pipe, the velocity of which is comparable to the velocity of the Lamb waves and the SH-wave. The calculated velocities for these modes are presented in table 2.

To excite the symmetric Lamb wave, one main component of the displacements is required, which is directed along the wave propagation, while a horizontally polarized shear wave will propagate in the perpendicular direction and possessing all three components of the antisymmetric Lamb wave will propagate in all directions.
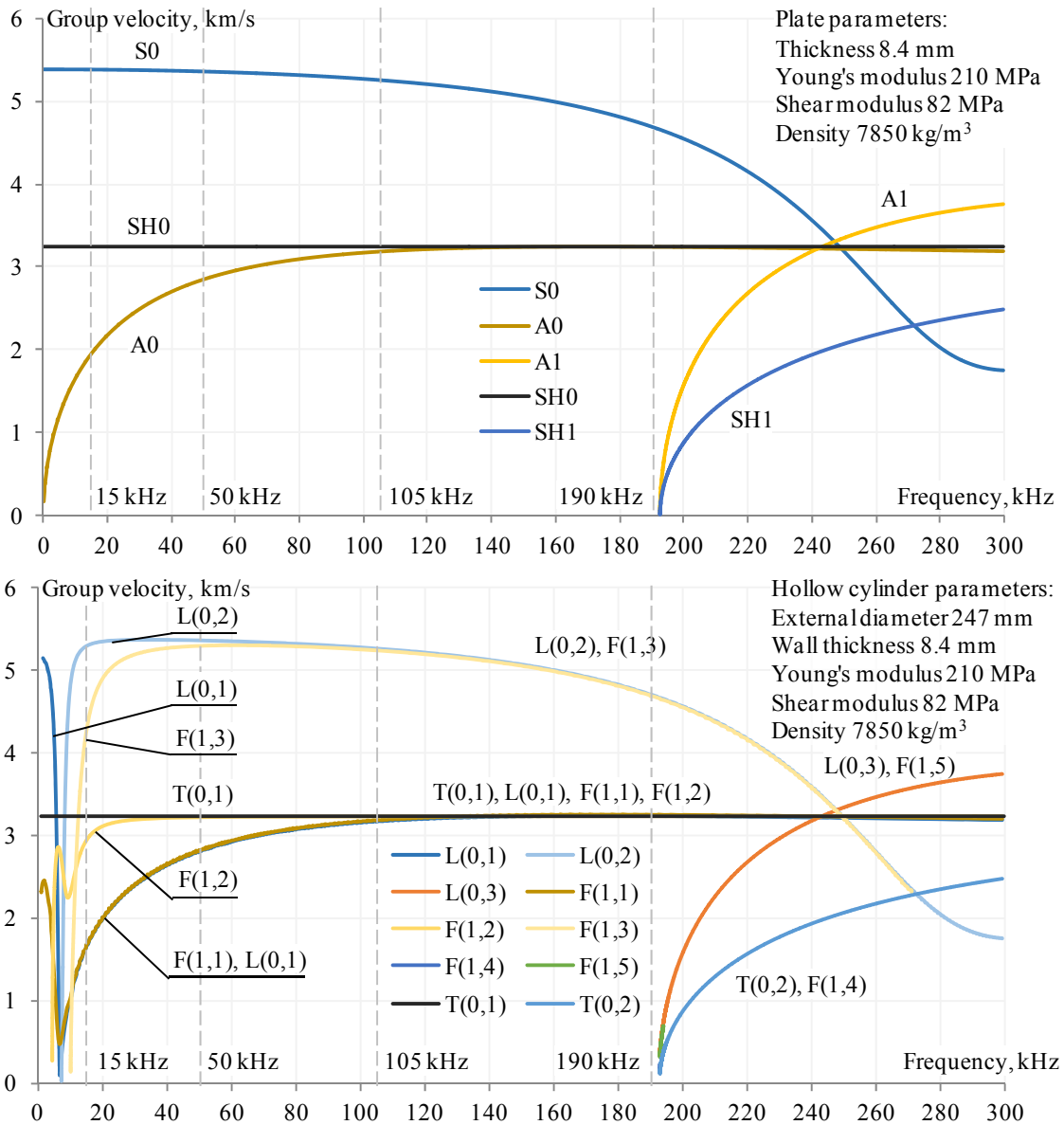

Figure 1. Dispersion curves of group velocities in a steel plate (a) and an steel hollow cylinder (b): S – symmetrical mode of Lamb wave, A – antisymmetrical mode of Lamb wave, SH – horizontally polarized shear wave, L – longitudinal wave, F – flexural wave, T – torsional wave

Table 1. Geometric and material properties

Parameter	Value	Dimension	Parameter	Value	Dimension
External radius	123.5	mm	Shear modulus, G	82	GPa
Wall thickness	8.4	mm	Poisson's ratio, η	0.28	–
Internal radius	115.1	mm	Shear wave velocity, C	3232	m/s
Young's modulus, E	210	GPa	Density, ρ	7850	kg/m^3

Table 2. Group velocities at the frequency of 50 kHz

Mode in plate	Group velocity (m/s)	Mode in pipe	Group velocity (m/s)
A0	2825	F(1,1), F(1,2), F(1,3)	2778, 5300, 3218
S0	5365	L(0,1), L(0,2)	2785, 5362
SH0	3242	T(0,1)	3232

FINITE ELEMENT PREDICTION

The model for studying the propagation of the symmetric Lamb wave (Figure 2) included a pipe section with length of 1 m, an external diameter of 246.7 mm and an average wall thickness of 8.4 mm. The geometric parameters, as well as the elastic and physical properties of the pipe material are presented in table 3.
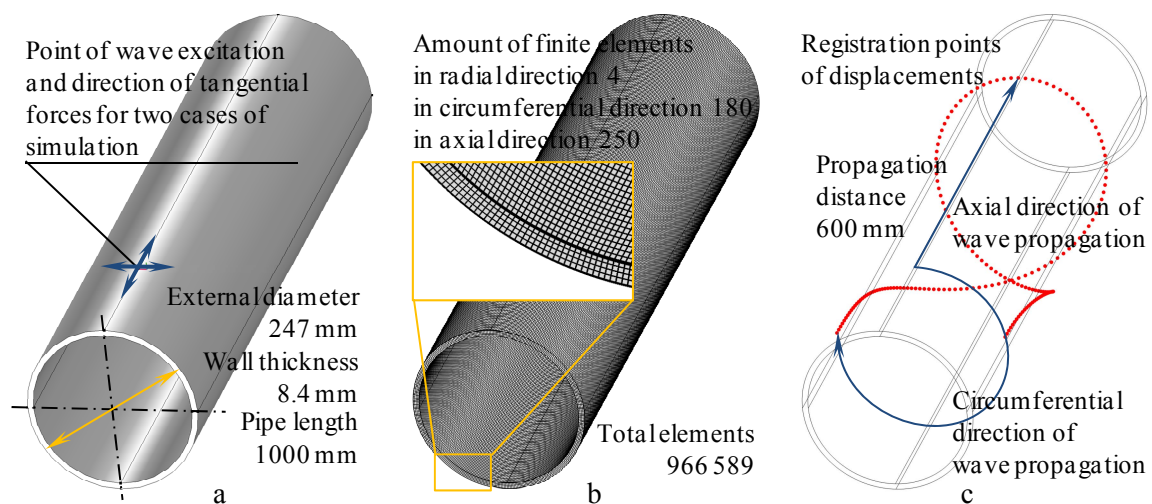

Figure 2. 3D model of the pipe (a), finite element mesh (b) and locations of registrations points (c): pipe length 1.0 m, point of application of tangential force is located at a distance of 0.2 m from the pipe end

Table 3. Model parameters and properties

Parameter	Value	Dimension	Parameter	Value	Dimension
Poisson's ratio, η	0.281	–	External diameter of cylinder, D_{ext}	246.7	mm
Shear wave velocity, C	3250	m/s	Internal diameter of cylinder, D_{int}	229.9	mm
Density, ρ	7850	kg/m^3	Cylinder length, L	1000	mm
Shear modulus, G	$\rho C^2 = 82.9$	GPa	Frequency, f	50	kHz
Young's modulus, E	$2G(1 + \eta) = 212.4$	GPa	Time step, Δt	100	ns

The boundary condition *Point Load* was applied at a distance of 200 mm from the pipe end at a point on the external cylindrical surface in the form of a tangential force action, the direction of which was specified in two ways: in the axial and circumferential directions. The shape of tangential force is shown in Figure 3.

Elastic oscillations were recorded at a distance of 600 mm from the point of excitation at angles of 0-360 degrees in increments of 1 degree relative to the generatrix of the pipe, taking

into account displacements corresponding to the wave oscillation plot. As an example, Figure 4 shows the recorded oscillations when the wave propagation path deviates from the generatrix of the pipe by 20 degrees. The result shows the signals of the direct symmetric Lamb wave and reflected from the pipe end, merging with the through signal of the symmetric Lamb wave, and the through signal of the horizontally polarized shear wave.
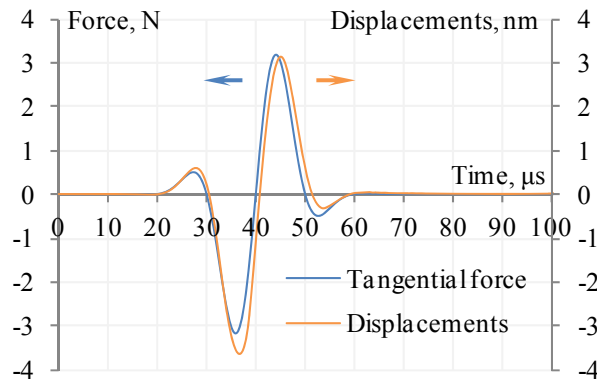

Figure 3. Pulse of the tangential force action and the shape of the elastic displacements pulse (calculated in the program): arrows indicate the correspondence of the graphs to the axes
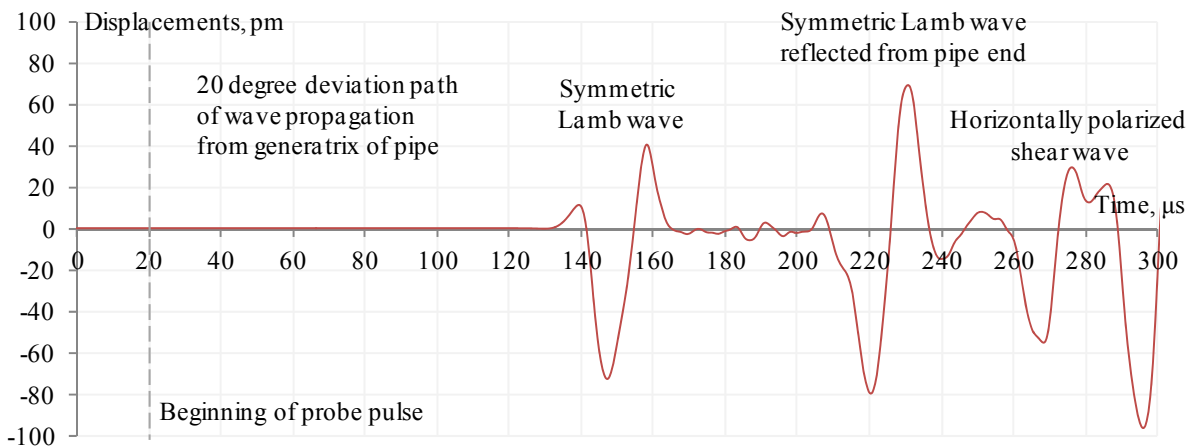

Figure 4. The signal received at a point at a distance of 600 mm from the excitation point when the wave propagation path deviates from the generatrix of the pipe by 20 degrees

The model was divided into finite elements based on the criterion of the minimum number of elements per wavelength necessary to obtain a satisfactory simulation result, which should be at least 4. Thus, taking into account the calculated value of the propagation velocity of the symmetric Lamb wave, the maximum size of the finite elements was 4 mm, and their total number according to the results of meshing is 966 589.

The time step was selected based on the Courant-Friedrichs-Levy criterion with a parameter for solving the wave equations of 0.1 and amounted to 20 ns. Thus, taking into account the distance traveled by the wave, the total number of iteration steps in time was 3076.

The simulation results in the form of a distribution of the axial component of displacements at a time of 50 μs and then with a step of 50 μs are presented in Figure 5. The distributions also show a symmetric Lamb wave and the SH wave propagating in mutually perpendicular directions.

The directions of displacements in the symmetric Lamb wave at its propagation in the axial and circumferential directions are presented in Figure 6 and Figure 7, respectively. In addition to the main axial component, the wave has a radial component that reaches its maximum at the moment of the change of the oscillation phase. A similar character of the oscillations is observed on the displacement diagrams (Figure 8) obtained at the moment of maximum displacements in the wave, at the moment of the phase change of the oscillations, and the average value of the displacements over the wave period. In this case, the ratio of the longitudinal component of the displacements to the vertical shear component is the greater, the closer the wave propagation path to the generatrix of the pipe, which varies from 6 to 30.

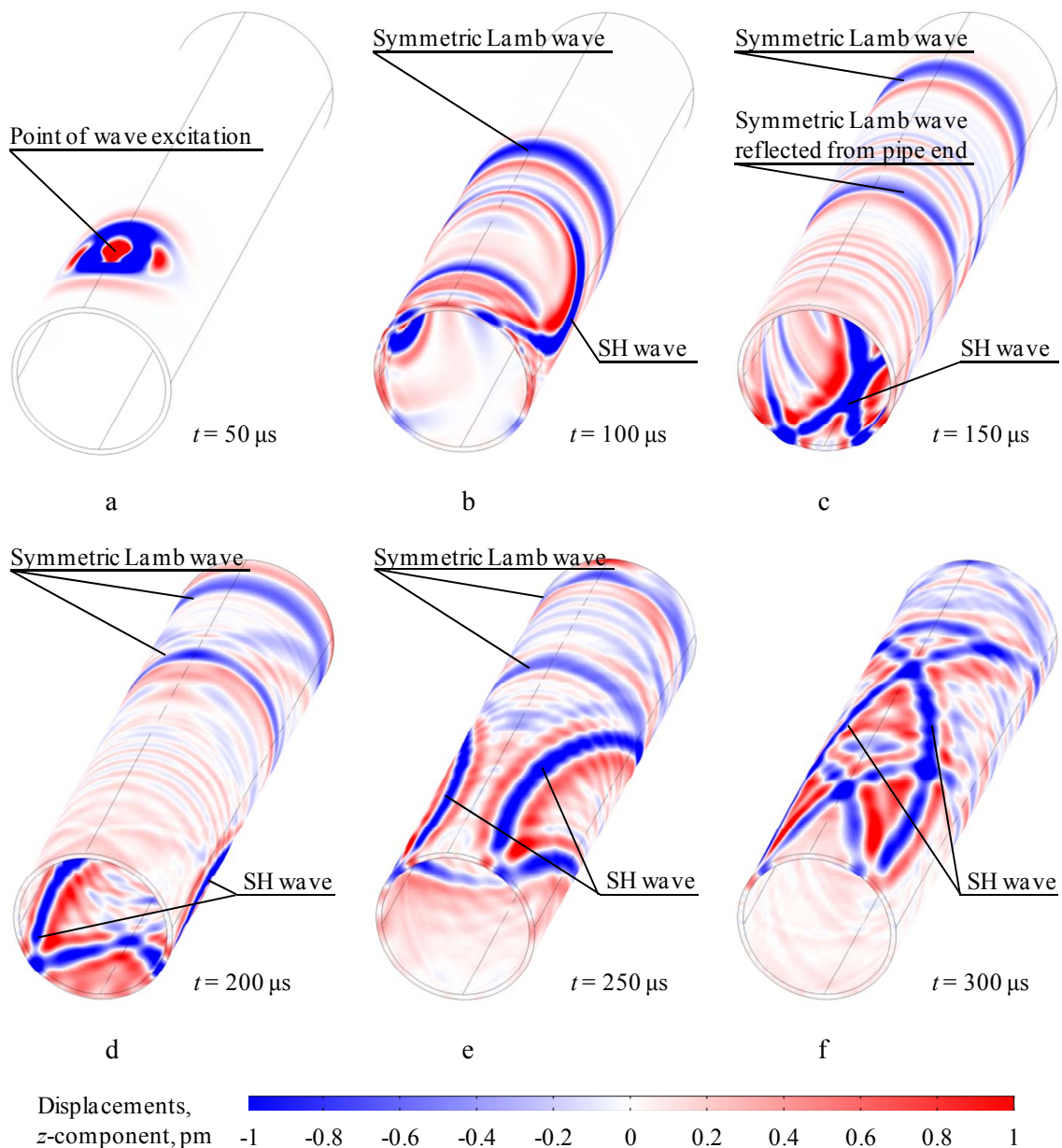**Figure 5.** Distribution of displacements on the surface of the pipe at different points in time, $t = 50\ \mu s$ (a), $t = 100\ \mu s$ (b), $t = 150\ \mu s$ (c), $t = 200\ \mu s$ (d), $t = 250\ \mu s$ (e), $t = 300\ \mu s$ (f): light wave graduation is used, the dark blue color corresponds to the maximum negative displacements, the dark red corresponds to the maximum positive displacements (approximately 50 pm)
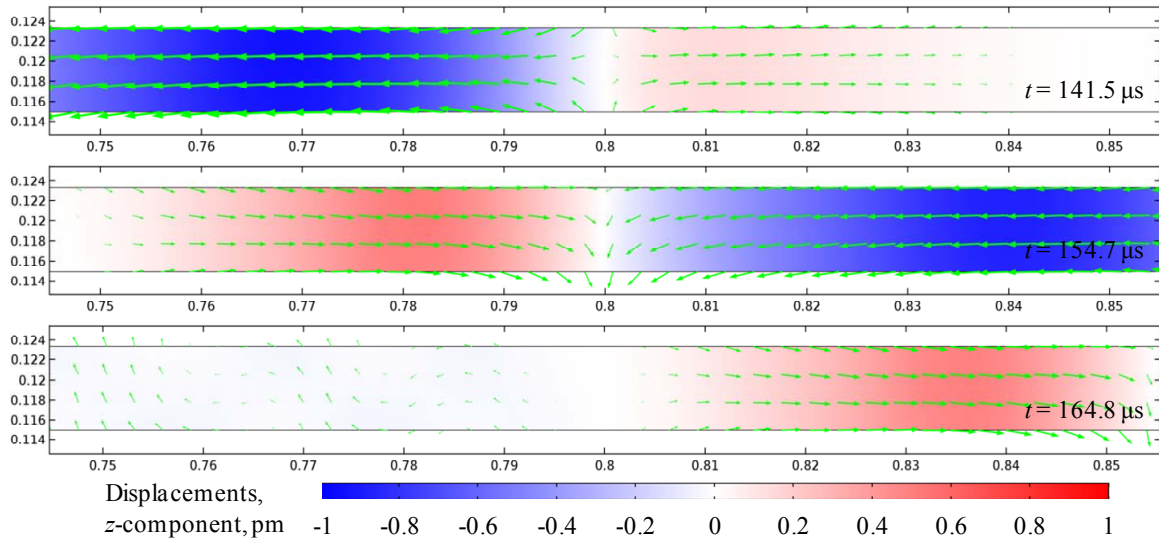
Figure 6. Longitudinal sectional distribution of displacements near the registration point at different points in time, $t = 141.5$ μs (corresponds to the beginning of the pulse), $t = 154.7$ μs (a half period of the pulse), $t = 164.8$ μs (the whole period of the pulse): light wave graduation is used, the dark blue color corresponds to the maximum negative displacements, the dark red corresponds to the maximum positive displacements (approximately 50 pm)

Figure 7. Cross sectional distribution of displacements near the left side of the pipe at different points in time, $t = 66.3$ μs (corresponds to the beginning of the pulse), $t = 76.2$ μs (a half period of the pulse), $t = 88.6$ μs (the whole period of the pulse): light wave graduation is used, the dark blue color corresponds to the maximum negative displacements, the dark red corresponds to the maximum positive displacements (approximately 50 pm)
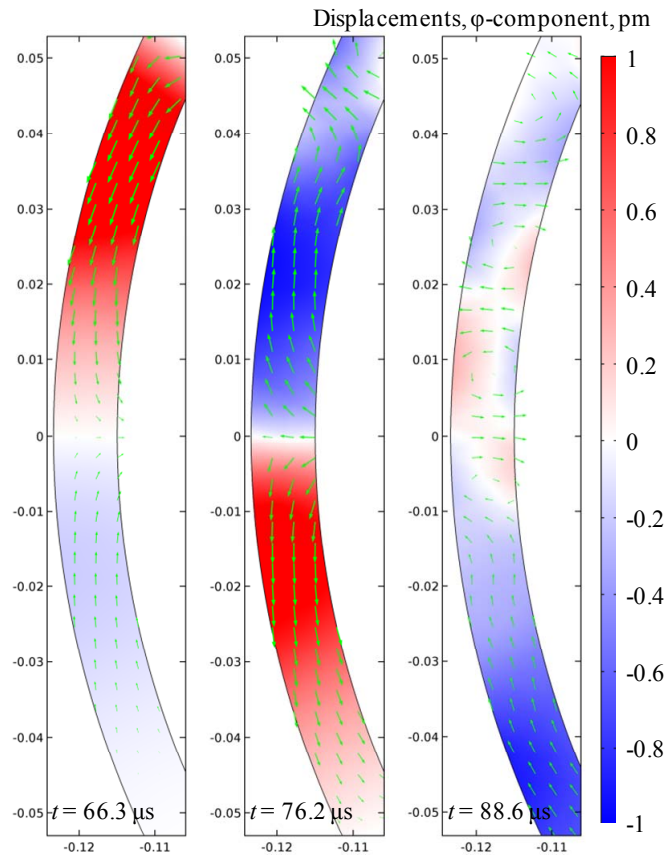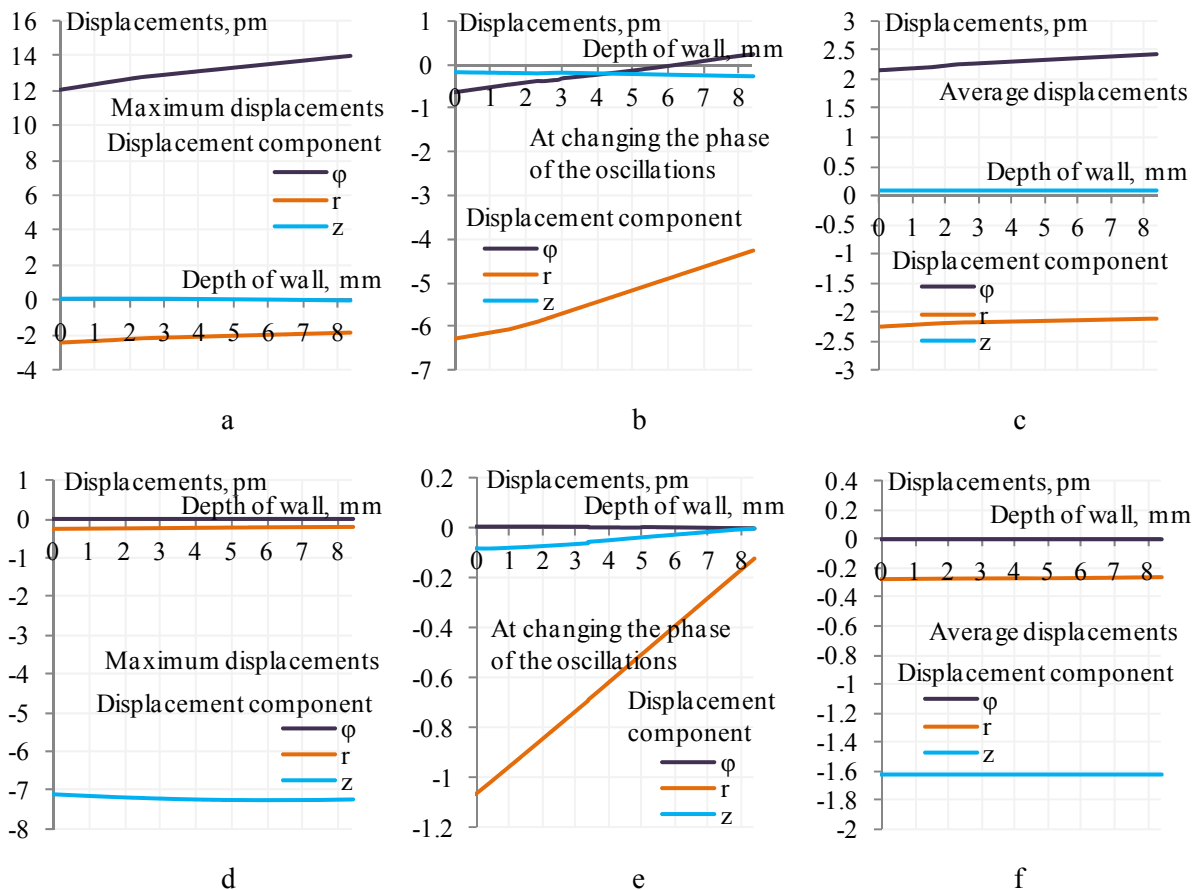
91

Figure 8. Displacement diagrams in cross section (a, b, c) and longitudinal section (d, e, f) at maximum displacements (a, d) at changing the phase of the oscillations (b,e) and at average displacements (c, f)

EXPERIMENTAL SETUP

To confirm the simulation results, an experiment was performed and conducted. The experimental setup is similar to that described in [35] and is shown in Figure 9. The setup includes a pipe, two low-frequency piezoelectric transducers with a dry point contact for studying the wave propagation velocity, a high-frequency piezoelectric transducer for thickness measurement, and a DIO-1000 ultrasonic flaw detector. The symmetric Lamb wave was excited at a frequency of 50 kHz by a piezoelectric transducer with a dry point contact at a distance of 200 mm from the pipe end from the outer cylindrical surface of the pipe and was received by a second similar transducer at a distance of 600 mm from the excitation point at angles of deviation of the wave propagation path from the pipe generatrix 0-180 degrees in increments of 1 degree. The wave was excited and received mainly due to shear stresses directed along its propagation and provided by the orientation of the transducers. Excitation was carried out on both sides of the pipe ends.

In addition to the wave propagation velocity, the pipe wall thickness was measured according to the scheme shown in Figure 9b. To do this, it is used a transducer at a frequency of 5 MHz, which was installed on the outer cylindrical surface of the pipe at 234 points with a step along the generatrix of 50 mm and an envelope of 20 degrees (approximately 43 mm). For increased accuracy, the pipe wall thickness was calculated from the fifth bottom echo pulse.
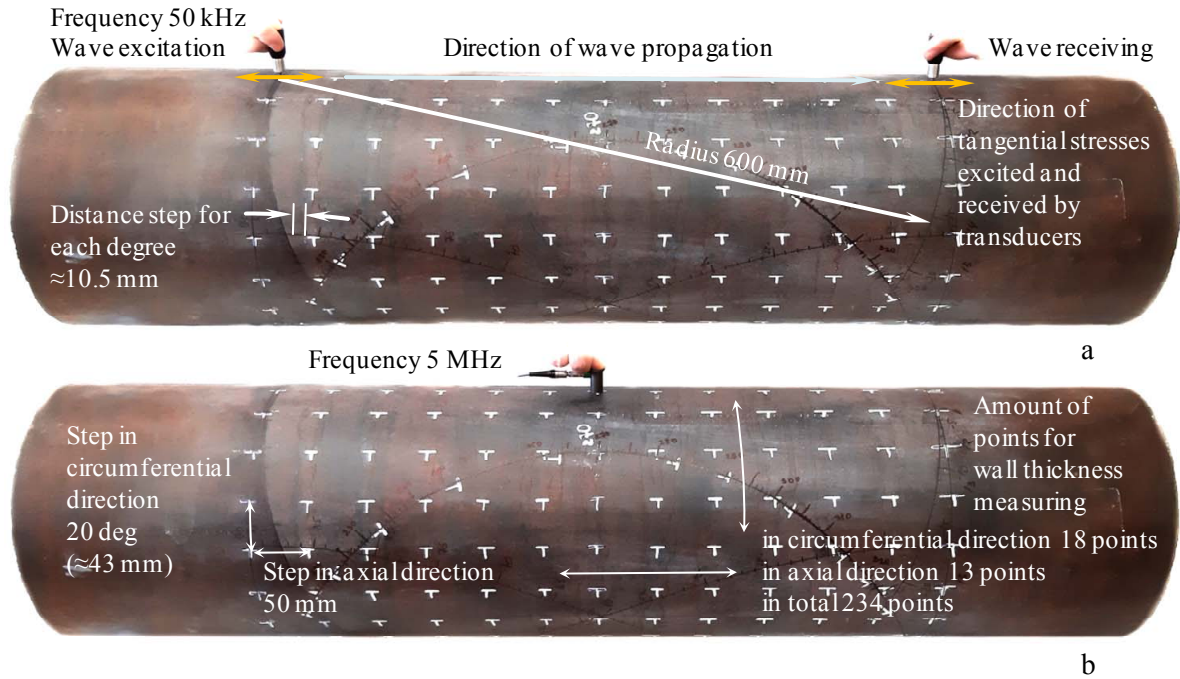
Figure 9. The experimental setup: for measuring the propagation velocity
of the symmetric Lamb wave (a), for measuring the wall thickness (b)

RESULTS AND DISCUSSION

The results of measuring the wall thickness of the pipe are presented in Figure 10. In the presented distribution there is a section of heterogeneity along the wall thickness, indicating the presence of a longitudinal weld. The remaining values have small deviations within 0.15 mm from the average value of the pipe wall thickness, which amounted to 8.43 mm. The total measurement error of the pipe wall thickness was 0.02 mm.

Figure 11 shows the dependences of the propagation velocity of the symmetric Lamb wave on the angle of deviation of the wave propagation path in the polar coordinate system. For clarity, the influence on the wave propagation velocity in the figures also shows maps of the distribution of the pipe wall thickness. The dependency graphs are characterized by an increase in values in the circumferential direction (90 and 270 degrees), reaching 5615 m/s, which is 250 m/s more than the calculated theoretical velocity values without taking into account geometric anisotropy. In the direction along the generatrix, the average value of the velocity within 20 degrees does not differ from the theoretical one and is equal to the propagation velocity in the plate. Further, with an increase in the angle by 1 degree, the velocity increases by 2.5 m/s to 80 degrees. Thus, the velocity of the symmetric Lamb wave varies from 5325 to 5615 m/s with a total range of 290 m/s.

The spikes in the graph in velocity are related to the inaccurate arrangement of the transducer, the quality of the acoustic contact, the unevenness in the wall thickness and the heterogeneity of the properties of the pipe material. Taking these factors into account, the total velocity calculation error was 20 m/s.

In the range of angles of deviation of the wave propagation path from the generatrix of the pipe by 20 degrees, a maximum in wave propagation velocity is observed, which exceeds the average velocity by 20 m/s and is associated with the presence of bulge in the studied section of the pipe.
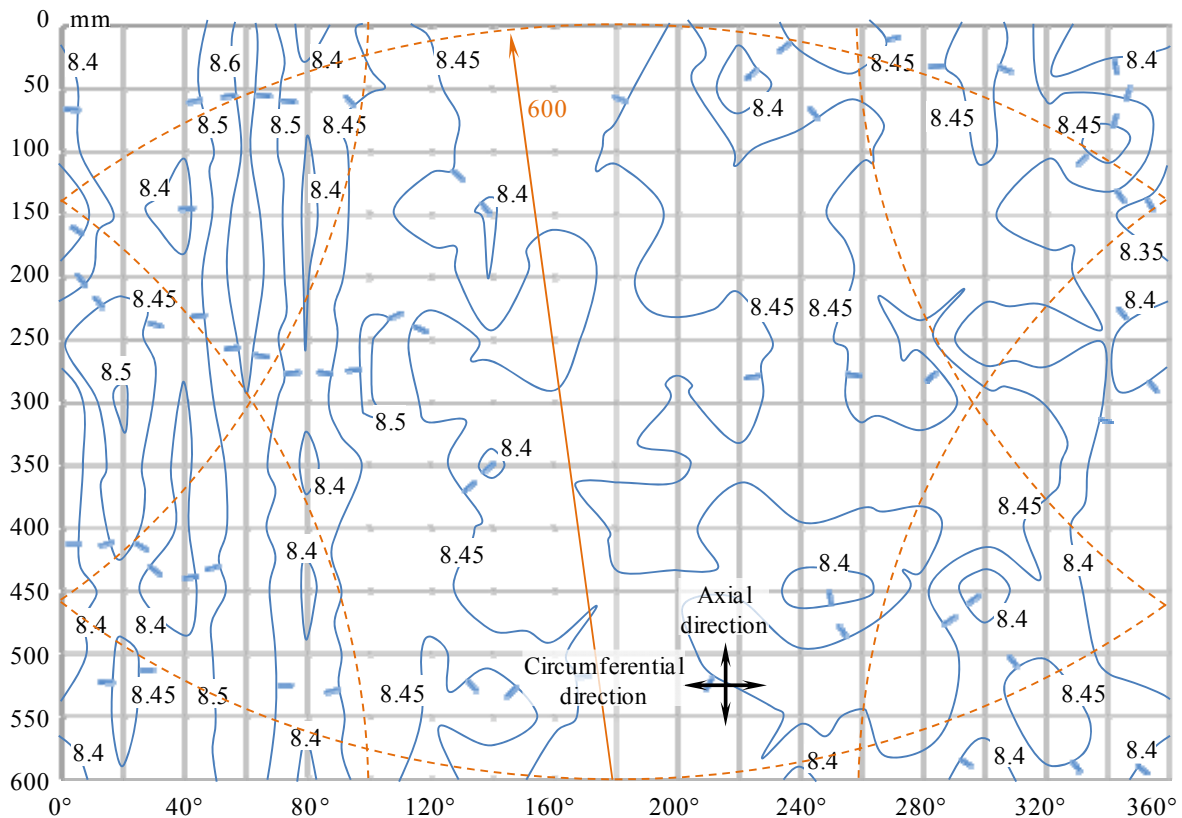
Figure 10. Results of thickness measurement: solid lines indicate the lines of the contour with the same value of the wall thickness; the dashed line corresponds to the location of the transducer for measuring the propagation velocity of the symmetric Lamb wave

CONCLUSIONS

Thus, according to the results of studies of the propagation of the symmetric Lamb wave in a hollow cylinder, the following conclusions can be drawn.

• The velocity of the wave depends on the direction of its propagation (the phenomenon of geometric dispersion): in the circumferential direction, the velocity is greater than in the direction along the generatrix and for a pipe with a diameter of 247 mm, the velocity difference is 290 m/s.

• The pipe wall thickness affects the wave propagation velocity: the smaller the wall thickness, the lower the velocity.

• The ratio of the longitudinal displacement component to the vertical shear is greater, the closer the wave propagation path to the pipe generatrix, which can increase up to 5 times.

• Simulation results are in satisfactory agreement with experimental data.

The study results can be used to create and develop methods for monitoring the residual thickness of the pipe wall, taking into account the phenomenon of geometric dispersion in focusing algorithms, and analyzing and calculating the coordinates of a defect at guided wave testing.
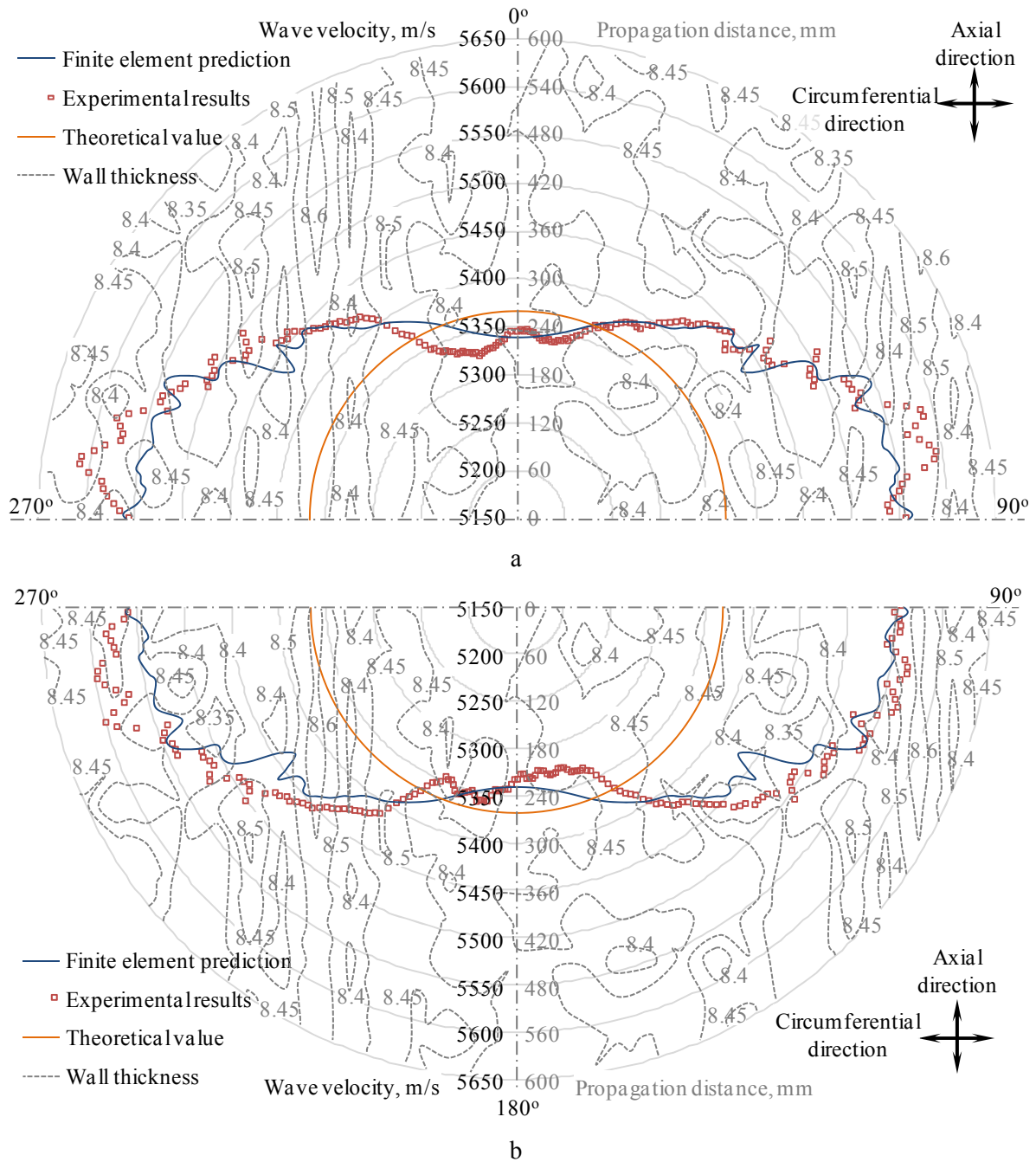
Figure 11. Dependence of symmetric Lamb wave on direction of the propagation in the hollow steel cylinder: left black scale (wave velocity) refers to experimental result, finite element prediction, and theoretical value; right gray scale (propagation distance) refers to wall thickness

ACKNOWLEDGEMENTS

REFERENCES

1. Zlobin, D. V., & Muravieva, O. V. (2012). Development features of electromagnetic acoustic defectoscopy equipment for bar iron using rod waves. *Bulletin of Kalashnikov ISTU,* (4), 099–104. (in Russian).

2. Strizhak, V. A., Hasanov, R. R., & Pryakhin, A. V. (2018). Features of excitation of an electromagnetic acoustic transducer under a waveguide method of testing. *Bulletin of Kalashnikov ISTU, 21*(2), 159–166. (in Russian). doi: 10.22213/2413-1172-2018-2-159-166

3. Muravyova, O. V., & Murashov, S. A. (2011). Use of torsional waves for detection of operational defects in pump rods and tubing. *Bulletin of Kalashnikov ISTU,* (2), 149–154. (in Russian).

4. Strizhak, V. A., Pryakhin, A. V., Khasanov, R. R., & Mkrtchyan, S. S. (2019). Flaw detection of composite rebar by acoustic wave guided technique. *Bulletin of Kalashnikov ISTU, 22*(1), 78–88. (in Russian). doi: 10.22213/2413-1172-2019-1-78-88

5. Myshkin, Y. V., & Muravieva, O. V. (2017). The features of the guided wave excitation and propagation at testing of pipes. *Journal of Physics: Conference Series, 881*(1), 012019. doi: 10.1088/1742-6596/881/1/012019

6. Evans, M., Lucas, A., & Ingram, I. (2018). The inspection of level crossing rails using guided waves. *Construction and Building Materials, 179,* 614–618. doi: 10.1016/j.conbuildmat.2018.05.178

7. Wu, J., Tang, Z., Lü, F., & Yang, K. (2018). Ultrasonic guided wave focusing in waveguides with constant irregular cross-sections. *Ultrasonics, 89,* 1-12. doi: 10.1016/j.ultras.2018.04.003

8. Myshkin, Y. V., & Muravieva, O. V. (2016). Influence of the viscoelastic media properties on the lowest Lamb wave mode propagation in pipe. In: *Instrumentation Engineering, Electronics and Telecommunications-2015* (pp. 152–156). Izhevsk, Russia: Publishing House of Kalashnikov ISTU.

9. Rose, J. L. (2014). *Ultrasonic guided waves in solid media.* Cambridge university press.

10. Jenot, F., Ouaftouh, M., Duquennoy, M., & Ourak, M. (2001). Corrosion thickness gauging in plates using Lamb wave group velocity measurements. *Measurement Science and Technology, 12*(8), 1287–1293. doi: 10.1088/0957-0233/12/8/341

11. Lowe, M. (1998). Characteristics of the reflection of Lamb waves from defects in plates and pipes. In: Thompson, D. O., Chimenti, D. E. (Eds.). *Review of progress in quantitative nondestructive evaluation* (pp. 113-120). Boston, USA: Springer. doi: 10.1007/978-1-4615-5339-7_14

12. Xu, H., Xu, C., Li, X., & Wang, L. (2011). Study on single mode Lamb wave interaction with defect of plate by finite element model. *Procedia Engineering, 15*, 5067–5072. doi: 10.1016/j.proeng.2011.08.941

13. Nagy, P. B., Simonetti, F., & Instanes, G. (2014). Corrosion and erosion monitoring in plates and pipes using constant group velocity Lamb wave inspection. *Ultrasonics, 54*(7), 1832–1841. doi: 10.1016/j.ultras.2014.01.017

14. Lowe, M. J. S., Alleyne, D. N., & Cawley, P. (1998). The mode conversion of a guided wave by a part-circumferential notch in a pipe. *Journal of Applied Mechanics, 65*(3), 649–656. doi: 10.1115/1.2789107

15. Demma, A., Cawley, P., Lowe, M., & Pavlakovic, B. (2005). The effect of bends on the propagation of guided waves in pipes. *Journal of Pressure Vessel Technology, 127*(3), 328–335. doi: 10.1115/1.1990211

16. Zhao, Y., Shen, Z., Lu, J., Ni, X., & Cui, Y. (2012). A numerical study of the interaction of laser-generated circumferential wave with defect on hollow cylinder. *Optics & Laser Technology, 44*(2), 407–411. doi: 10.1016/j.optlastec.2011.08.004

17. Pei, J., Yousuf, M. I., Degertekin, F. L., Honein, B. V., & Khuri-Yakub, B. T. (1996). Lamb wave tomography and its application in pipe erosion/corrosion monitoring. *Journal of Research in Nondestructive Evaluation, 8*(4), 189–197.

18. Tapkov, K. A. (2018). Strain stress modeling of differential hardening rails. *Intelligent Systems in Manufacturing (Intellekt. Sist. Proizv.), 16*(2), 78–83. (in Russian). doi: 10.22213/2410-9304-2018-2-78-83

19. Murav'ev, V. V., Volkova, L. V., Platunov, A. V., Buldakova, I. V., & Gushchina, L. V. (2018). Investigations of the structural and strain-stress state of the rails of current production by the acoustic elasticity method. *Bulletin of Kalashnikov ISTU, 21*(2), 13–23. (in Russian). doi: 10.22213/2413-1172-2018-2-13-23

20. Rudd, K. E., Leonard, K. R., Bingham, J. P., & Hinders, M. K. (2007). Simulation of guided waves in complex piping geometries using the elastodynamic finite integration technique. *The Journal of the Acoustical Society of America, 121*(3), 1449–1458. doi: 10.1121/1.2431335

21. Strizhak, V. A., Hasanov, R. R., & Pryakhin, A. V. (2018). Features of excitation of an electromagnetic acoustic transducer under a waveguide method of testing. *Bulletin of Kalashnikov ISTU, 21*(2), 159–166. (in Russian). doi: 10.22213/2413-1172-2018-2-159-166

22. Nishino, H., Asano, T., Taniguchi, Y., Yoshida, K., Ogawa, H., Takahashi, M., & Ogura, Y. (2011). Precise measurement of pipe wall thickness in noncontact manner using a circumferential Lamb wave generated and detected by a pair of air-coupled transducers. *Japanese Journal of Applied Physics, 50*(7S), 07HC10. doi: 10.1143/JJAP.50.07HC10

23. Nishino, H., & Yoshida, K. (2006). Simple method of generating for circumferential shear horizontal waves in a pipe and their mode identifications. *Acoustical Science and Technology, 27*(6), 389–392. doi: 10.1250/ast.27.389

24. Leonard, K. R., & Hinders, M. K. (2003). Guided wave helical ultrasonic tomography of pipes. *The Journal of the Acoustical Society of America, 114*(2), 767–774. doi: 10.1121/1.1593068

25. Matuszyk, P. J. (2017). Modeling of guided circumferential SH and Lamb-type waves in open waveguides with semi-analytical finite element and perfectly matched layer method. *Journal of Sound and Vibration, 386,* 295–310. doi: 10.1016/j.jsv.2016.09.019

26. Clough, M., Fleming, M., & Dixon, S. (2017). Circumferential guided wave EMAT system for pipeline screening using shear horizontal ultrasound. *NDT & E International, 86,* 20–27. doi: 10.1016/j.ndteint.2016.11.010

27. Nishino, H., Yokoyama, R., Kondo, H., & Yoshida, K. (2007). Generation of circumferential guided waves using a bulk shear wave sensor and their mode identification. *Japanese Journal of Applied Physics, 46*(7S), 4568. doi: 10.1143/JJAP.46.4568

28. Zhao, X., & Rose, J. L. (2004). Guided circumferential shear horizontal waves in an isotropic hollow cylinder. *The Journal of the Acoustical Society of America, 115*(5), 1912–1916. doi: 10.1121/1.1691037

29. Sun, Z., Zhang, L., & Rose, J. L. (2005). Flexural torsional guided wave mechanics and focusing in pipe. *Journal of Pressure Vessel Technology, 127*(4), 471–478. doi: 10.1115/1.2065587

30. Nishino, H., Takashina, S., Uchida, F., Takemoto, M., & Ono, K. (2001). Modal analysis of hollow cylindrical guided waves and applications. *Japanese Journal of Applied Physics, 40*(1R), 364. doi: 10.1143/JJAP.40.364

31. Mineo, C., Cerniglia, D., & Pantano, A. (2013). Surface waves on cylindrical solids: Numerical and experimental study. *Ultrasonics, 53*(4), 913–921. doi: 10.1016/j.ultras.2013.01.003

32. Park, M. H., Kim, I. S., & Yoon, Y. K. (1996). Ultrasonic inspection of long steel pipes using Lamb waves. *NDT & E International, 29*(1), 13–20. doi: 10.1016/0963-8695(95)00030-5

33. Li, J., & Rose, J. L. (2001). Excitation and propagation of non-axisymmetric guided waves in a hollow cylinder. *The Journal of the Acoustical Society of America, 109*(2), 457-464. doi: 10.1121/1.1315290

34. Viktorov, I. A. (1967). *Rayleigh and Lamb waves: Physical theory and applications*. Springer US.

35. Myshkin, Yu. V., Murav'eva, O. V., Sannikova, Yu. O., & Chukhlanceva, T. S. (2018). The propagation of horizontally polarized shear wave in the hollow cylinder. In: *Instrumentation Engineering, Electronics and Telecommunications – 2018* (pp. 51–65). doi: 10.22213/2658-3658-2018-51-65

Formalization of the Problem of Building an Optimal Infocommunication Platform by the Criterion of the Effectiveness of Support for Business Processes

V. Ryzhakov [1], F. Chapparov [2], R. Karaban [3]

[1] Dept. of Radioelectronics and Electricity, Surgut State University, Surgut, Russia
E-mail: [1] v.ryzhakov@gmail.com, [2] fchapparov@mail.ru, [3] romakaraban@mail.ru

Abstract. The article presents a description of a general approach to solving a class of design for network tasks supporting the activities of small and medium-sized companies based on modeling their business processes. Optimization of the infocommunication platform is formulated as a linear programming problem. The interpretation of the parameters of the optimization model and their relationship with the company's business processes and the characteristics of the infocommunication platform are given. An interpretation of the linear programming problem of the infocommunication platform is given as an optimization task in predicting changes in the input factors of the constructed model.

Keywords: business process, business function, infocommunication platform, linear programming, design for network, network optimization

INTRODUCTION

Network design to support the activities of small and medium-sized companies has problem with finding the optimal ratio of attracted resources of computing and telecommunication networks and systems, software and applied cloud services. The problem is the need to determine a large number of basic properties and functionalities, such as the architecture and structure of the network, the list of supported services, the procedure for collecting, storing and processing user data, bandwidth of communication channels, methods of operation and management, economic indicators, etc. [1, 11-20]. It is also necessary to consider business development forecasts and trends in changing information and communication technologies used to solve the company's daily tasks. At present, expert assessments are mainly used for designing networks of small and medium-sized companies. The fact is that the task of designing infocommunications does not have a strict formalization, and this does not allow using the mathematical techniques to optimize systems and processes. This paper presents an approach to formalizing the problem of infocommunication designing to support the activities of small and medium-sized companies based on a linear programming mathematical techniques.

V. Ryzhakov, F. Chapparov, R. Karaban
"Formalization of the problem of building an optimal infocommunication platform
by the criterion of the effectiveness of support for business processes"

Optimization Problem

The task of selecting the above basic properties and functionality of infocommunication platforms can be solved as a result of multiparameter optimization by the criterion of the effective implementation of the company's business processes by the designed platform taking into account business development and telecommunication technologies forecast.

Correct formulation of a common optimization problem needs the definition of the following elements: [6-10].

- input factor set:

$$\bar{X} = x_1, x_2, \ldots, x_m, \tag{1}$$

their values can be measured, but cannot be changed for management and optimization purposes;

- set of disturbing factors:

$$\bar{\bar{\Xi}} = \xi_1, \xi_2, \ldots, \xi_s, \tag{2}$$

they randomly change over time and affect the state of a system or process, but cannot be measured directly;

- driving factor set:

$$\bar{U} = u_1, u_2, \ldots, u_n, \tag{4}$$

they change during the optimization process, which is why the optimization goal is achieved;

- set of output parameters (state parameters):

$$\bar{Y} = y_1, y_2, \ldots, y_n, \tag{5}$$

they characterize the state of the system or process under consideration with the cumulative effect of input, disturbing and driving factors;

- optimality criterion (objective function):

$$R = f\left(\bar{X}, \bar{\bar{\Xi}}, \bar{Y}, \bar{U}\right), \tag{6}$$

finding its extremum with varying driving factors $\bar{U}$ is the ultimate goal of solving the optimization task;

- allowable set of driving factors

$$G = \left\{\bar{U} \middle| g_i\left(\bar{U}\right) \le x_i, i = 1, \ldots, m\right\} \in \mathbb{R}^n, \tag{7}$$

it is given by a set of limiting inequalities $g_i\left(\bar{U}\right)$.

Determining the composition and setting these elements for a specific infocommunication platform is a problem of formalizing the optimization task. For its successful solution, it is necessary to find an acceptable interpretation of the factors, parameters and objective function of the optimization task on the basis the information and communication platform is optimized by the criterion of the effective implementation of the company's business processes by the designed platform taking into account business development and telecommunication technologies forecast.

Network Optimization

The infocommunication platform of a small or medium-sized enterprise is designed to support the following basic functions: [2, 3].

- customer management;
- management of activities;
- resource management;
- management of financial flows.

They are user-oriented infocommunication platform services. To implement them, it is necessary to develop business processes that determine the order of implementation and interaction of basic functions, and to design a support these business processes infocommunication platform.

Because the purpose of any infocommunication platform is to support the company's business processes, the solution of the network design task should begin with a description of the organization's business processes. [4].

The activities of a small or medium-sized company can often be described by a single business process, which is a set of business process structure business functions. The business functions and the relations between them determine the set of input factors $\overline{X}$, and the results of the implementation of the business process, that are the set of output parameters $\overline{Y}$, for the problem of optimal design of the infocommunication platform.

Must be define the following elements for designing business processes: [3].

1) Business functions that describe the actions of a business process. They are the input factors of the optimization model. It is necessary to take into account those business functions that require information and communication support for their implementation. Input factors for business functions is the data value that must be processed by the infocommunication platform during the implementation of these business functions, in the formation of limiting inequalities $g_i(\overline{U})$. Arguments of inequalities $g_i(\overline{U})$ are the intensity of use of information and communication platform technologies in the implementation of relevant business functions, and the inequality coefficients are the norms of using company resources in the implementation of business functions.

2) The defining moments of the launch and the results of business functions inbound and outbound events. They are the input factors of the optimization model. Since define the call flows and the intensity of the use of business functions it suffices to take into account only incoming events. To describe the incoming flows in the compilation of limiting inequalities $g_i(\overline{U})$, we will use the intensity of the call flow ψ [5], defined as the mathematical expectation of the number of calls of the corresponding business function arriving per unit time. Each input factor is determined by its value of flow rate. It is necessary to take into account only independent flows of incoming calls when describing incoming factors of this type. Flows that arise as a result of the occurrence of other events are not independent and are not used in building an optimization model of the infocommunication platform.

3) Representing input and output data Input and output documents are also the optimization model input factors. The formation of each of the documents is accompanied by the generation of a certain amount of traffic that is not included in the final document. Therefore, when describing inequalities $g_i(\overline{U})$, it is necessary to determine the average data volume of each document instance generated in the infocommunication platform, for each of the document type optimization parameter that represents the input parameter.

4) Representing the functional responsibilities of enterprise role employees. They are the input factors of the optimization model. The roles of employees are determined by the scope of the company. Roles are included in inequalities $g_i(\overline{U})$ as the number of employees of the

V. Ryzhakov, F. Chapparov, R. Karaban
"Formalization of the problem of building an optimal infocommunication platform
by the criterion of the effectiveness of support for business processes"

respective roles, and the coefficients of these inequalities determine the intensity of use by employees of infocommunication technologies.

5) Resources that are used to complete the business process. Are the input factors of the optimization model as well. The input factors of this type include various types of material and financial resources that are used to implement the business process. In inequalities $g_i\left(\bar{U}\right)$ in the allowable amount of attraction of these resources are limited.

6) Used to quantify the metrics of the implementation of a business process metrics, for example, the required number of customers, annual turnover, etc. Represent a set of output parameters of the optimization model $\bar{Y}$. Output parameters are used to take into account the development trends of the company when solving the task of planning the development of the infocommunication platform. It is necessary to use only a set of independent metrics when determining output parameters, i.e. have no functional or statistical relationships between the metrics.

An introduction to the model of disturbing factors $\bar{\Xi}$ is possible when specifying the optimization task of the information and communication platform. Their use makes sense only with relatively large variations of the input factors and output parameters of the optimization model and the stochastic processes used to build the model.

The infocommunication platform for supporting small and medium-sized companies in general can contain the following components - office cloud and local services, network printers and scanners, e-mail, telephony and IP-telephony, video conferencing, data storage, information security subsystems, wireless and wired access networks , personal computers, cloud and local client management services, content management, video surveillance and security, accounting support, etc.

Different combinations of these components can give different options for building an infocommunication platform, each of which represents its own controlling factor u_i from the set $\bar{U}$. Each of the driving factors u_i is a set of infocommunication platform components necessary to obtain the corresponding metric from the set of output parameters $\bar{Y}$. It is necessary to determine the elements and technologies that should be used to obtain the target value of the metric y_i when building an optimization model. Numerical value u_i means the intensity of use of the corresponding set of infocommunication platform components. Variable factors u_i are set by a combination of components of the information and communication platform, providing a single intensity of their use, i.e. it is necessary to determine the used volume of technologies group u_i of the infocommunication platform that corresponds to a unit value of its metric y_i.

For the same output parameter y_i, various combinations of components of the information and communication platform can be used, i.e. different driving factors u_i may correspond to the same metric, which should be included in the general optimization model as independent elements representing independent options for building an infocommunication platform to achieve a given value of the corresponding metric

Since for small and medium-sized companies the total effect from their activities is most interesting, the objective function R can be a linear weighted sum of the intensities of using sets of technologies u_i, that ensure the achievement of the required values of the corresponding metrics y_i.

RESULTS

The above procedure for formalizing the task of designing an infocommunication platform to support the activities of small and medium-sized companies makes it possible to present the task of finding the best option design for network as a linear programming task:

It is required to find the values $u_1, u_2, \ldots, u_n$ delivering the minimum of the linear function:

$$R = f\left(\overline{Y}, \overline{U}\right) = y_1 \cdot u_1 + y_2 \cdot u_2 + \ldots + y_n \cdot u_n, \tag{8}$$

on a set of values $u_1, u_2, \ldots, u_n$ satisfying the constraints given by inequalities of the form:

$$
\begin{aligned}
a_{11} \cdot u_1 + \ldots + a_{1n} \cdot u_n &\leq x_1, \\
\ldots \quad \ldots \quad \ldots & \\
a_{m1} \cdot u_1 + \ldots + a_{mn} \cdot u_n &\leq x_m,
\end{aligned}
\tag{9}
$$

y_i – means a set of company performance targets; x_i – resource support of the company's activities for the implementation of business processes with given target indicators $\overline{Y}$; u_i are the intensity of use of the set of components of the infocommunication platform to achieve the corresponding target indicators y_i; a_{ij} is the utilization rate of the resource x_i when implementing the set of components of the infocommunication platform u_i of unit intensity; the objective function R shows the total intensity of the use of infocommunication resources used to achieve the specified target indicators $\overline{Y}$.

Minimization of the objective function R will provide an optimal supporting infocommunication platform minimized by the intensity of its use. In turn, this will allow to determine the required amount of attracted resources of computing and telecommunication networks and systems, software and applied cloud services.

The definition of the necessary resource support for the company, expressed by the set of input factors $\overline{X}$, is carried out by rationing the performance of individual business functions when it is necessary to achieve the target indicators $\overline{Y}$.

Planning the development of a company's business processes ultimately leads to setting target values for $\overline{Y}$ target indicators and solving an optimization problem for these indicators.

Accounting technological trends through the forecast for changing norms a_{ij}.

CONCLUSIONS

The proposed optimization model can be used to build an optimal infocommunication platform to support the activities of small and medium-sized companies, whose activities can be described by a single end-to-end business process, taking into account the company's development plan and trends in changing infocommunication technologies. The application of the proposed model involves the localization of tasks for a particular company and the definition of specific indicators of the model. As a result of solving the optimization task, an infocommunication network will be obtained with the minimum amount of hardware and software required for achieving the planned performance of the company, necessary for the implementation of the infocommunication platform with the required set of infocommunication resources.

V. Ryzhakov, F. Chapparov, R. Karaban
"Formalization of the problem of building an optimal infocommunication platform
by the criterion of the effectiveness of support for business processes"

References

1. Metsälä, E., & Salmelin, J. (Eds.) (2015). *LTE backhaul: Planning and optimization.* John Wiley & Sons. doi: 10.1002/9781118924655

2. Brambilla, M., Cabot, J., & Wimmer, M. (2012). *Model-driven software engineering in practice.* Morgan & Claypool Publishers. doi: 10.2200/S00441ED1V01Y201208SWE001

3. Russell, N., van der Aalst, W. M. P., & ter Hofstede, A. H. M. (2016). *Workflow patterns: The definitive guide.* The MIT Press. doi: 10.7551/mitpress/8085.001.0001

4. Wang, Z.-Yu., Li, Q., Cao, Z.-Ch., Li, W.-H., Li, J., & Du, R.-Ya. (2012). A model-based deployment framework of integrated public cloud service. In: *2012 International Conference on Computer Science and Service System* (pp. 723–728). Nanjing, China: IEEE. doi: 10.1109/CSSS.2012.186

5. Shortle, J. F., Thompson, J. M., Gross, D., & Harris, C. M. (2018). *Fundamentals of queueing theory.* 5th ed. John Wiley & Sons. doi: 10.1002/9781119453765

6. Xu, H., Wang, S., & Wu, S.-Yi. (Eds.). (2015). *Optimization methods, theory and applications.* Springer-Verlag Berlin Heidelberg. doi: 10.1007/978-3-662-47044-2

7. Neely, M. (2010). *Stochastic network optimization with application to communication and queueing systems.* Morgan & Claypool Publishers. doi: 10.2200/S00271ED1V01Y201006CNT007

8. Demydov, I. (2017). Approaches to solving the problem of improving the efficiency of scalable telecommunication platforms. In: *2017 4th International Scientific-Practical Conference Problems of Infocommunications. Science and Technology (PIC S&T)* (pp. 560–563). Kharkov, Ukraine: IEEE. doi: 10.1109/INFOCOMMST.2017.8246462

9. Bezruk, V., Svid, I., & Korsun, I. (2006). Methods of multicriteria optimization in telecommunication networks planning and controlling. In: *2006 International Conference – Modern Problems of Radio Engineering, Telecommunications, and Computer Science* (pp. 381–383). Lviv-Slavsko, Ukraine: IEEE. doi: 10.1109/TCSET.2006.4404558

10. Lemeshko, O. V., & Sterin, V. L. (2013). Structural and functional optimization of transport telecommunication network. In: *2013 23rd International Crimean Conference "Microwave & Telecommunication Technology"* (pp. 490–491). Sevastopol, Ukraine: IEEE. Retrieved from: https://ieeexplore.ieee.org/document/6652918

11. Bezruk, V., & Rybalko, D. (2007). Multicriteria optimization in telecommunication networks planning. In: *2007 17th International Crimean Conference - Microwave & Telecommunication Technology* (pp. 338–340). Crimea, Ukraine: IEEE. doi: 10.1109/CRMICO.2007.4368739

12. Zhang, J., Yang, J., Aydin, M. E., & Wu, J. Y. (2006). Mathematical modelling and comparisons of four heuristic optimization algorithms for WCDMA radio network planning. In: *2006 International Conference on Transparent Optical Networks, 3* (pp. 253–257). Nottingham, UK: IEEE. doi: 10.1109/ICTON.2006.248446

13. Hou, X., & Shu, H. (2012). Research on radio network planning and optimization in TETRA digital trunking system. In: *2012 Second International Conference on Instrumentation, Measurement, Computer, Communication and Control* (pp. 821–824). Harbin, China: IEEE. doi: 10.1109/IMCCC.2012.198

14. Moskalets, M., & Kuzminich, I. (2016). Methods of femtocells planning using methods of packaging optimization. Publisher: IEEE. Published in: 2016 Third International Scientific-Practical Conference Problems of Infocommunications Science and Technology (PIC S&T). Date of Conference: 4-6 Oct. 2016. INSPEC Accession Number: 16836954. DOI: 10.1109/INFOCOMMST.2016.7905385

15. Bondarenko, O., Ageyev, D., & Mohammed, O. (2019). Optimization model for 5G network planning. In: *2019 IEEE 15th International Conference on the Experience of Designing and Application of CAD Systems (CADSM)* (pp. 211–213). Kharkiv, Ukraine: IEEE. doi: 10.1109/CADSM.2019.8779298

16. Doherty, D., Morawski, T., Sackett, R., Tang, B., Carlos-Urrutia-Valdes, & Zhao, J. (2008). Next generation networks – multi-service network design. In: *Networks 2008 – The 13th International Telecommunications Network Strategy and Planning Symposium* (pp. 1–14). Budapest, Hungary: IEEE. doi: 10.1109/NETWKS.2008.4763684

17. Patri, S. K., Grigoreva, E., Kellerer, W., & Mas Machuca, C. (2019). Rational agent-based decision algorithm for strategic converged network migration planning. *Journal of Optical Communications and Networking, 11*(7), 371–382. doi: 10.1364/JOCN.11.000371

18. Xianxiang, W., Yan, M., & Juan, W. (2011). An improved path planning approach based on Particle Swarm Optimization. In: *2011 11th International Conference on Hybrid Intelligent Systems (HIS)* (pp. 157–161). Melacca, Malaysia: IEEE. doi: 10.1109/HIS.2011.6122097

19. Giuliano, R., Mazzenga, F., & Petracca, M. (2012). Planning optimization for TDMA-based radio mobile systems with power consumption constraints. In: *2012 IEEE First AESS European Conference on Satellite Telecommunications (ESTEL)* (pp. 1–4). Rome, Italy: IEEE. doi: 10.1109/ESTEL.2012.6400159

20. Bezruk, V., & Bukhanko, A. (2013). Optimal project solution decision making in telecommunication systems using multicriteria optimization methods. In: *East-West Design & Test Symposium (EWDTS 2013)* (pp. 1–5). Rostov-on-Don, Russia: IEEE. doi: 10.1109/EWDTS.2013.6673210

Robot Drives Diagnostics by Identifiability Criterion Based on State Matrix

S. A. Trefilov, Yu. R. Nikitin

Department of Mechatronic Systems, Kalashnikov Izhevsk State Technical University, Izhevsk, Russia
E-mail: nikitin@istu.ru

Abstract. The paper discusses robot drives diagnostics and optimal decision-making algorithm according to the identifiability criterion based on discrete digital control model. We consider discrete control algorithm for quality criterion that minimizes the energy of control and displacement. The optimal control algorithm is based on the Riccati equation solving for control system with modified state and control matrices. The criteria of observability, controllability and identifiability of robot drives are considered as rank function of the extended matrix with measurement matrix. An algorithm is proposed for calculating the criterion for identifiability of nonlinear control system in discrete linearization variant is proposed. Decision theory is applied for the robot drives diagnosis. It is suggested or we suggest to use identification in terms of mathematical model compliance to object operation results. A robot drives control using discrete vector-matrix algorithm involves calculating the state matrix at each step. Consequently, the expanded matrix determinant is calculated at each step and is compared with some constant that numerically divides the space of state matrices. Therefore, robot drives operation allows its identification. As the identification algorithm optimality criterion was chosen the optimal decision making criterion in combination with the identifiability criterion for the optimal control algorithm by the quadratic form criterion minimum. The vector-matrix model of robot drives in the state space is presented, taking into relative account state measuring accuracy of the information-measuring subsystem of robot drives. The drive model was developed in the Russian software package "Dynamic Simulation of Technical Systems SimInTech". It proposed to determine the identifiability criterion for practical tasks. The criterion of optimal decision making (threshold) can be chosen depending on the a priori data on the loss matrix and the probabilities of the hypothesis about the object mathematical model correspondence to the results of operation and the alternative - not about the correspondence of the model and experiment. In this paper, the identifiability conditions are considered not only in relation to the rank of the extended matrix [C, AC, ...], but also as a condition for ensuring the accuracy of the model with respect to the object. It is proposed to model the identifiability threshold by exhaustive search of the object states for this model.

Keywords: identification, diagnostics, robot drives, state space, discrete model, optimal algorithm, Riccati equation, Cauchy matrix, Bayes criterion

INTRODUCTION

A robot drives work in extreme conditions. An effective diagnostic system is required to provide for high reliability robot drives. An optimal algorithm is proposed for deciding on robot drives identifiability, based on discrete digital control model. The diagnostic process de-

termines the adequacy of the model applicability to the object. The algorithm is based on calculating the value of the identifiability criterion for discrete non-linear model of robot drives in the state space.

The identification method in the state space has been actively developing over the past two decades. P. Eykhoff is one of the first who performed the theoretical identification justification, as well as developed algorithms and methods of identification [1, 2]. The works of the following authors are devoted to the dynamic systems identification research: D. Graupe [3], L. Ljung [4], E. P. Sage and J. L. Melsa [5, 6], and among Russian authors – Ya. Z. Tsypkin [7], N. S. Rybman [8], S. E. Steinberg [9] and others.

R. V. Beard developed a scheme for detecting defects based on observers [10]. H. L. Jones continued these studies and developed the Beard-Jones Fault Detection Filter [11]. In the 1980s and early 1990s, the main approaches of quantitative diagnostics were developed: an observer-based approach, a parameter estimation method, etc. Some important study in this direction are works of P. M. Frank [12], R. Isermann [13, 14]. Theoretically well-substantiated developed techniques are classic diagnostic methods. These techniques are based on analytical redundancy, which is a model describing the diagnosed technical system.

SETTING THE RESEARCH TASK

A robot drives are represented by nonlinear differential control and observation equations in the state space.

$$\dot{\mathbf{x}} = \mathbf{A}(t)\mathbf{x}(t) + \mathbf{B}(t)\mathbf{u}(t), \tag{1}$$

$$\mathbf{y}_k = \mathbf{C}_k \mathbf{x}_k,$$

where $\mathbf{A}(t)$ is a functional matrix of size $n \times n$, called the matrix of the system (object) state; $\mathbf{B}(t)$ is a functional matrix of size $n \times r$, called the control (input) matrix; $\mathbf{C}(t)$ is a functional matrix of size $m \times n$, called the state exit matrix or measurement matrix.

In general, when at least one of the matrix $\mathbf{A}(t)$, $\mathbf{B}(t)$, $\mathbf{C}(t)$ is time dependent, the task is nonlinear and has only particular solutions.

To find the state equation, we represent equations (1) in a discrete form, the discretization time Δt tends to zero, and the trajectory on each discrete segment is linear. We write equations (1) in the form

$$\frac{\mathbf{x}_{k+1} - \mathbf{x}_k}{\Delta t} = \mathbf{A}_k \mathbf{x}_k + \mathbf{B}_k \mathbf{u}_k,$$

$$\mathbf{y}_k = \mathbf{C}_k \mathbf{x}_k, \tag{2}$$

Multiply the left and right sides of the first equation (2) by Δt, we get

$$\mathbf{x}_{k+1} = \tilde{\mathbf{A}}_k \mathbf{x}_k + \tilde{\mathbf{B}}_k \mathbf{u}_k, \tag{3}$$

where $\tilde{\mathbf{A}}_k = \Delta t \mathbf{A} + \mathbf{E}$, $\tilde{\mathbf{B}}_k = \Delta t \mathbf{B}_k$.

This equation relates the transition of the system from the state $\mathbf{x}_k$ to the state $\mathbf{x}_{k+1}$. On the segment Δt, we take the values of the matrices $\mathbf{A}_k$, $\mathbf{B}_k$, and $\mathbf{C}_k$ to be constant. Find the solution to equation (3). For convenience, we will remove the "wavy line" sign in subsequent entries.

The quadratic quality functional determining the control and displacement energy is expressed as follows

$$I = \frac{1}{2} \int_{t_0}^{t_f} \left(\mathbf{x}^{\mathrm{T}} \mathbf{Q} \mathbf{x} + \mathbf{u}^{\mathrm{T}} \mathbf{G} \mathbf{u} \right) dt, \qquad (4)$$

where $\mathbf{Q} \geq 0$ and $\mathbf{G} > 0$ are arbitrarily defined matrices.

The equation solution (1) for the quality criterion (4), which minimizes the energy of control and displacement. It is determined by the following expression [15, 16].

$$\mathbf{u} = -\mathbf{G}^{-1} \mathbf{B}^{\mathrm{T}} \mathbf{K} \mathbf{x},$$

$$\mathbf{x} = -\mathbf{C}^{-1} \mathbf{y}, \qquad (5)$$

where $\mathbf{K}$ is the Cauchy matrix, $\mathbf{K} = \mathbf{K}^{\mathrm{T}}$, which can be found by solving the Riccati equation [15].

$$-\dot{\mathbf{K}} = \mathbf{Q} + \mathbf{A}^{\mathrm{T}} \mathbf{K} + \mathbf{K}^{\mathrm{T}} \mathbf{A} - \mathbf{K}^{\mathrm{T}} \mathbf{B} \mathbf{G}^{-1} \mathbf{B}^{\mathrm{T}} \mathbf{K}, \qquad (6)$$

where $\mathbf{K}(t_f) = 0$.

Cauchy Matrix:

$$\mathbf{K} = \begin{bmatrix} k_{11} & k_{12} & \ldots & k_{1(n-1)} & k_{1n} \\ k_{21} & k_{22} & \ldots & k_{2(n-1)} & k_{2n} \\ \ldots & \ldots & \ldots & \ldots & \ldots \\ k_{(n-1)1} & k_{(n-1)2} & \ldots & k_{(n-1)(n-1)} & k_{(n-1)n} \\ k_{n1} & k_{n2} & \ldots & k_{n(n-1)} & k_{nn} \end{bmatrix}, \qquad (7)$$

where $k_{ij} = k_{ji}$, should be positively defined, since as positive definite matrices $\mathbf{Q}$ and $\mathbf{G}$ is used in the quadratic quality functional (4), which is also positive.

Matrices $\mathbf{Q}$ and $\mathbf{G}$ are chosen arbitrary. Matrices $\mathbf{Q}$ and $\mathbf{G}$ are selected by the assortment method, since they are not always possible to obtain a satisfactory solution of equation (5), when calculating the control vector $\mathbf{u}$. In [15, 16], it is proposed to select these matrices by assortment or simulation.

Thus, the driver control is carried out by solving (6) according to the model (5) by calculating at each step the state matrix $\mathbf{A}_k$ and the control matrix $\mathbf{B}_k$ (3).

We assume that the matrix $\mathbf{C}^{-1} = \mathbf{C}_k^{-1}$ at each step k does not change, is determined by the information-measuring system, can be represented as

$$\mathbf{C}^{-1} = \begin{bmatrix} 1+\xi_1 & 0 & \ldots & 0 \\ 0 & 1+\xi_2 & \ldots & 0 \\ \ldots & \ldots & \ldots & \ldots \\ 0 & 0 & \ldots & 1+\xi_n \end{bmatrix}, \qquad (8)$$

where $\xi_n = \begin{bmatrix} \xi_1 & \xi_2 & \ldots & \xi_n \end{bmatrix}^{\mathrm{T}}$ is random vector, that reflects the random nature of measurements by the information-measuring system, that is part of the drives [17, 18].

DRIVE IDENTIFICATION

Consider the issue of identifying drives in terms of analyzing expression (9), where at each step of linearization the criterion of identifiability and observability is the rank of the extended matrix.

$$\text{rank}\begin{bmatrix} \mathbf{C}_k^{\mathrm{T}} & \mathbf{A}_k^{\mathrm{T}}\mathbf{C}_k^{\mathrm{T}} & \left(\mathbf{A}_k^{\mathrm{T}}\right)^2 \mathbf{C}_k^{\mathrm{T}} & \dots & \left(\mathbf{A}_k^{\mathrm{T}}\right)^{n-1} \mathbf{C}_k^{\mathrm{T}} \end{bmatrix} = n. \tag{9}$$

The matrix $\mathbf{C}_k^{\mathrm{T}}$ is completely determined by the information-measuring system, that is, by relative measurement error or accuracy class. We write the model of information-measuring system in the form

$$\mathbf{y}_k = \mathbf{C}_k \mathbf{x}_k, \tag{10}$$

or

$$\begin{bmatrix} y_1 \\ y_2 \\ \dots \\ y_n \end{bmatrix} = \begin{bmatrix} 1+h_1\xi_1 & 0 & \dots & 0 \\ 0 & 1+h_2\xi_2 & \dots & 0 \\ \dots & \dots & \dots & \dots \\ 0 & 0 & \dots & 1+h_n\xi_n \end{bmatrix} \begin{bmatrix} x_1 \\ x_2 \\ \dots \\ x_n \end{bmatrix}, \tag{11}$$

where h_i is the relative measurement error, ξ_i is implementation of a normally distributed random variable with standard deviation $\sigma_i = \dfrac{h_i}{3}, \ i = \overline{1, n}.$

Then for the maximum downward errors in the worst case for all measuring channels, given the continuous and infinite nature of the implementation of a normally distributed random variable, assuming that most of the values fall within the interval $-3\sigma_i \leq \xi_i \leq 3\sigma_i,$ $i = \overline{1, n},$ we can write approximately

$$\mathbf{C}_n = \begin{bmatrix} 1-h_1 & 0 & \dots & 0 \\ 0 & 1-h_2 & \dots & 0 \\ \dots & \dots & \dots & \dots \\ 0 & 0 & \dots & 1-h_n \end{bmatrix}.$$

In our case, the measurement channels are independent and the determinant of the matrix will be equal to

$$\det \mathbf{C}_n^{T} = \left(1-h_1\right)\left(1-h_2\right)\dots\left(1-h_n\right). \tag{12}$$

Open the brackets in (12), exclude the terms of the second and higher order of smallness, we get

$$\det \mathbf{C}_n^{\mathrm{T}} = 1-h_1-h_2-\dots-h_n = 1-\sum_{i=1}^{n} h_i. \tag{13}$$

If the relative accuracy of all measuring channels is the same $h_i = h, \ i = \overline{1, n},$ then from (13), we get

$$\det \mathbf{C}_n^{\mathrm{T}} = 1-nh.$$

Similarly, for maximum errors in a big way in the worst case for all measuring channels we can write

$$\det \mathbf{C}_n^{\mathrm{T}} = 1 + h_1 + h_2 + \ldots + h_n = 1 + \sum_{i=1}^{n} h_i. \tag{14}$$

$$\det \mathbf{C}_n^{\mathrm{T}} = 1 + nh. \tag{15}$$

The value of the determinant in (14) and (15) is always greater than one, since the value of relative accuracy is always positive,

$$h_i > 0, \;\; i = \overline{1, n}.$$

Thus, the identifiability condition (10) in the case

$$\det \mathbf{A}_k^{\mathrm{T}}(n)^i > 0, \;\; i = \overline{1, n}$$

will be the condition

$$\det \mathbf{C}_n^{\mathrm{T}} = 1 - \sum_{i=1}^{n} h_i > 0$$

or

$$\sum_{i=1}^{n} h_i < 1. \tag{16}$$

The following is DC motor model in the state space, depending on the accuracy of measuring the state matrix under the assumption that the given path accuracy is no worse than 10%. Going beyond this value will be considered a loss of identifiability, that is, the model does not match the object.

Figure 1 shows the scheme for calculating the model output parameters at different accuracy of measuring the state vector of the DC motor in a vector-matrix form with the "State variables" block in the dynamic modeling environment of technical systems SimInTech.
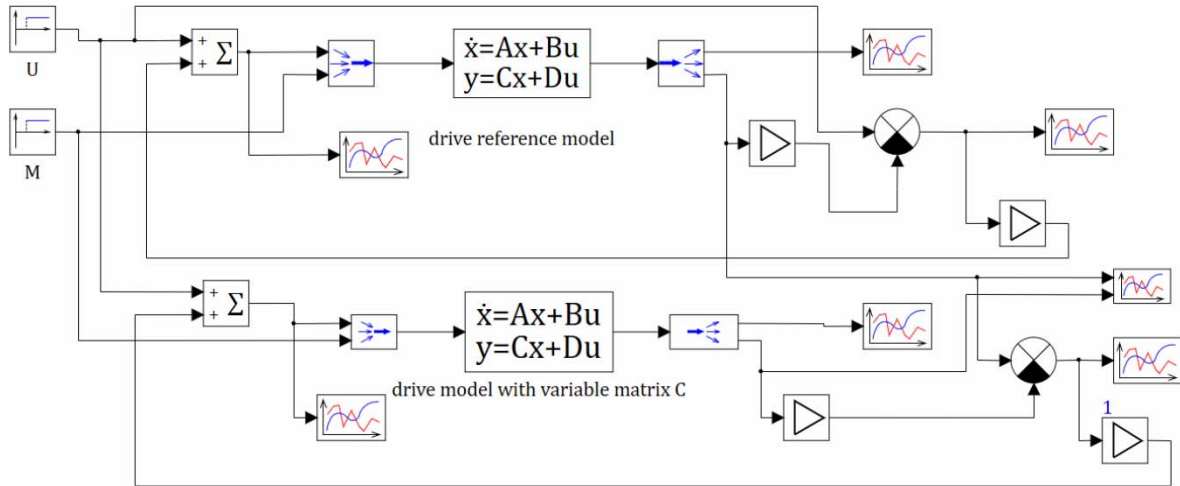

Figure 1. DC motor model with a reference and variable measuring matrix

The simulation results at torque $M = 1.91$ N, a relative measurement error $h_1 = 0$ (reference measuring matrix without measurement errors), $h_2 = 0.1$ (measuring matrix in the presence of a relative measurement error of 0.1) are presented in Fig. 2.

Figure 2. Simulation results at torque $M = 1.91$ N, $h_1 = 0$ (reference measuring matrix),
$h_2 = 0.1$ (variable measuring matrix)

Fig. 3 shows the dependence of the relative difference in the angular velocities of the reference model and the model with a modified measurement matrix.
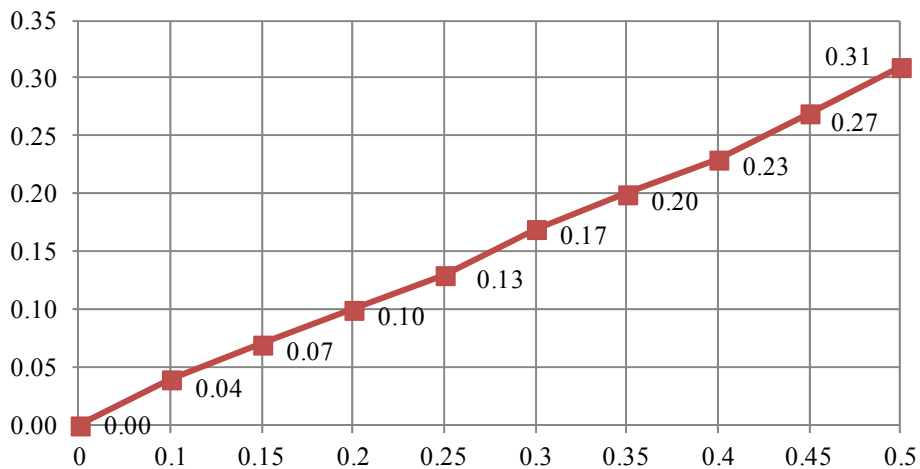

Figure 3. Dependence of the relative difference in the angular velocities
of the reference model and the model with modified observation matrix
(the abscissa axis is h, the ordinate axis is the relative difference of angular velocities)

Considering that in many practical problems of managing tasks, the dimensions of problems do not exceed ten, and the relative accuracy of measurement is equal to units of percent, it can be concluded that only the state matrices affect the identifiability

$$\mathbf{A}_k^{\mathrm{T}}, \quad k = \overline{1, n},$$

which will ultimately determine the rank of the matrix (9).

It is proposed for practical tasks to determine identifiability in the form

$$\min(\det \mathbf{A}_k^{\mathrm{T}}(n)^i \det \mathbf{C}_k^T(n)) > \gamma. \tag{17}$$

where k is the step number in the nonlinear model; n is the dimension of the model; γ is the identifiability criterion chosen by modeling the state matrix for the cases when the parameters of matrix $\mathbf{A}$ are exited from the space of realizable values of a serviceable system.

DRIVE DIAGNOSTICS

Apply the decision theory [19, 20] to the choice of the threshold in (17). Let's write the source data for this task:
 – S_0 is system state corresponding to identifiability;
 – S_1 is system state corresponding to non-identifiability;
 – X_0 is the space of samples corresponding to condition (17) of the identifiability of the system with probability $P\{x \in X_0 \mid S_0\}$;
 – X_1 is the sample space corresponding to condition (17) of the system's non-identifiability with probability $P\{x \in X_1 \mid S_1\}$;
 – q is the probability that the state of the system corresponds to the state S_0;
 – p is an alternative, i.e. $p = 1 - q$ is the probability that the state of the system corresponds to the state S_1;
 – H_0 is hypothesis about the belonging of the observed vector $\mathbf{x} = (x_1, x_2, \ldots, x_n)^{\mathrm{T}}$ to the state S_0;
 – H_1 is hypothesis about the belonging of the observed vector $\mathbf{x} = (x_1, x_2, \ldots, x_n)^{\mathrm{T}}$ to the state S_1;
 – γ_0 is the decision to accept the true hypothesis H_0 with probability $P\{\mathbf{x} \in X_0 \mid S_0\}$;
 – γ_1 is the decision to accept the true hypothesis H_1 with probability $P\{\mathbf{x} \in X_1 \mid S_1\}$;
 – $W_n(\mathbf{x} \mid S_0)$ is conditional density function for samples corresponding to the state S_0;
 – $W_n(\mathbf{x} \mid S_1)$ is conditional density function for samples corresponding to the state S_1;
 – $l(x) = \dfrac{W_n(\mathbf{x} \mid S_0)}{W_n(\mathbf{x} \mid S_1)}$ is likelihood statistics.
Then if the likelihood statistics

$$l(x) = \frac{W_n(\mathbf{x} \mid S_0)}{W_n(\mathbf{x} \mid S_1)} > c, \tag{18}$$

then we decide γ_0 on the correctness of the hypothesis H_0, that the observed vector (sample) $\mathbf{x} = (x_1, x_2, \ldots, x_n)^{\mathrm{T}}$ belongs to the state S_0, i.e. the robot drive is identifiable. Otherwise, the likelihood statistics

$$l(x) = \frac{W_n(\mathbf{x} \mid S_0)}{W_n(\mathbf{x} \mid S_1)} \le c, \tag{19}$$

then we decide γ_1 on the correctness of the hypothesis H_1, that the observed vector (sample) $\mathbf{x} = (x_1, x_2, \ldots, x_n)^{\mathrm{T}}$ belongs to the state S_1 – the decision on the system's non-identifiability. Optimal decision-making on the selected criterion implies errors: $\alpha = P\{x \in X_1 \mid S_0\}$ - decision making γ_1, although the state was true S_0 (error of the first kind) and $\beta = P\{x \in X_0 \mid S_1\}$ - decision-making γ_0, although the state was true S_0 (error of the second kind).

The threshold c is selected as one of the decision methods. For example, for the Bayes method [19, 20], we can record the statistics of the correct decision on the identifiability of drives in the form

$$l(x) = \frac{W_n(\mathbf{x} \mid S_0)}{W_n(\mathbf{x} \mid S_1)} > \frac{\prod_{01} - \prod_{00}}{\prod_{10} - \prod_{11}} \frac{q}{p},$$

where $\prod_{00}$, $\prod_{11}$, $\prod_{01}$, $\prod_{10}$ – elements of the loss matrix, and $\prod_{00}$, $\prod_{11}$ are weights for correct decisions, and $\prod_{01}$, $\prod_{10}$ – for erroneous ones. For a simple loss matrix of identical probabilities p and q [19, 20], we obtain the statistics of the correct decision on the identifiability of the system in a simpler form

$$l(x) = \frac{W_n(\mathbf{x} \mid S_0)}{W_n(\mathbf{x} \mid S_1)} > 1,$$

which meets the maximum likelihood criterion.

Thus, solving together (17, 18, 19) for a given threshold c, going through all possible values $\mathbf{x} = (x_1, x_2, \ldots, x_n)^{\mathrm{T}}$ from the space $X_0 + X_1$ for all states S_0 and S_1, we obtain the value γ. Note that solution (17) presupposes the dependence of the matrix $\mathbf{A}_k^{\mathrm{T}}$, $k = \overline{1, n}$ on the state $\mathbf{x} = (x_1, x_2, \ldots, x_n)^{\mathrm{T}}$ and, therefore, it has greater computational complexity of the numerical solution. Considering the universality of the likelihood statistics (18, 19), the criterion of optimal decision making (threshold c) can be chosen depending on a priori data on the loss matrix and the probabilities of the hypothesis and alternative [19, 20].

CONCLUSION

Currently the development of control algorithms based on discrete models is a very important task, because almost all tasks of controlling practice of robots drives cannot be accurately represented by linear models and the solution of nonlinear models is generally absent. Discrete models of nonlinear systems of the form (3) presuppose variable matrices of state, control, and measurement. Matrices are defining an infinite number of the model variants. Therefore, some tools are needed to calculate of adequacy degree of mathematical models and real objects. This paper presents the optimal algorithm for identifying nonlinear complex systems based on a discrete digital control model. As the criterion for the optimality of the identification algorithm was chosen the criterion of optimal decision making in combination with the identifiability criterion for the optimal control algorithm by the minimum criterion of the quadratic form.

The paper investigates the influence of the parameters of the measurement matrix on the identifiability of the robot drive model based on the DC motor for control and diagnostic tasks.

It is shown that at a threshold value h>0.2 of the measurement matrix, the difference in the angular velocities of the reference model and the model with the modified observation matrix is more than 10%, the drive model becomes unidentifiable, which leads to a loss of controllability and the inability to diagnose. To study the influence of the measurement matrix on the identifiability of the model, a vector-matrix model of the drive in the state space is developed taking into account viscous friction.

Identification criteria (16) and (17) allow to determine the models conformity degree to the control object by the model of the measuring matrix or by the models combination of the state matrix and the measuring matrix.

The threshold γ in (17) is optimal and is calculated numerically by solving the system of inequalities (17, 18, 19). It is possible to require, though it is not necessary, in the criterion (16) for the measurement matrix, that the sum of the relative errors be substantially less than one. The criterion of optimal decision making (threshold c) can be chosen depending on the apriori data by the loss matrix and the probabilities of the hypothesis and the alternative.

In this paper are new:

1) the conditions of identifiability are considered not only with respect to the rank of the extended matrix [C, AC, …], but also as a condition for ensuring the accuracy of the model with respect to the object;

2) it is proposed to model the identifiability threshold by exhaustive search of the state of an object for this model.

ACKNOWLEDGMENT

REFERENCES

1. Eykhoff, P. (1974). *System identification: Parameter and state estimation*. Wiley-Interscience, New York. 555 p.

2. Eykhoff, P. (Ed.). (1981). *Trends and progress in system identification*. Oxford, England: Pergamon. 402 p.

3. Graupe, D. (1976). *Identification of system*. New York: R. E. Krieger Publishing Company. 302 p.

4. Ljung, L. (1999). *System identification. Theory for the user*. 2nd ed. PTR Prentice Hall, Upper Saddle River. 609 p.

5. Sage, A., & Melsa, J. (1971). *System identification*. New York: Academic press. 221 p.

6. Sage, A., & Melsa, J. (1971). *Estimation theory with applications to communications and control*. New York: McGraw-Hill. 496 p.

7. Cypkin, Ja. Z. (1984). *Osnovy informacionnoj teorii identifikacii [Fundamentals of identification information theory]*. Moscow, USSR: Nauka. 320 p. (in Russian).

8. Rajbman, N. S. (1970). *Chto takoe identifikacija? [What is identification?]*. Moscow, USSR: Nauka. 118 p. (in Russian).

9. Shtejnberg, Sh. E. (1987). *Identifikacija v sistemah upravlenija [Identification in control systems]*. Moscow, USSR: Energoatomizdat. 80 p. (in Russian).

10. Beard, R. V. (1971). *Failure accommodation in linear system through selfreorganization* (PhD thesis). Massachusetts, USA: MIT. 376 p.

11. Jones, H. L. (1973). *Failure detection in linear systems* (PhD thesis). Massachusetts, USA: MIT. 459 p.

12. Frank, P. M. (1990). Fault diagnosis in dynamic systems using analytical and knowledge-based redundancy: A survey and some new results. *Automatica, 26*, 459–474. doi: 10.1016/0005-1098(90)90018-D

13. Isermann, R. (2006). *Fault-diagnosis systems: An introduction from fault detection to fault tolerance.* Springer-Verlag Berlin Heidelberg. 475 p. doi: 10.1007/3-540-30368-5

14. Isermann, R. (2017). *Combustion engine diagnosis. Model-based condition monitoring of gasoline and diesel engines and their components.* Springer Vieweg. 303 p. doi: 10.1007/978-3-662-49467-7

15. Sage, A.P., & White, C.C. III. (1993). *Optimum systems control*. Englewood Cliffs, USA: Prentice Hall. 392 p.

16. Krasovskij, A. A. (1987) *Spravochnik po teorii avtomaticheskogo upravlenija* [Handbook of automatic control theory]. Moscow, USSR: Nauka, Gl. red. fiz.-mat. lit. 712 p. (in Russian).

17. Trefilov, S., & Nikitin, Y. (2018). Automatic warehouses with transport robots of increased reliability. *Acta Logistica, 5*(1), 19–23. doi: 10.22306/al.v5i1.86

18. Trefilov, S. A., Kalinkin, A. A., & Nikitin, Y. R. (2007). High-maneuverable transport robot. *University Review, 1*(2), 34–39. Trencin, Slovakia: Alexander Dubcek University of Trencin; Izhevsk, Russia: Izhevsk State Technical University.

19. Levin, B. R. (1968). *Teoreticheskie osnovy statisticheskoj radiotehniki* [Theoretical foundations of statistical radio engineering]. Vol. 2. Moscow, USSR: Sovetskoe radio. 504 p. (in Russian).

20. Pugachev, V. S., & Sinicyn, I. N. (1990). *Stohasticheskie differencial'nye sistemy. Analiz i fil'tracija* [Stochastic differential systems. Analysis and filtering]. Moscow, USSR: Nauka. 632 p. (in Russian).

Improving Safety of Oil Storage Tanks Operation

L. E. Zemlerub, E. R. Kharasov, V. M. Avdeev

Petroleum Faculty of Technology, Samara State Technical University,
Samara, Russian Federation
E-mail: oaoatt25@mail.ru

Abstract. Tank batteries for storage of crude oil and refined products are hazardous industrial facilities. Almost half of the accidents (including fires) occurs at the tank batteries at oil and gas industry. The most effective way to improve safety of facilities operation is to introduce additional functions to the existing automated control systems of technological processes. In this article it is proposed to add to automated control systems of technological processes of tank batteries two new subsystems. First one is the subsystem of bottom water drainage from an oil tank by installing on a siphon crane an analyzer of oil concentration in water. The other one is the subsystem of remote leak detection with receiving information from the gas monitoring sensors installed in the leak detection wells and in the area around the tank. Implementation of this additional subsystems to automated control systems of technological processes will allow to receive timely and reliable information about the status of equipment, to increase the efficiency of control and to ensure trouble-free operation which will significantly enhance the safety and efficiency of tank batteries for storage of crude oil and refined products.

Keywords: vertical tank, automated system, technological process, operation safety, bottom water, leak detection

INTRODUCTION

Tank battery (TB) is an essential part of the oil transportation and storage process and allows to maintain pumping cycle. At the same time, tanks have several specific features.

When such a complex product as a crude oil is taken into the tank it starts to stratify and bottom water (BW) appears during the process of water precipitation. Since crude oil contains sulphur, its compounds and other salts, BW is a dilute solution of sulphuric acid and other compounds that accelerate tank's lower ring corrosion and bottom corrosion.

Precipitation of mechanical impurities and bottom water drainage (BWD) reduces the weight of ballast which results in improving crude oil quality and in increasing net weight percent and profitability of crude oil pipeline transportation because payment between suppliers and recipients of oil are made by net weight.

In the Tank Operation Rules it is stated that after taking oil into the tank it is settled for at least two hours, then BWD is performed, and only after that oil is sampled and quality controlled in metrological laboratory.

In addition, TB for crude oil and refined products are facilities that present potential environmental hazards. The main source of contamination is steam-and-gas mixture displaced from the tanks when they have been filled and when the product volume increases due to temperature rise from night to day. [1]. Product leakage is also a serious risk, therefore tanks for oil and oil products with a volume of more than 2000 m3 are equipped with a primary leak detection system. LDS consists of a polyethylene film 1 mm thick, laid under the bottom of the tank at a depth of 70 cm and a drainage pipe connected to the leak detection well (Fig. 1) [2–3].
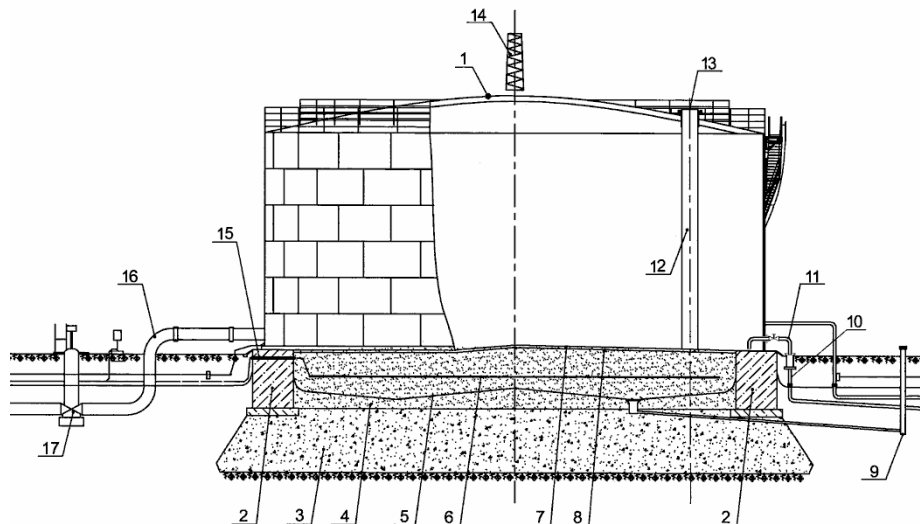
Figure 1. Cross section of the tank: 1 – storage tank; 2 – ring foundation of the tank; 3 – basement of the tank; 4 – sand and gravel mixture; 5 – impervious film; 6 – long anode grounding; 7 – bottom of the tank; 8 – hydrophobic layer; 9 – leak detection well; 10 – industrial sewage; 11 – siphon crane; 12 – pontoon guide (pontoon is not shown); 13 – product level measurement system; 14 – lightning protection; 15 – passage of ECP cables through the foundation; 16 – technological pipelines; 17 – pipeline valve

During the operation of TB emissions and leakages are released into the air, waste water and soil. The size of these leaks can be great. This is primarily represented by the fact that they are not detected immediately and it is extremely difficult to prevent them. Therefore, reducing emissions and timely detecting leaks is one of the most important environmental and tank safety operation concerns. [4, 5]

AUTOMATED SYSTEM OF BOTTOM WATER DRAINAGE

These days BW drainage is carried out manually through a siphon crane installed on the tank wall, technical inspection of which should be performed before each process of drainage. The manual method of BWD has following drawbacks: higher labor costs and relatively high losses during a visual control of BWD process. As a result of the search, several patents of automated system of BWD (AS BWD) were found. For instance, the following design was proposed by colleagues of Omsk State Technical University (Fig. 2).

Its peculiarity is that the bottom 2 of the tank 1 is proposed to be made in the form of outward cone. The amount of BW is determined by the position sensor of an interface level "oil-water" 3, then water is pumped through the pipeline 4 by the pump unit (PU) 6 through the analyzer 5 which determines presence of an oil in a water. When oil appears analyzer sends a signal to the control unit 8 to close the regulator 7. [6]
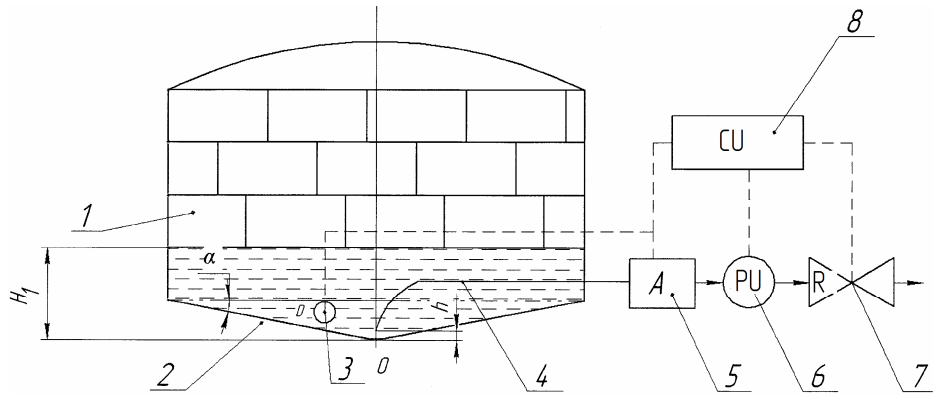
Figure 2. AS BWD of the invention patent number RU 151321 U1

In the design of automatic BWD offered by Saudi company for automation SAFIA determination of oil presence in water is carried out with the help of a device installed on a drainage pipeline. Its operating principal is based on measuring of difference in ultrasound speed in different substances. [7]

In this article it is proposed to use an automated system that reduces crude oil losses during BWD process. The design of AS BWD is similar to that proposed in the patent number RU 151321 U1 and includes a siphon to which a ball valve with electric drive and an oil presence alarm are connected. All devices are made in an explosion-proof design.
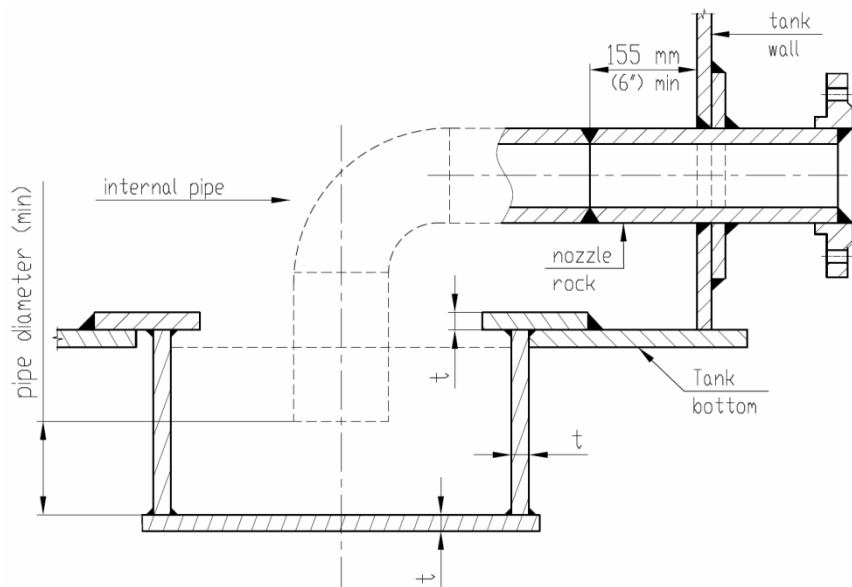
Figure 3. Drain sump on the bottom of the tank

In the design of AS BWD there is no need in using a pump unit since the duration of BWD process is determined by a diameter of syphon cranes and their number which increases proportionally to the increase in a tank volume. The proposal to construct bottom of the tank in the form of outward cone will lead to an increase in stresses and bending moment that occurs when filling the tank in the T-bar welded connection of the wall and bottom which in turn will lead to a decrease in the reliability of the tank. To prevent the inlet of BW into oil a manifold it is enough to provide a small pit (drain sump) on the bottom of the tank with a diameter of 0.5–1.5 m and to increase the length of siphon crane offset by 3–6 cm towards

the tank bottom. For example, in API 650 a water collection pit is proposed to be constructed as shown on Fig. 3. [8]

Selected as an example alarm CH-1T is designed for continuous monitoring of water quality at explosive facilities, signalization of oil concentration over-limit in water and controlling of executive mechanisms of TP. CH-1T is a device operating principle of which is based on the effect of fluorescence of oil under ultraviolet irradiation (Fig. 4).

Figure 4. Alarm device CH-1T

BWD is carried out by automatic opening of the ball valve after the time required for water precipitation after taking the crude oil into the tank. During the process of BWD alarm device continuously monitors the concentration of oil in the drainage pipe. When the specified concentration is reached the alarm device will notify about this and send a signal to close the ball valve and stop drainage. The difference of the proposed design lies in its simplicity and in the algorithm of iterative drainage termination when relatively small concentration of oil in water appears, which will lead to a reduction of oil losses.

Since the proposed design is not provided with manual rotation mechanism of a siphon crane as on the tank with manual BWD, it is proposed to heat external part of the system to prevent water freezing at a negative temperature.

The implementation of AS BWD will lead to a reduction in labor costs and elimination of the influence of "human factor" not only during the process of BWD but also during the process of level gaging. It will be required for TB operators to carry out the additional start-up of the system before taking any measurements and sample drawing.

AUTOMATED SYSTEM OF REMOTE LEAK DETECTION

Standard ACS TP designed to provide centralized monitor and control of TB consists of the following subsystems:
- system of tank gaging;
- bottom sediments erosion system;
- fire extinguisher system;
- system of gate valves control.

The following parameters are remotely measured and transmitted to local control room:
- oil level in tanks;
- average oil temperature (measured by product layers);
- air temperature in TB.

At the local control room following parameters are monitored:
- reliability of measured parameters by intervals of allowed values;
- volume of product oil and free capacity;
- position of gate valves of TB process pipelines;
- status of local automatics and communication channels.

ACS TP provides automatic protection against fire and crude oil over fill in tanks. In case of emergency situations automatic light and sound alarming is provided. [9, 10, 11].

In this article it is proposed to install additional sensors and systems to the existing ACS TP to provide following features:
- continuous control of gas-air environment in leak detection wells and in the area around the tank (Fig. 5) [12];
- monitoring of tank cathode protection system (CPS) operation using the potentials obtained from the reference electrodes and signals from corrosion rate sensors located under the tank bottom (Fig. 6) [13, 14, 15].
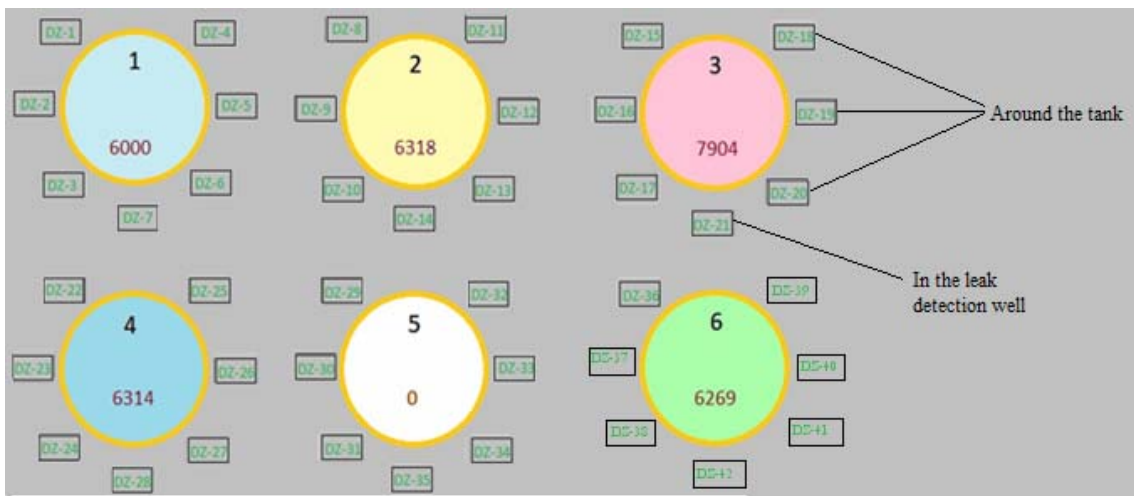
Figure 5. Mnemonic scheme of gas monitoring sensors location at TB
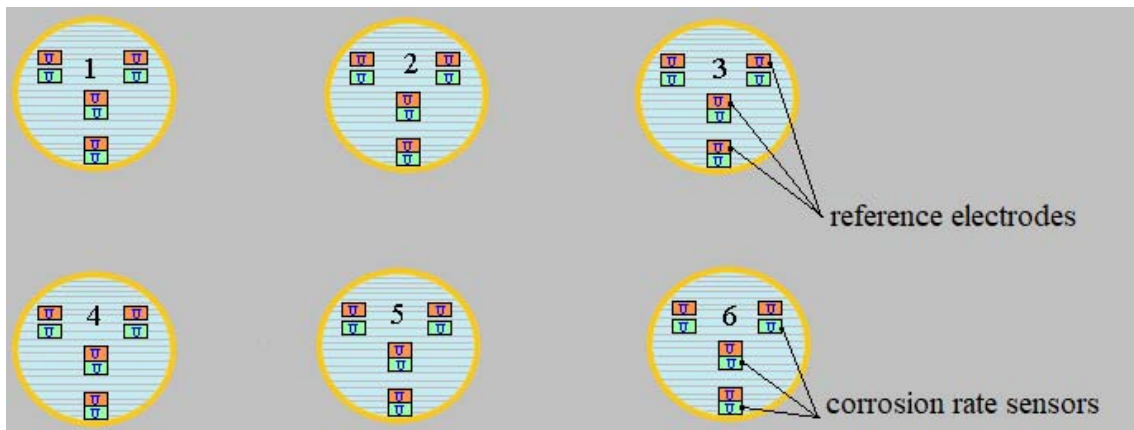
Figure 6. Mnemonic scheme location of reference electrodes and corrosion rate sensors in TB

Information obtained from tank gaging system and additional sensors and systems will provide the development and implementation of combined automated system of remote leak detection (AS RLD) at TB [16, 17].

For the development of the AS RLD it is proposed to use the existing certified software package of ACS TP to which subsystems with following features will be added:

- receiving signals from sensors installed in leak detection wells;
- receiving signals from gas pollution sensors in the area around the tank;
- receiving signals from reference electrodes measuring electric potentials of cathodic protection and corrosion rate sensors installed under the bottom of the tank;
- display of received sporadically arising information on the operator's workstation screen.

In addition to the above mentioned functions AS RLD should perform the analysis of the received information and necessary calculations and separate unreliable data and notify about the approaching accident.

CONCLUSION

Implementation of AS BWD will lead to a reduction of labor costs, elimination of the "human factor" influence and minimization of oil losses during the process of BWD.

Equipping TB with a system of continuous monitoring of the gas-air environment using sensors installed in the area around the tank and leak detection wells at TB facilities will result in ensuring safe working conditions as well as preventing fires and explosions. [18, 19].

Using the method of adding new functions to existing ACS TP will allow to develop and implement AS RLD for a relatively short period of time and at low cost. Such indicators of AS RLD development can be obtained in the process of technical, informational, mathematical and software development by analogy with the corresponding sections of the current ACS TP [20].

Introduction of additional subsystems of ACS TP will allow to receive timely and reliable information about the status of equipment, to increase the efficiency of control and to ensure trouble-free operation which will significantly enhance the safety and efficiency of TB operation.

REFERENCES

1. Danilov, V. F., & Shurygin, V. Y. (2017). Sistema avtomatizirovannogo obnaruzheniya utechek nefteproduktov [System of automatic leak detection of refined products]. *Uspekhi sovremennogo estestvoznaniya [The successes of modern science], 2017*(11), 63–67. (in Russian).

2. Abbasi, M. H., Benhelal, E., & Ahmad, A. (2014). Designing an optimal safe layout for a fuel storage tanks farm: Case study of Jaipur oil depot. *International Journal of Chemical, Molecular, Nuclear, Materials and Metallurgical Engineering, 2014*(8), 147–155. doi: 10.5281/zenodo.1092134

3. Sengupta, A., Gupta, A. K., & Mishra, I. M. (2011). Engineering layout of fuel tanks in a tank farm. *Journal of Loss Prevention in the Process Industries, 24*, 568–574. doi: 10.1016/j.jlp.2010.06.016

4. Ibrahim, H. A., & Syed, H. S. (2018). Hazard analysis of crude oil storage tank farm. *International Journal of ChemTech Research, 11*(11), 300–308. doi: 10.20902/IJCTR.2018.111132

5. Chang, J. I., & Lin, Ch.-Ch. (2006). A study of storage tank accidents. *Journal of Loss Prevention in the Process Industries, 19*, 51–59. doi: 10.1016/j.jlp.2005.05.015

6. Tokarev, V. V., Kucherenko, M. V. & Pohlebaeva, D. P. (2015). Ustrojstvo dlya udaleniya podtovarnoj vody iz rezervuara [Device for bottom water drainage from a tank]. *Ru Patent No. 151321 U1* (in Russian).

7. Safia: Innovative Measureemnts. (n.d.). *Automatic Tank Dewatering System.* Retrieved from https://www.ksafia.com/automatic-tank-dewatering

8. API standard 650. Welded Steel Tanks for storage of petroleum products. 11th edition, June 2007.

9. Ickovich, E. L. (2009). *Metody racional'noj avtomatizacii proizvodstva [Methods of rational production automation]*. Moscow, Russia: Infra-Inzheneriya. (in Russian).

9. Caouette, R., & Eng, P. (2015). Automation infrastructure upgrades at an oil storage terminal. In: *Process Control & Safety Symposium, 2015*. Retrieved from: https://23.235.204.252/~letico/wp-content/uploads/2017/04/TP15PCS073.pdf

10. Sharma, R. K., Gurjar, B. R., Singhal, A. V., Wate, S. R., Ghuge, S. P., & Agrawal, R. (2015). Automation of emergency response for petroleum oil storage terminals. *Safety Science, 72*, 262–273. doi: 10.1016/j.ssci.2014.09.019

11. Thompson, J. (2013). *Choosing the correct leak detection for tanks*. Retrieved from the PetrolPlaza website: https://www.petrolplaza.com/knowledge/2888

12. Bae, J.-H., Ha, T.-H., & Lee, H.-G. (2003). Development of remote corrosion monitoring and control system for oil tanks by using a high efficiency CP rectifier. *IFAC Proceedings Volumes, 36*, 951–955. doi: 10.1016/S1474-6670(17)34596-2

13. Meroufel, A., Al Hajri, M., & Abed, K. (2016). Mitigation of soil-side corrosion on storage tank bottoms in the absence of deficient CP system. *NACE 16th Middle East Corrosion Conference & Exhibition* (pp. 1–13). NACE Paper No. MECCFEB16-7995. Retrieved from: https://www.cortecvci.com/Publications/Papers/8-MECCFEB16-7995.pdf

14. Welsh, R. A., & Benefield, J. (2006). Environmental protection through automated remote monitoring of fuel storage tank bottoms using electrical resistance probes. *Materials Performance, 45*(3), 38–40.

15. Yang, L. (Ed.). (2008). *Techniques for corrosion monitoring*. Woodhead Publishing.

16. Ali, M., & Al Beed, A. A. (1998). Above-ground tank bottom corrosion due to inappropriate construction practices and corrosion control using cathodic protection. In: *CORROSION 98 (March 22–27, 1998)*. San Diego, USA: NACE International. Retrieved from: https://www.onepetro.org/conference-paper/NACE-98596

17. Hamatdinova, A. V., & Smorodova, O. V. (2015). Pribornyj kontrol' sostoyaniya gazo-vozdushnoj sredy na predpriyatitah neftepererabotki [Instrumental monitoring of the gas and air environment at oil refineries]. *Tekhnologiya tekhnosfernoj bezopasnosti [Technology of technospheric safety], 62,* 1–7. (in Russian).

18. Li, S. C. (2004). Oil tank fire statistical analysis. *Fire Control Theory Research, 04,* 0117.

19. Argyropoulosa, C. D., Christolisa, M. N., Nivolianitou, Z., & Markatos, N. C. (2012). A hazard assessment methodology for large liquid hydrocarbon fuel tanks. *Journal of Loss Prevention in the Process Industries, 25,* 329–335. doi: 10.1016/j.jlp.2011.12.003